JOÃO PAULO DE CARVALHO PEDROSO

ECONOMIC POWER SHARING USING DROOP STRATEGY FOR PARALLEL CONVERTERS IN A LOW-VOLTAGE AC ISLAND MICROGRID

LAVRAS – MG

2021

JOÃO PAULO DE CARVALHO PEDROSO

ECONOMIC POWER SHARING USING DROOP STRATEGY FOR PARALLEL CONVERTERS IN A LOW-VOLTAGE AC ISLAND MICROGRID

Dissertation submitted in partial fulfillment of the requirements of the Graduate Program in Systems and Automation Engineering for the Degree of Master of Science at the Federal University of Lavras.

Prof^{a}. Dr^{a}. Sílvia Costa Ferreira

Supervisor

LAVRAS – MG

2021

Ficha catalográfica elaborada pelo Sistema de Geração de Ficha Catalográfica da Biblioteca Universitária da UFLA, com dados informados pelo(a) próprio(a) autor(a).

Pedroso, João Paulo de Carvalho.
Economic Power Sharing Using Droop Strategy for Parallel Converters in a Low-voltage AC Island Microgrid / João Paulo de Carvalho Pedroso. - 2021.
167 p. : il.

Orientador(a): Sílvia Costa Ferreira.

Dissertação (mestrado acadêmico) - Universidade Federal de Lavras, 2021.
Bibliografia.

1. Estratégia de Despacho Econômico de Potência. 2. Controle Droop. 3. Microrredes Resistivas. I. Ferreira, Sílvia Costa. II. Título.

JOÃO PAULO DE CARVALHO PEDROSO

ECONOMIC POWER SHARING USING DROOP STRATEGY FOR PARALLEL CONVERTERS IN A LOW-VOLTAGE AC ISLAND MICROGRID

Dissertation submitted in partial fulfillment of the requirements of the Graduate Program in Systems and Automation Engineering for the Degree of Master of Science at the Federal University of Lavras.

APROVADA em 25 de Julho de 2021.

Prof^a. Dr^a. Sílvia Costa Ferreira	UFLA, Brazil
Prof. Dr. Rondinelli Rodrigues Pereira	UNIFEI, Brazil
Prof. Dr. Vinicius Miranda Pacheco	UFLA, Brazil
Prof. Dr. Felipe Oliveira e Silva	UFLA, Brazil

Prof^a. Dr^a. Sílvia Costa Ferreira
Orientadora

LAVRAS – MG
2021

AGRADECIMENTOS

A Deus, por permitir desfrutarmos uma pequena parte de Sua infinita criação.
A minha esposa Julia, pelo amor durante todos esses anos.
Aos meus pais Sérgio e Silene, e também ao meu irmão Sérgio Henrique, pelo apoio incondicional.
A minha orientadora Prof^{a}. Sílvia C. Ferreira, pela orientação, dedicação e empenho ímpar na realização desse trabalho.
Ao Prof. Vinícius M. Pacheco, pela oportunidade de trabalhar como docente voluntário.
Ao Prof. Danton D. Ferreira e aos demais professores do Programa de Pós-graduação em Engenharia de Sistemas e Automação - PPGESISA pelos ensinamentos.
Aos meus colegas Rayane, Marielle, Thales, Letivan e muitos outros, os quais, sem eles, a realização desse trabalho seria impossível.
A Fundação de Amparo à Pesquisa do Estado de Minas Gerais - FAPEMIG, pelo fomento à pesquisa e inovação científica e tecnológica.
A Universidade Federal de Lavras - UFLA e ao povo brasileiro, pela oportunidade.

A todos vocês, meu mais sincero obrigado.

"The adventure of life is to learn. The purpose of life is to grow. The nature of life is to change. The challenge of life is to overcome. The essence of life is to care. The opportunity of like is to serve. The secret of life is to dare. The spice of life is to befriend. The beauty of life is to give."
(William Arthur Ward)

"If you want to find the secrets of the universe, think in terms of energy, frequency and vibration."
(Nikola Tesla)

RESUMO

As unidades de geração participantes de uma microrrede podem fazer o uso de diferentes fontes primárias de energia, tais como combustíveis fósseis, recursos renováveis ou sistemas de bateria. Dada a diversidades de tais fontes, é natural que haja diferenças nos custos de operação das unidades de geração distribuída. Quando uma microrrede encontra-se desconectada do sistema elétrico principal, suas unidades geradoras devem ser capazes de manter níveis adequados de tensão e frequência para atendimento das cargas locais. Além disso, nessa condição também é necessário coordenar o fornecimento de energia de cada gerador com base em seus respectivos custos operacionais, visando minimizar o custo global de operação do sistema ilhado. O controle local de uma microrrede nessa condição pode ser realizado por dois métodos: empregando um sistema de controle central, o qual baseia-se em tecnologias de comunicação para coordenar a operação das fontes de energia, ou então através de um sistema distribuído de gestão econômica dos geradores, o qual realiza o despacho de potência sequencial dessas unidades baseado nos seus respectivos custos de operação, sem a necessidade de um sistema paralelo de comunicação. A coordenação dessa estratégia se dá através da variação de parâmetros da própria rede local, como frequência e amplitude da tensão. Esse método de controle é conhecido como estratégia *Droop* e apresenta como vantagem a dispensa do uso de meios de comunicação secundários entre os conversores, o que aumenta a confiabilidade, simplicidade e velocidade de atuação do sistema. Nesse contexto, esse trabalho consiste em adaptar uma estratégia de compartilhamento de potência baseada em aspectos econômicos inerentes à fonte energética primária das unidades de geração distribuídas para uma microrrede monofásica ilhada de baixa tensão, visando minimizar custos globais de operação. Essa estratégia foi implementada empregando-se o controle preditivo baseado em modelo com conjunto de dados finito como método de controle local dos conversores eletrônicos, adicionando adequada capacidade de seguir sinais de referência com ajuste dinâmico, de rejeição de distúrbios e de lidar com não-linearidades no sistema, com desempenho comparável a técnicas de controle tradicionais. A validação da estratégia econômica adaptada é realizada em simulações computacionais empregando o software MATLAB/*Simulink* para uma microrrede de baixa tensão com cargas distintas e com demanda de potência variável ao longo do tempo.

Palavras-chave: Estratégia de Despacho Econômico de Potência Adaptada. Controle *Droop*. Microrredes Resistivas.

ABSTRACT

Distributed generation units participating in a microgrid may be employing different primary energy sources such as fossil fuels, renewable resources or battery systems. Given the diversity of such sources, it is natural that the operational costs will probaly vary between such units. When a microgrid is disconnected from the main electrical system, its distributed generators must be able to maintain adequate voltage and frequency levels to meet local loads. In addition, at this condition it is also necessary to coordinate the power dispatch of each generator based on their respective operational costs in order to minimize the overall islanded system operational cost. The microgrid local control in island operation can be accomplished by two methods: utilizing a central control system, which relies on communication technologies to coordinate the operation of local power sources, or by means of a distributed economic power-sharing management system, which performs sequential power dispatch of the distributed generators based on each unity operational cost, without a paralell communication system being required. The coordination of this strategy is based on the variation of grid parameters, such as voltage amplitude and frequency. This control method is known as *Droop* strategy and has the advantage of avoiding the use of secondary communication channels between converters, increasing system reliability, simplicity and speed response performance. In this context, this study consists of adapting a power sharing strategy based on economic aspects inherent to the primary energy source of the distributed generation units for a single-phase low-voltage microgrid, aiming system overall operational cost reduction. This strategy was implemented using finite-control-set model predictive control as local control method for the power-electronic converters, which added adequate ability to follow reference signals with dynamic adjustment, disturbance rejection and to deal with nonlinearities in the system, with performance comparable to traditional control techniques. The validation of the adapted economic strategy is performed in computer simulations using the MATLAB/*Simulink* software for a low-voltage microgrid with distinc loads and variable power demand over time.

Keywords: Adapted Economic Power Dispatch Strategy. Droop Control. Resistive Microgrids.

LIST OF FIGURES

LIST OF TABLES

SUMMARY

1 INTRODUCTION

A microgrid can be described as a cluster of loads, distributed generation and energy storage systems operating in coordination to reliably supply electricity, and is connected to the electrical power system at a single point of connection, the PCC (*Point of Common Coupling*). The adoption of microgrids as the paradigm for the massive integration of distributed generation will allow technical problems to be solved in a decentralized fashion, reducing the need for an extremely ramified and complex central coordination and facilitating the realization of the Smart Grid (OLIVARES et al., 2014).

A microgrid is capable of operating in grid-connected and stand-alone, or islanded, modes and handle the transitions between these two states. In the grid-connected mode, the power deficit can be supplied by the main grid and excess power generated can be traded with the power system. In the islanded mode of operation, the active and reactive power generated within the microgrid should be in balance with the demand of local loads (OLIVARES et al., 2014). A special attention must be given to the microgrid during island operation since it is necessary to generate proper voltage and frequency references within the local distributed generation units.

Microgrids usually comprise different types of small DG units, controlled as grid-forming converters, such as microturbines, internal combustion engines, and other storage technologies. Being conceptually distinct, their operating characteristics and generation costs will normally vary. It is, therefore, important to control the power dispatch of those converters optimally based on their operating characteristics and costs (NUTKANI et al., 2017).

Usually, optimized or economic operation of microgrid is achieved by a traditional centralized communication-based system. The concept of centralized management of microgrid has been adopted from the traditional power system, where generation dispatch decision is made based on load forecasting and economic unit commitment. Although the centralized management system has advantages of maximizing benefits in terms of economic operation, and better voltage and frequency regulations, it may not be suitable for all applications due to its inflexibility for plug-n-play and dependence on communication infrastructure (NUTKANI et al., 2017).

A decentralized power sharing control technique is of great interest in terms of reliability as it does not rely on communication systems and also presents fast response due to power network local parameters measurement at the DG converter connection point. According to Han et al. (2017), in order to ensure stability and economical operation of the microgrid,

the active and reactive powers of the distributed generation units should be shared simultaneously. To address this question, the droop control strategy was proposed by Chandorkar, Divan e Adapa (1993) to allow power sharing without communication lines by imitating steady-state characteristics of synchronous generators in islanded microgrids. For the microgrid overall cost reduction, Nutkani et al. (2017) presented an economic approach for power sharing based on operational costs of each generator within the microgrid.

Microgrid functionalities, operation modes and hierarchical control are presented at the present work. An adapted droop-based economic power-sharing strategy for low-voltage microgrids is also presented. This control strategy should be able to dispatch active and reactive power for supplying the microgrid load demand proportionally between the DG units based on their operational costs and without the necessity of a secondary communication system. The objective is to achieve cost reduction for microgrids in stand-alone operation in a decentralized manner, maintaining system stability and reliability with online power reserve for supporting load variations and also maintaining voltage and frequency withing acceptable limits. In this sense, grid-feeding and grid-forming with finite set model predictive control converter operational modes are also considered.

1.1 Project motivation and contributions

Several control strategies have been proposed in technical literature for proper parallel connected grid-forming converters operation in an islanded microgrid, such as Han et al. (2016), Rocabert et al. (2012), Dragičević (2018) and Guerrero et al. (2005). These methods can be classified into centralized or distributed control strategies, and also as communication based and non-communication based techniques. Among these methods, droop control has been widely accepted in the scientific community and has been focus of a massive amount of studies, Nutkani et al. (2017), Nutkani et al. (2015) and Guerrero et al. (2005). The main feature of this technique is the power sharing among the parallel distributed generators being coordinated based on grid parameters measured at each converter connection point, for instance voltage amplitude and frequency. Another benefit of droop control is that it is a decentralized control strategy that does not require the use of a central controller, which makes the system more reliable and increases the plug-and-play capability for new units.

The vast majority of works applies the traditional droop scheme with the purpose of sharing power proportionally among multi parallel converters (YOUNG; BASTIAS, 2018; HAO;

ZHEN, 2017; CHANDORKAR; DIVAN; ADAPA, 1993). However, it is of paramount importance to improve the operation of these converters in order to achieve more adequate power sharing, and subsequent generation cost reduction. To achieve that, different modified droop schemes have been proposed aiming to improve economic operation of the microgrid (NUTKANI et al., 2017; VERGARA et al., 2019a; AUGUSTINE et al., 2012; ALVAREZ et al., 2009).

This work aims to apply an economic dispatch strategy for proportional cost-related active and reactive power sharing between parallel single-phase converters in a low-voltage islanded microgrid using the droop control technique.

1.2 General Objective

The present work proposes an adaptation of a droop-based economic dispatch strategy for converters using finite-control-set model predictive control for an island low-voltage distribution level AC microgrid with mainly resistive impedance behavior.

1.3 Specific Objectives

The specific objectives of this work are:

a) Develop using *software* MATLAB/*Simulink* a fully decentralized low-voltage island AC microgrid, which allows the connection of multiple finite-control-set model predictive control grid-forming converters in order to implement an adapted droop-based economic power sharing strategy with the absence of secondary communication systems between distributed generators;

b) Perform software simulations of the proposed system under distinct loads and time-varying power demand conditions;

c) Validate the adapted economic strategy using a MATLAB/*Simulink* implementation of a traditional resistive droop power sharing method for comparative cost analysis;

d) Include converters operational mode transition within the adapted strategy in order to improve the dynamic behavior of the system during short-time low-load variations;

e) Evaluate the proposed adapted power sharing strategy expandability with the inclusion of a new cost-distinct distributed generation unity in software simulations.

2 LITERATURE REVIEW

This chapter present a literature review over this work main subject, which includes microgrids and its functionalities, active and reactive power sharing methods and control strategies.

2.1 Microgrids

The increased penetration of distributed generation units, especially the renewable energy sources including micro-turbines, fuel cells, photovoltaic systems, and wind energy plants have been a paradigm shift in the electrical power systems in the past decades (BLAABJERG; CHEN; KJAER, 2004). The distributed generation units make a major contribution in reducing pollution, decreasing power transmission losses, and improving local utilization of renewable energy resources, which becomes a strong support for the large-scale power grid (MINXIAO et al., 2013).

The concept of microgrid was first introduced in the technical literature by Lasseter (2001) and Lasseter (2002) as a solution for the reliable integration of distributed energy resources, including energy storage systems and controllable loads. Such microgrid would be perceived by the main grid as a single element responding to appropriate control signals. Although a detailed definition of microgrids is still under discussion in technical forums, a microgrid can be described as a cluster of loads, distributed generation units and energy storage systems operated in coordination to reliably supply electricity, connected to the distribution power system at a single point of connection (OLIVARES et al., 2014). In general, according to Barklund et al. (2007) a microgrid can be considered as a small-scale power system in which all generation, storage and load systems are electrically interconnected and hierarchically controlled with the capacity of operating connected to the main grid, isolated or in the transition between them. The microgrid basic architecture is presented in Figure 2.1

The adoption of microgrids as the paradigm for the massive integration of distributed generation will allow technical problems to be solved in a decentralized fashion, reducing the need for an extremely ramified and complex central coordination and facilitating the realization of the Smart Grid. In order to successfully integrate renewable distributed energy resources in a microgrid, many technical challenges must yet be overcome to ensure that the present levels of reliability are not significantly affected, and the potential benefits of distributed generation are

Figure 2.1 – Microgrid basic architecture.

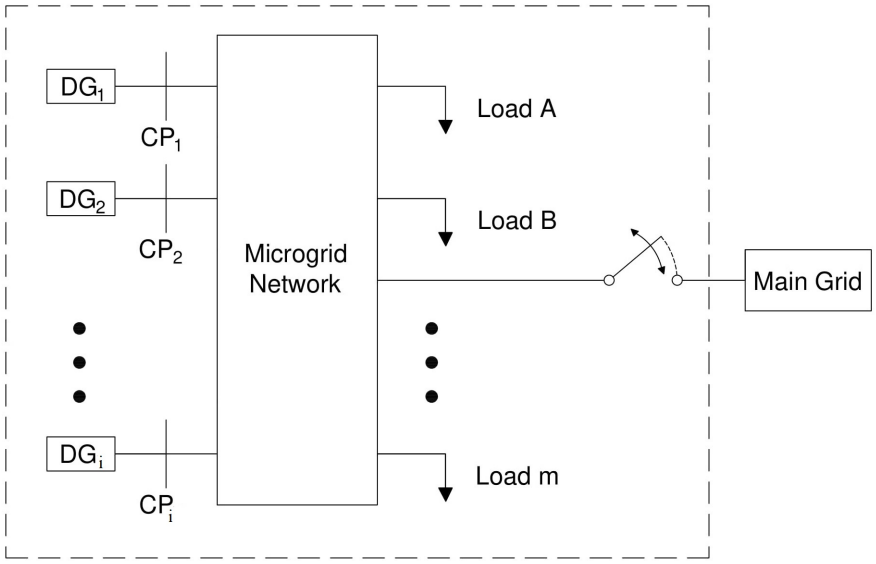

Source: Adapted from: Olivares et al. (2014)

fully harnessed (OLIVARES et al., 2014). In this sense, the main issues listed by Olivares et al. (2014) include:

a) **Bidirectional power flows:** while distribution feeders were initially designed for unidirectional power flow, integration of distributed generation units at low voltage levels can cause reverse power flows and lead to complications in protection coordination, undesirable power flow patterns, fault current distribution, and voltage control;

b) **Stability issues:** local oscillations may emerge from the interaction of the control systems of DG units, requiring a thorough small-disturbance stability analysis. Moreover, transient stability analyses are required to ensure seamless transition between the grid-connected and island modes of operation in a microgrid;

c) **Modeling:** prevalence of three-phase balanced conditions, primarily inductive transmission lines, and constant-power loads are typically valid assumptions when modeling conventional power systems at a transmission level; however, these do not necessarily hold valid for microgrids, and consequently models need to be revised;

d) **Low inertia:** unlike bulk power systems where high number of synchronous generators ensures a relatively large inertia, microgrids might show a low-inertia characteristic, especially if there is a significant share of power electronic-interfaced generation units. Although such an interface can enhance the system dynamic performance, the low iner-

tia in the system can lead to severe frequency deviations in island operation if a proper control mechanism is not implemented;

e) **Uncertainty:** the economical and reliable operation of microgrids requires a certain level of coordination among different distributed energy resources. This coordination becomes more challenging in islanded microgrids, where the critical demand-supply balance and typically higher component failure rates require solving a strongly coupled problem over an extended horizon, taking into account the uncertainty of parameters such as load profile and weather forecast. This uncertainty is higher than those in bulk power systems due to the reduced number of loads and highly correlated variations of available energy resources.

In particular, as enumerated by Olivares et al. (2014), the desirable features of the control system must include:

a) **Output control:** output voltages and currents of the various distributed energy resources units must track their reference values and ensure oscillations are properly damped;

b) **Power balance:** generation units in the microgrid must be able to accommodate sudden active power imbalances, either excess or shortage, keeping frequency and voltage deviations within acceptable ranges;

c) **Demand side management:** where applicable, proper demand side management mechanisms must be designed in order to incorporate the ability to control a load portion. Additionally, for the electrification of remote communities with abundant local renewable resources, the active participation of the local community may be beneficial in order to design cost-effective demand side management strategies that enhance load-frequency control;

d) **Economic dispatch:** an appropriate dispatch of distributed generation units participating in the operation of a microgrid can significantly reduce the operational costs, or increase the profit. Reliability considerations must also be taken into account in the dispatch of units, especially in island operation;

e) **Transition between modes of operation:** a desirable feature of microgrids is the ability to operate in both grid-connected and island modes, including a smooth transition

between them. Different control strategies might be defined for each mode of operation and, therefore, a high-speed islanding detection algorithm is very important in order to adjust the control strategy accordingly.

As mentioned, one of the main features of a microgrid is its capacity of operating both connected to the main grid or as a small autonomous power system. According to Karimi, Nikkhajoei e Iravani (2008), the microgrid must be able to handle the transition between these two modes, increasing the system reliability in cases of energy shortages and permitting energy costs reduction by the high integration capacity of renewable resources and storage systems.

The steady-state operation of an islanded microgrid are being considered at the present work, focusing on a decentralized droop-based control strategy for resistive biased lines of grid-forming distributed generation units, where active and reactive power sharing, voltage and frequency stability and economic aspects regarding the local power sources nature and instantaneous operating set-point are considered all together. Main power system disconnection and re-synchronization, power quality recovery and compensation and other diverse features and capabilities regarding microgrids are not being addressed at the present moment.

2.1.1 Microgrid island operation

The microgrid isolated, or island, operation mode is significantly more challenging than the grid-connected mode once the active and reactive power control, system stability and power quality management must be more strict and locally coordinated. Therefore, for this kind of operation it is of keen importance proper control strategies to maintain balance among distributed power sources and local loads.

The microgrid disconnection from the main power grid can be either intentional or unintentional. Intentional islanding can occur in situations such as scheduled maintenance, or when degraded power quality of the main grid can endanger microgrid operation. Unintentional islanding can occur due to faults and other unscheduled unknown events. Proper detection of such a disconnection is imperative for safety of personnel, proper operation of the microgrid, and implementation of changes required in the control strategy (OLIVARES et al., 2014).

Dispatchable renewable or nonrenewable power sources can be integrated as the primary energy sources among the diverse distributed generators geographically spread over a microgrid. In case of a power grid disconnection event, these units are capable of maintaining the voltage reference while attending the local loads. Also, energy storage systems, such as

battery banks, acting as an UPS (*Uninterruptible Power Sources*) units are an attractive solution to attend high load variation capacity for an island microgrid, increasing the system reliability.

Therefore, operational costs will vary among the different power sources that might integrate the microgrid, being of great interest to perform a gradual dispatch of these distributed generators based on economic criteria in order to achieve overall cost reduction during stand-alone operation. Thus, the microgrid operating independently from the main grid may also have to integrate the power sources dispatch control in ways to sequence the distributed generators operation as load demand increases, tending to prioritize the less costly of those.

According to Hao e Zhen (2017), voltage-source power converters or synchronous generators are required to provide stable voltage reference for other local current-source distributed generation units in island operation. Dispatchable units are of most importance for this case once they are also responsible for the power flow management within the microgrid. Main control methods applied to perform these objectives, especially for power electronic-based converters, are the centralized P-Q and V-f control and the diverse decentralized strategies, such as conventional droop-based control and its variations.

In the next section, classification and operational features of power electronic-based converters will be presented.

2.2 Classification of power converters in AC microgrids

The power electronic converters are the main responsible for the microgrid proper operation once they are, in most cases, the connection element between the power source and the electric grid. As reported by Araujo (2017), some sorts of power electronic based converters are capable of controlling the active and reactive power flow and also achieve better power quality rates.

Depending on their objectives in an AC microgrid, power converters can be classified into grid-forming, grid-feeding, and grid-supporting power converters. The grid-forming converters can be represented as an ideal AC voltage source with a low-output impedance, setting the voltage amplitude and frequency of the local grid by using a proper control loop. On the other hand, the grid-feeding power converters are mainly designed to deliver power to a previously energized grid. This last can be represented as an ideal current source connected to the grid in parallel with a high output impedance. Finally, the grid-supporting converters can be

represented either as an ideal AC-controlled current source in parallel with a shunt impedance, or as an ideal AC voltage source in series with a link impedance (ROCABERT et al., 2012).

A grid-feeding power converter, in order to be controlled as a current source, it require a synchronous generator or a grid-forming power converter to previously create the grid voltage to properly operate. Therefore, this kind of converter cannot operate independently in island mode. On the contrary, a grid-forming power converter usually operates specifically in islanded mode, since in the main grid the AC voltage is conventionally formed by synchronous generators (GREEN; PRODANOVIC, 2007). A grid-supporting power converter is in between a grid-feeding and a grid-forming power converter, being its main objective to deliver proper values of active and reactive power to contribute to the regulation of the grid frequency and voltage amplitude (ROCABERT et al., 2012). A more detailed description of the operation and control loops of grid-forming and grid-feeding converters are presented next as both converter control modes will be applied in the present work. The grid-supporting converter control will not be addressed, though a detailed description of its control structure can be found in Rocabert et al. (2012).

2.2.1 Grid-forming power converters

The grid-forming power converters are controlled in closed loop to operate as an ideal AC voltage sources with a given amplitude E_{ref} and frequency ω_{ref} references. As voltage sources, they present a low output impedance, so they need an extremely accurate synchronization system to operate in parallel with other grid-forming converters. Power sharing among parallel connected grid-forming converters is a function of the value of their output impedances (ROCABERT et al., 2012). When a microgrid operates in island mode, its grid-forming power converters are responsible to set the microgrid nominal voltage and frequency by adjusting their internal voltages and virtual impedance parameters.

According to Araujo (2017), the grid-forming power converter is suitable to operate in island mode, being necessary in this case to be fed by a stable DC external power source, like fuel cells or energy storage systems such as batteries. A practical example of a grid-forming power converter can be a standby UPS system. This backup system remains disconnected from the main grid when the operating conditions are within nominal standard limits. In the case of a grid failure or degraded signal quality, the UPS power converter provides the local grid voltage. In an island microgrid, the AC voltage generated by the grid-forming power converter will be

used as reference for the other local grid-feeding power converters connected to it (ROCABERT et al., 2012).

Figure 2.2 – PI-based control structure for a grid-forming power converter.

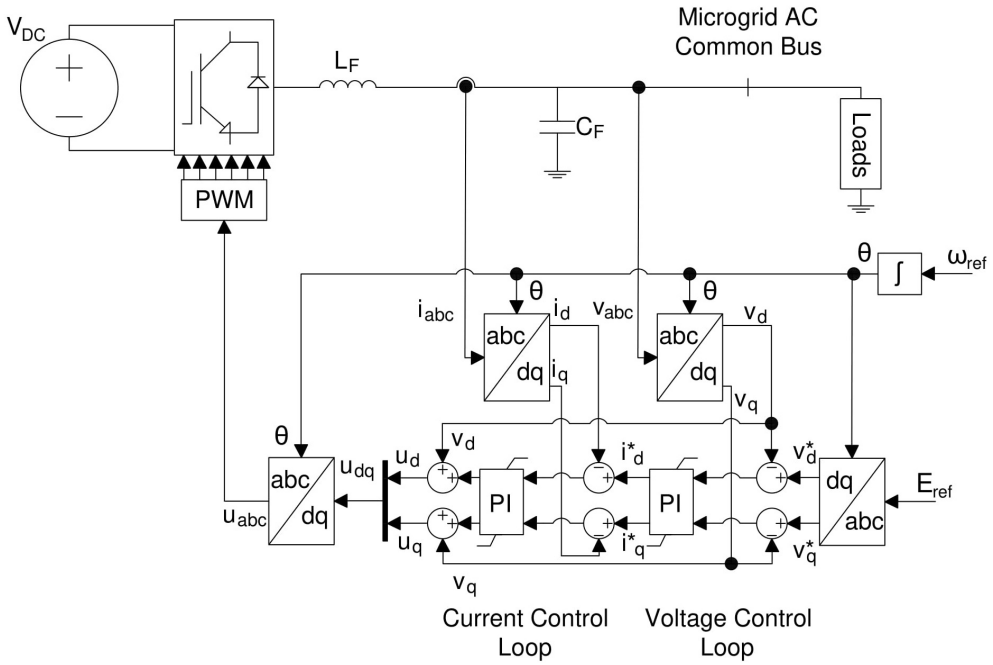

Source: Adapted from: Rocabert et al. (2012)

Figure 2.2 shows an example of a controller scheme for a grid-forming power converter, which, like the grid-feeding converter, is traditionally implemented by using two cascaded synchronous controllers working on the *dq* reference frame. The inputs to the control system are the voltage amplitude E_{ref} and the frequency ω_{ref} to be formed by the power converter at the point of common coupling (PCC).

As stated by Guimaraes (2019), the converter external loop controls the grid voltage to match its reference value by calculating the error between the reference and converter output voltage, v^*_{dq} and v_{dq}, respectivelly. The signal difference is then feeded into the internal control loop as it regulates the current supplied by the converter i^*_{dq}. Therefore, the controlled current flowing though the inductor L_f charges the capacitor C_f to keep the output voltage close to the reference provided to the voltage control loop. As stresses by Rocabert et al. (2012), it is important to outline that the voltage control loop of a grid-forming power converter will only be activated when the microgrid is disconnected from the main power system and working in island mode.

Although the synchronous reference based PI controller is one of the most widely used in technical literature, it has some disadvantages compared to more modern controllers such

as fuzzy, adaptive, sliding mode and predictive (GUIMARAES, 2019). Rodriguez et al. (2013) compared the PI based controler using PWM (*Pulse width modulation*) to the finite control set model predictive control, FCS-MPC. In this paper the authors demonstrated that the FCS-MPC is comparable to the classical control solutions, having a better performance in terms of flexibility. It was also pointed out that the advantages of the FCS-MPC control strategy are the elimination of the cascaded controllers, the capacity in dealing with nonlinearities and the possibility of including restrictions such as output filter resonance elimination algorithms (GUIMARAES, 2019).

Due to technical restrictions on the classical control strategies, new control techniques such as the model predictive control has been gaining ground in research and applications, especially in industrial and energy sectors (GUIMARAES, 2019). The present study will employ the FCS-MPC control technique at the primary control level of the grid-forming converters in order to track a dynamically adjusted voltage reference set by a higher controller.

2.2.2 Grid-feeding power converters

The grid-feeding power converter is designed to provide power to an already energized power grid and depends of an existing reference voltage signal for synchronization (ARAUJO, 2017). Grid-feeding power converters are controlled as current sources, presenting high parallel output impedance. These power converters are suitable to operate in parallel with other grid-feeding power converters in grid-connected mode. Actually, most of the power converters belonging to distributed generation systems nowadays operate in grid-feeding mode, like in photovoltaic or wind power systems (BIALASIEWICZ, 2008).

In this application, the current source should be perfectly synchronized with the AC voltage at the connection point in order to regulate accurately the active and reactive power exchanged with the power grid. As reported by Vazquez et al. (2014) and Gonzatti et al. (2017), in order to control the injected current, solutions based in proportional-integral technique using synchronous reference frame or resonant controllers with stationary reference are commonly applied. Also, more robust control methods such as predictive or hysteresis-based controllers can also be applied (ROCABERT et al., 2012)

Figure 2.3 presents a typical synchronous reference-based control structure for an AC grid-feeding power converter. The synchronous reference system uses two sequential transformations: the Clarke transformation which changes the *abc* three-phase system to an orthogo-

nal stationary reference $\alpha\beta$ system, and the Park transformation, which modifies the $\alpha\beta$ to a synchronous dq reference, where the fundamental components at 60Hz are seen as a DC signal (GUIMARAES, 2019). As these are well known transformations in technical literature they will not be detailed on the present work, but they can be found at the following references: (CLARKE, 1926; MIRANDA; ROLIM; AREDES, 2005; BLAABJERG et al., 2006).

Figure 2.3 – PI-based control structure for a grid-feeding power converter.

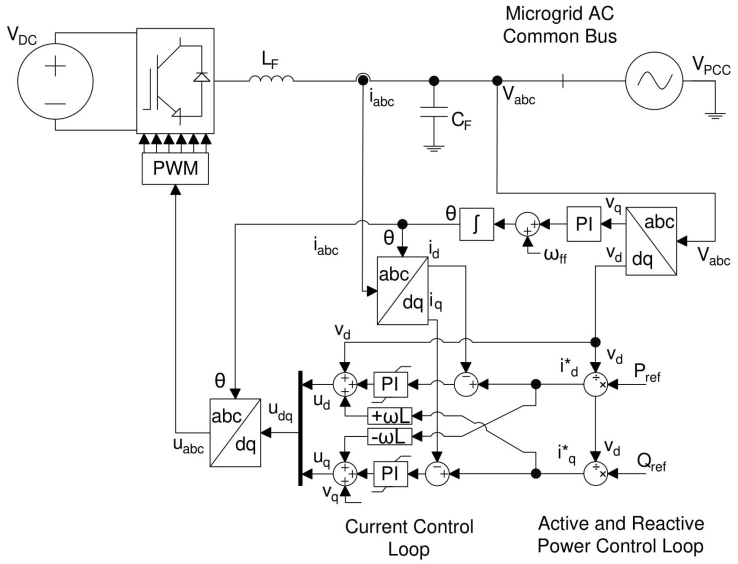

Source: Adapted from: Rocabert et al. (2012)

As stated by Rocabert et al. (2012), the operation of the grid-feeding converters is often regulated by a high-level controller, such as a maximum power point tracking method or a power plant controller, which sets reference values for active and reactive powers, P_{ref} and Q_{ref}, respectively. As can be seen in Figure 2.3, the converter controller receives the power references and the output current i_{abc}, and voltage, v_{abc} measurements. The v_{dq} voltage, obtained after the Park transformation at the outer voltage control loop, enables the achievement of the current reference i^*_{dq} from P_{ref} and Q_{ref}, as it is necessary as part of the inner current control loop. The L_f and C_f represents the LC filter inductor and capacitor, respectively. Also, θ and ω represents the phase angle and the voltage signal frequency (GUIMARAES, 2019).

It is important to outline that the grid-feeding power converters is unable to set an AC reference voltage signal, being dependent of a previously energized grid to properly provide power to the system. Therefore, in order to a grid-feeding converter to operate in an island microgrid it is essential that at least a single grid-forming or grid-supporting power converter, or local synchronous generator, be previously in operation as a voltage reference provider. The present study will apply a change in converters operational mode from grid-forming to grid-

feeding control as a transient process between turning on and off the relative costly power sources. This operation is governed by the adopted economic power dispatch strategy and was developed as an improvement of the economic power sharing strategy presented by Nutkani et al. (2017) to enhance the system performance during short-time low load demand conditions.

2.3 Microgrids hierarchical control

In order to interconnect the different converters into an island microgrid, a coordinated control structure is required in pursuance of grid signal parameters stability, proper power sharing, power quality regulation and economic operation. As stated by Olivares et al. (2014), interconnected power systems usually cover extended geographic areas, making the implementation of a fully centralized microgrid control approach infeasible due to the extensive communication and computational needs. At the same time, a fully decentralized approach is also not possible due to the strong coupling between the operations of various units in the system with multiple control objectives, requiring a minimum level of coordination that cannot be achieved by using only local variables.

According to Peng, Li e Tolbert (2009), power ratings, distribution of loads and generation systems, electrical market prices, generation costs, and energy availability from stochastic primary sources are the main issues to be considered when determining the optimum operation point of a microgrid. This way Rocabert et al. (2012) states that in a microgrid, where different power generation systems based on different technologies and power ratings are interconnected, it is necessary to implement a multiple stage control structure oriented to minimize the operation cost, while maximizing efficiency, reliability, and controllability.

A compromise between fully centralized and fully decentralized control schemes can be achieved by means of the hierarchical control scheme consisted of three control levels: primary, secondary, and tertiary as proposed by Olivares et al. (2014). These control levels differ in their speed of response and the time frame in which they operate, and infrastructure requirements such as communication systems. Therefore, to guarantee a proper regulation of the microgrid operation set point, the hierarchical control can be organized into three main layers with distinct control objective as depicted in Figure 2.4. Some extra ancillary services, many of them implemented locally in the generation units, have been included in Figure 2.4 as well (ROCABERT et al., 2012).

Figure 2.4 – Block diagram of primary, secondary and tertiary microgrid hierarchical control.

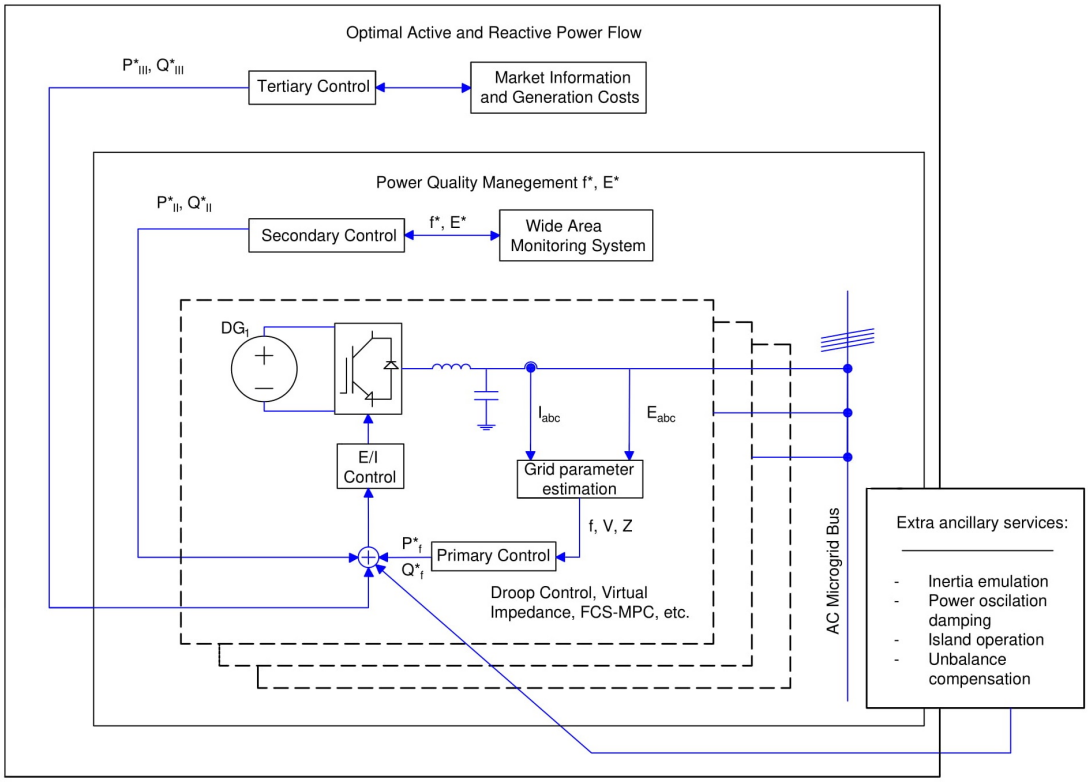

Source: Adapted from: Rocabert et al. (2012)

2.3.1 Primary Control

Primary control, also known as local control or internal control, is the first level in the control hierarchy, featuring the fastest response. This control is based exclusively on local grid parameters measurements and requires no secondary communication systems. Given their speed requirements and reliance on local measurements, islanding detection, distributed generators output grid parameters control and power sharing control are all included in this category (KARIMI; NIKKHAJOEI; IRAVANI, 2008; KATIRAEI; IRAVANI; LEHN, 2004).

In synchronous generators, output control and power sharing is performed by the voltage regulator governor and the inertia of the machine itself. Grid-forming converters operating as voltage sources are used as interface for DC sources, or as part of back-to-back converters, requiring a specially designed control to simulate the inertial characteristic of synchronous generators and provide appropriate frequency regulation. For this purpose, grid-forming primary level converter controllers are composed of two stages: a distributed generation power sharing controller and an inverter output controller (OLIVARES et al., 2014).

Power sharing controllers are responsible for the adequate share of active and reactive power mismatches within the microgrid, whereas inverter output controllers should control and regulate the output voltages and currents. Inverter output control typically consists of an outer loop for voltage control and an inner loop for current regulation (BLAABJERG et al., 2006). Power sharing at this lower hierchical control stage can be performed without the need for communication by using grid local parameters emulating the droop characteristics of a synchronous generators to set instantaneously all microgrid distributed generators operating point.

2.3.2 Secondary Control

The secondary control works as a centralized automatic generation controller and compensates the steady-state errors in microgrid voltage and frequency, restoring their values to nominal defined references. In addition, the secondary control is responsible for controlling the voltage profile along the AC buses in order to keep it within its operational limits at any point of the microgrid structure. This control level makes use of communications and wide-area monitoring systems to coordinate the action of all the generation units within a given area, being its time response in the range of minutes, thus having a slow dynamic if compared with the primary control (ROCABERT et al., 2012).

2.3.3 Tertiary Control

Tertiary control is the highest level of control and is responsible for optimizing the long term microgrid operation and setting its interaction with the distribution network by controlling the active and reactive power dispatch references for each distributed generation unit. This optimization is usually based on economic criteria, which considers the relationship between the demand and the energy supply balance, together with the marginal generation cost of each distributed generation unit (ROCABERT et al., 2012). The estimation of the short-term load changes, the generation forecast, and energy storage capability, as well as the specific demands set by the transmission and/or distribution system operators and the prize signals provided by the electrical market are taken into account in the microgrid operation analysis (NUTKANI et al., 2017).

This work will focus in aspects related to the primary and tertiary hierarchical control levels. The covered aspects of primary hierarchical control layer are related to an island microgrid power sharing management and controlling grid voltage signal parameters as grid references set

signals. In order to incorporate economic operation to the microgrid primary control, some aspects of the tertiary layer will also be considered. An adaptation for low-voltage microgrids distributed generators droop-based control sequencing with regards to individual unit operational costs of the economic power management strategy developed by Nutkani et al. (2017) will be proposed.

2.4 Power sharing control strategies for islanded operation of AC microgrids

With regard to the architecture of primary control, two very distinctive opposite approaches can be identified: centralized and decentralized. A fully centralized control relies on the data gathered in a dedicated central controller that performs the required calculations and determines the control actions for all the generation units at a single point, requiring extensive communication between the central controller and controlled units. On the other hand, in a fully decentralized control each unit is controlled by its local controller, which only receives local information and is neither fully aware of system-wide variables nor other controllers actions (HAN et al., 2016).

As listed by Han et al. (2016), power sharing control strategies of distributed generation units based on communication include concentrated control, master/slave control, and distributed control. Alternatively, the control strategies without communication are generally based on the droop concept, which include four main categories: conventional and variants of the droop control, virtual framework structure-based method, “construct and compensate” based methods and the hybrid droop/signal injection method (HAN et al., 2016).

2.4.1 Communication-based control techniques

Communication-based control techniques can achieve excellent voltage regulation and proper power sharing. Moreover, the output voltage amplitude and frequency are generally close to their ratings without using a secondary control (VANDOORN; MEERSMAN, 2013). However, these control strategies, which require communication lines between the modules, result in increased cost of the system. Long distance communication lines will be easier to get interfered, thus reducing system reliability and expandability (ARAUJO, 2017). In the following sections, some typical communication-based control strategies are reviewed.

2.4.1.1 Concentrated control strategy

The concentrated or central control method mimics the control architecture of large power systems where all the generation units are operated by a single controller. This method was presented by Shanxu et al. (1999) and Abdelaziz et al. (2014), and the control scheme is illustrated in Figure 2.5.

Figure 2.5 – Control schematic of concentrated control strategy.

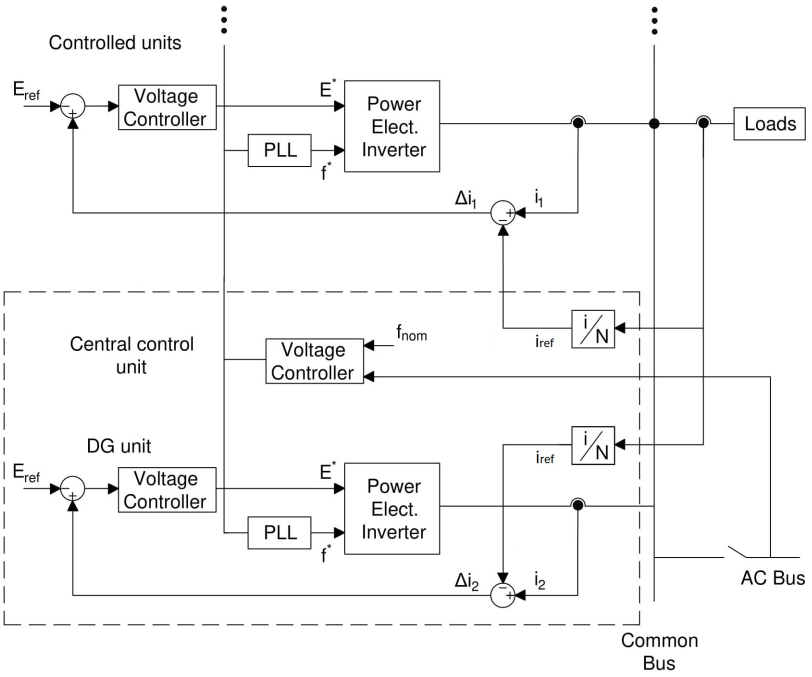

Source: Adapted from: Han et al. (2016)

This control method requires common synchronization signals and current sharing modules. The PLL (*Phase Locked Loop*) circuit of each module can ensure the consistency between the frequency and phase of the output voltage and the synchronization signal. Also, the current sharing modules can detect the total load, which define the reference value of the current for each module. This reference current (i_{ref}) is a fraction of the load current (i_{load}). For N equal modules, $i_{ref} = i_{load}/N$. In the meantime, every inverter unit measures itself output current in order to calculate the current error. In case of parallel units controlled by synchronization signals, they have negligible differences of frequency and phase among each other, thus the current sharing error of each unit can be caused by voltage amplitude inaccuracies. Therefore, this method directly adds current error to each inverter unit as a compensation component of the voltage reference in order to eliminate the differences among their output currents (HAN et al., 2016).

The advantage of the concentrated method is that current sharing is maintained during both steady-state and transients. However, this control scheme must include a centralized controller, which makes difficult to expand the system and reduces system redundancies. Moreover, current reference has to be distributed to all converters by using high-bandwidth communication links, in order to achieve synchronization among the units. These techniques present high dependency on communications and reduce the reliability, which may be compromised with single-point faults (HAN et al., 2016).

2.4.1.2 Master/slave control strategy

For the master/slave control method, the function of parallel control units is built into each inverter. Through the mode-selecting switch or automatic software setting, the initially starting module in parallel acts as master inverter, which is in charge of parallel control, while the others serve as slave-inverters (SIRI; LEE, 1990; CHEN; CHU, 1995; PETRUZZIELLO; ZIOGAS; JOOS, 1990).

According to the master/slave control structure, the master module regulates the output voltage and specifies the current reference of the rest of slave modules. Then, slave units track the current reference provided by the master in order to achieve equal current distribution. Inverters do not need any PLL for synchronization since these units are communicated with the master units. However, the system is not redundant since it presents a single point of failure. If master unit fails, the whole system will fail (HAN et al., 2016).

In order to overcome this drawback, several researchers have improved the master/slave control method. In Petruzziello, Ziogas e Joos (1990), the rotating priority window, providing random selection of the master, is proposed to increase the reliability. An auto master–slave control strategy is proposed in Pei et al. (2004), which is a variant of the master/slave control. The control circuitry contains an active power share bus and a reactive power share communication bus interconnecting all the paralleled units. The inverter with the highest output power becomes the master inverter, which drives the power bus. Also, its power is the reference for the other inverters. The master/slave control in Caldognetto e Tenti (2014) regards the utility interface as master control at the common coupling point with the utility and the energy gateways, allows plug-and-play integration of distributed energy resources and ensures efficient and reliable operation of the microgrid in every operating condition (HAN et al., 2016).

In summary, master/slave control can achieve excellent power sharing performance with advantages of ease implementation. If the master inverter fails, the improved control strategy would switch to another normal inverter which is then used as the new master. Therefore, parallel operation would not be affected. However, an obvious issue with all master/slave control methods is that high-output current overshoot may occur during transients since the master output current is not controlled, so it does not ensure a good transient performance (HAN et al., 2016).

2.4.1.3 Distributed communication-based control

In this control technique, an individual control circuit is used in each inverter, but no central controller is needed. Further, average current sharing requires a current sharing bus and reference synchronization for the voltage. An additional current control loop is used to enforce each converter to track the same average reference current, provided by the current sharing bus. When a defect happen in any module, it can smoothly detach from the microgrid, and the rest of modules can still operate normally in parallel. The average current sharing bus value is regarded as a current reference of each paralleled converter (HAN et al., 2016).

The distinct feature of the distributed control is that the information required is not global but adjacent for any units. So, it only needs lower bandwidth than the centralized control method. In summary, the distributed control has no central control board and every module is symmetric. Voltage regulation and fundamental power sharing are well controlled. However, interconnections between the inverters are still necessary. This degrades the flexibility and redundancy of the system. As the number of parallel modules and distance of the interconnected lines increase, more interference is expected in the system (HAN et al., 2016).

In general, communication-based control techniques have good response in terms of grid parameters control and power sharing management. However, these solutions are conceived for parallel systems, which are close to each other and interconnected through high-bandwidth communication channels.

According to Han et al. (2016), Rocabert et al. (2012) and Olivares et al. (2014), these communication-based solutions are not the most suitable choice for controlling wide area microgrids, since distributed generators and loads these systems may be physically separated by several kilometers. To overcome this problem, droop control algorithms are used for power sharing coordination in microgrids without using communication channels, thereby eliminating

the limits imposed by the physical location and improving the microgrid performance (ROCABERT et al., 2012).

2.4.2 Droop characteristic-based control techniques

In order to achieve a fully decentralized control for an island AC microgrid without the necessity of high bandwidth communication systems, the participating converters must rely only on grid parameters measured locally at its own connection point. According to Han et al. (2016), operation without communication links is often essential to connect remote inverters. It can avoid complexity and high costs, and improve redundancy and reliability requirements of a supervisory system. Also, such a system is easier to expand because of the plug-and-play feature of the modules which allows replacing one unit without stopping the whole system.

In this context, Chandorkar, Divan e Adapa (1993) firstly proposed the droop control strategy for sharing power among multiple generator units, where the active and reactive powers delivered by each converters have a direct relation with the grid frequency and voltage amplitude, respectively. Originally developed for controlling parallel-connected inverters in AC UPS systems, the concept of droop has been borrowed from conventional power system, where it has been used for controlling synchronous generators in high voltage power lines with predominantly inductive behavior. For microgrids, the droop concept has been used in the primary layer of a control hierarchical architecture (OLIVARES et al., 2014). The main purpose of this control technique is to share power proportionally among multiple distributed generators or UPS systems in an autonomous and scattered manner.

As presented by Han et al. (2016), the control algorithm with conventional droop control is illustrated in Figure 2.6, where v_f and i_0 represents the converter output voltage and current, respectively. The k_p and k_q are the active and reactive droop curves coefficients and will be further detailed in this work. The power stage consists of a grid-forming converters with a LC filter and a coupling line inductor. The control algorithm is divided into three stages:

1) The grid voltage, frequency and delivered current are measured at the converter output and used for active and reactive power calculation;

2) A power sharing controller is used to generate the magnitude and frequency of the converter output voltage of the inverter according to the droop characteristic;

3) The new voltage reference is then used to coordinate the switching states of the converter, usually with a PWM (*Pulse Width Modulation*) controller;

Figure 2.6 – Control structure of conventional *P-f/Q-V* droop control

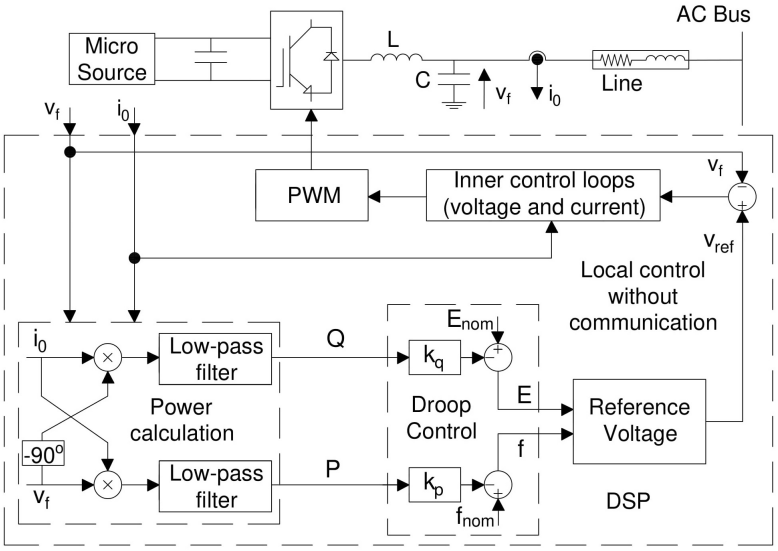

Source: Adapted from: Han et al. (2016)

Droop principle is used to set the new voltage amplitude and frequency, so, it is fundamental to control the droop parameters properly in order to achieve the desired levels of active and reactive power shared within the island microgrid.

Figure 2.7 – Equivalent schematic of two parallel grid-forming converters connected to a common AC microgrid busbar through complex impedances.

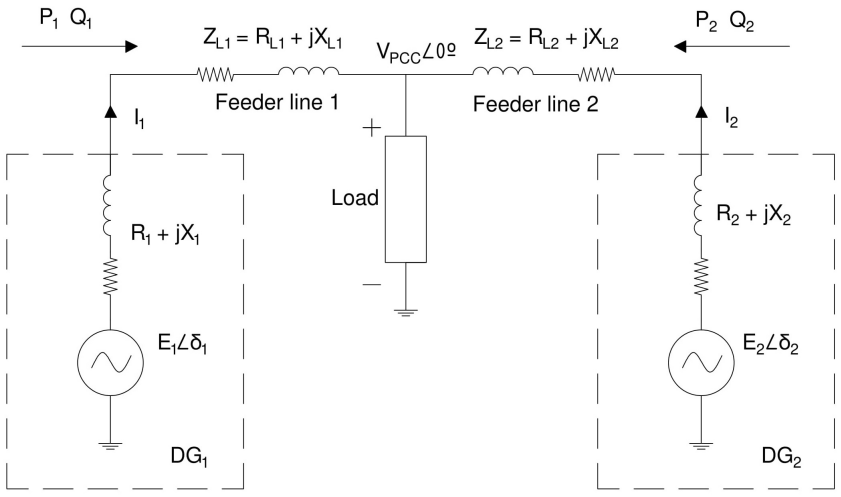

Source: Adapted from: Han et al. (2017)

As presented by Dragičević (2018), a single line diagram representing two grid-forming converters (DG_1 and DG_2) acting as ideal voltage sources connected to a common AC bus

through generic impedance power lines $Z_{Li} = R_{Li} + jX_{Li}$ is shown in Figure 2.7. In this figure, R_1, R_2, X_1 and X_2 are the converters 1 and 2 internal filter resistive and reactive impedances, respectively. Each converter is able to set a voltage amplitude E_i and power angle δ_i relative to the common busbar voltage, V_{PCC}. This results in an amount of active P_i and reactive Q_i powers being dispatched by each converter to supply the local load demand. According to the aforementioned author, the equivalent diagram is also applicable for situations with more parallel grid-forming units. In order to design the control strategy for them, the principle of active and reactive power exchange between one voltage source and a common AC bus needs to be understood first.

Considering the grid-forming converters as an ideal controllable voltage source, the power exchange is defined by the voltage amplitude and phase angle between the converters output and the common bus voltage signal. It is also influenced by the line impedances Z_L connecting the voltage sources to the microgrid PCC. Equations 2.1 and 2.2 demonstrated by Brabandere et al. (2007) describes those relationships.

$$P_i = \frac{E_i \cdot [(R_i + R_{Li}) \cdot (E_i - V_{PCC} cos\delta_i) + (X_i + X_{Li}) \cdot V_{PCC} sen\delta_i]}{(R_i + R_{Li})^2 + (X_i + X_{Li})^2} \tag{2.1}$$

$$Q_i = \frac{E_i \cdot [-(R_i + R_{Li}) \cdot V_{PCC} sin\delta_i + (X_i + X_{Li}) \cdot (E_i - V_{PCC} cos\delta_i)]}{(R_i + R_{Li})^2 + (X_i + X_{Li})^2} \tag{2.2}$$

where P_i and Q_i are the active and reactive powers, respectively, flowing from the voltage source i. E_i and V_{PCC} are the voltage values of converter i output and microgrid common busbar signal, and δ_i corresponds to the phase angle difference between these two voltage signals. The resistive and inductive parts of the complex line impedance are represented by R_{Li} and X_{Li}, respectively. Similarly, the internal impedance of each converter, mostly originated from passive filtering, are represented by R_i and X_i for resistive and reactive parts, respectively.

It can be seen from Equations 2.1 and 2.2 that the active power P_i and reactive power Q_i power exchange between the voltage source and the microgrid depends on both E_i and δ_i, and hence they cannot be controlled independently by each of those variables. However, some assumptions about the nature of grid impedance behavior can be made in order to decouple the active and reactive power shared by the local power sources.

2.4.2.1 Inductive grid condition

The grid impedance nature have a major importance in power sharing capacity and accuracy amid the geographically spread distributed generators and the microgrid common bus. In general, the circuit impedance can be classified into five categories: purely resistive, purely inductive, purely capacitive, resistive-inductive or resistive-capacitive. The grid impedance nature depends on the presence of transformers between different voltage buses and the resistance of electrical cables. It may also vary according to the loads conditions, and consequently the voltage and current phase-angle causing shifts in the grid impedance nature over time. Therefore, the system impedance characteristic affects the droop control and, consequently, the adopted power sharing strategy.

In order to evaluate the microgrid impedance condition, the Thevenin equivalent circuit theorem R_{eq}/X_{eq} ratio can be applied, Figure 2.8, where the influence of circuit mixed resistances and reactances can be analyzed. Usually, the inductive component of line impedances in high-voltage and medium-voltage networks is typically greater than the resistive one (ROCABERT et al., 2012). As stated by Rocabert et al. (2012), Young e Bastias (2018) and Han et al. (2016), to achieve active and reactive power decoupling in ways that these parameters can be associated with grid frequency and voltage amplitude, respectively, the Thevenin equivalent circuit must be purely inductive.

Figure 2.8 – Thevenin equivalent circuit.

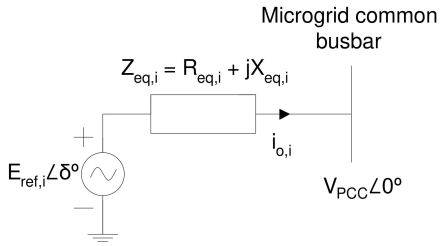

Source: Adapted from: Guerrero et al. (2005)

In Figure 2.8, $E_{ref,i}$ and δ^o represents the output voltage amplitude and phase angle of a controllable ideal voltage source. $R_{eq,i}$ and $X_{eq,i}$ represents the equivalent resistance and reactance components of the feeder impedance, respectively. The $Z_{eq,i}$=$R_{eq,i}$+$jX_{eq,i}$ equation represents the circuit complex impedance from the distributed generator i perspective to the microgrid point of common coupling. Lastly, $i_{o,i}$ and V_{PCC} indicates the voltage source output current and microgrid common busbar voltage, respectively.

The Equation 2.3 can be used to calculate the impedance ratio that indicates the grid condition. According to Rocabert et al. (2012) values over one, $R_{eq,i} \gg X_{eq,i}$, indicates a mainly resistive system while values closer or inferior to one, $R_{eq,i} \ll X_{eq,i}$, indicates a mainly inductive system behavior.

$$\frac{R_{eq,i}}{X_{eq,i}} \tag{2.3}$$

With the assumption of predominantly inductive lines $Z_{Li} \approx jX_{Li}$, and considering phase angles δ_i to be small, a simplification for Equations 2.1 and 2.2 was presented by Laaksonen, Saari e Komulainen (2005) resulting in Equations 2.4 and 2.5. For low δ_i values, it has been assumed that $sin\delta_i = \delta_i$ and $cos\delta_i = 1$.

$$P_i = \frac{E_i \cdot V_{PCC} \cdot \delta_i}{(X_i + X_{Li})} \tag{2.4}$$

$$Q_i = \frac{E_i \cdot (E_i - V_{PCC})}{(X_i + X_{Li})} \tag{2.5}$$

It is noticeable that the active power flow P_i provided by converter i is proportional to the phase angle δ_i. On the other hand, the reactive power Q_i is related with the voltage amplitude difference between the converter output and the common busbar voltage, $E_i - V_{PCC}$. Thereby, with the predominantly inductive grid assumption and for small power angles, δ_i, the active and reactive power dispatched by a voltage source converter are decoupled from one another, allowing both powers to be related independently with grid local parameters. Figure 2.9 illustrates the purely inductive grid condition current vectors behavior, were $\Delta\delta$ represents the phase angle difference between the voltage sources 1 and 2, and I_P and I_Q represents the shared active and reactive current vectors, respectively.

As a result of the power decoupling, the droop control strategy can set new grid references that are perceived by all distributed generators connected to the microgrid according to the instantaneous load demand. Suitable references for the frequency $f_{ref,i}$ and amplitude of the output voltage vector $E_{ref,i}$ at each grid-forming unit are calculated using droop characteristic curves.

Figure 2.10 presents the droop characteristic curves, which are obtained from Equations 2.6 and 2.7 (YOUNG; BASTIAS, 2018).

Figure 2.9 – Parallel operation of two ideal voltage sources under inductive output impedance: a) equivalent circuit and b) circulating current vectors.

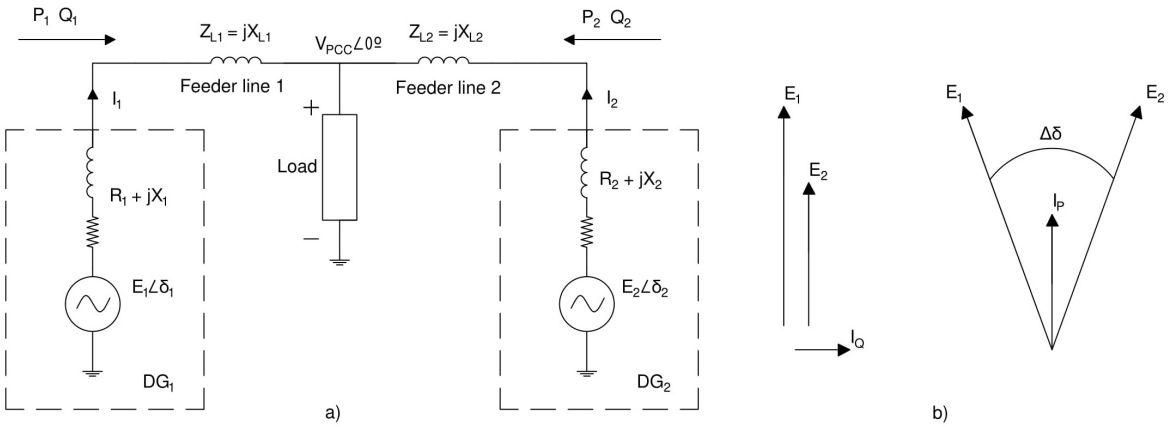

Source: Adapted from: Guerrero et al. (2005)

$$f_{ref,i} = f_{nom} - k_{p,i} \cdot P_{cal,i} \tag{2.6}$$

$$E_{ref,i} = E_{nom} - k_{q,i} \cdot Q_{cal,i} \tag{2.7}$$

Figure 2.10 – Dominant inductive behavior system frequency and voltage droop characteristics.

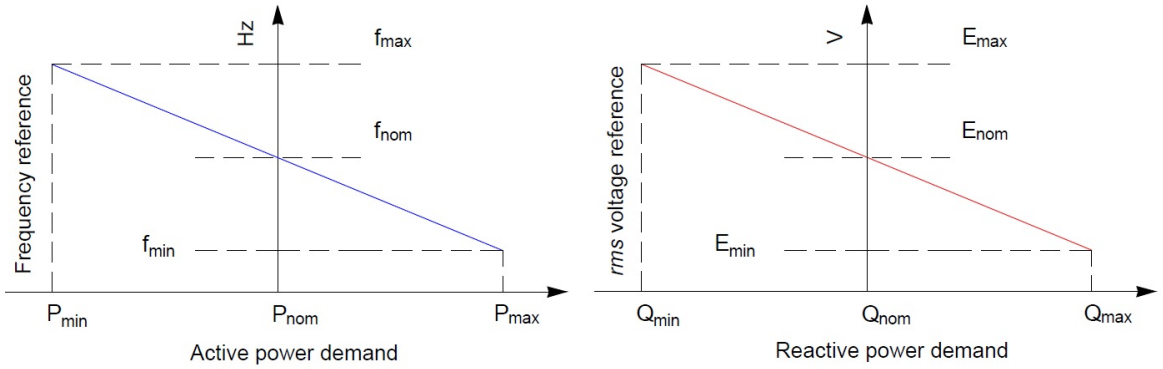

Source: Adapted from: Rocabert et al. (2012)

The f_{nom} and E_{nom} variables represent nominal reference values for microgrid frequency, usually 50Hz or 60Hz, and for *rms* nominal voltage. Although the main electric power system has strict rules for its nominal parameters, small variations are allowed within certain limits without largely compromising power quality. The droop control strategy explores the allowed variations around the nominal values in an island microgrid in order to eliminate the necessity of secondary high-bandwidth communications between distributed generators for fast-time primary control parameters.

At Equations 2.6 and 2.7, $P_{cal,i}$ and $Q_{cal,i}$ are the active and reactive power delivered by the distributed generator i and $k_{p,i}$ and $k_{q,i}$ are the droop coefficients which mimics the effects of a synchronous generator in a predominantly inductive system under load demand variations. These coefficients are calculated as presented by Young e Bastias (2018) in Equations 2.8 and 2.9, where f_{nom}, E_{nom}, f_{min} and E_{min} are the nominal and minimum frequency and voltage amplitude set references for the microgrid and $P_{nom,i}$, $Q_{nom,i}$, $P_{max,i}$ and $Q_{max,i}$ represents the nominal and maximum active and reactive rated power of each distributed generator i unity.

$$k_{p,i} = \frac{f_{nom} - f_{min}}{P_{nom,i} - P_{max,i}} \tag{2.8}$$

$$k_{q,i} = \frac{E_{nom} - E_{min}}{Q_{nom,i} - Q_{max,i}} \tag{2.9}$$

It is important to notice that the droop frequency reference $f_{ref,i}$ is a common variable for the entire microgrid, serving as an indicator for the phase angle δ_i to be set by each converter for proportional active power sharing. In an opposite way, the delivered reactive power depends mostly on the voltage amplitude difference between the converter output and the microgrid common bus. The block diagrams that represents the droop control implementation at the primary controller level are shown in Figure 2.11. The output voltage amplitude, frequency and phase angle are then used to obtain a voltage reference signal that will drive the switching states of the inverter semiconductor devices, either by a PWM controller or by other conversion techniques.

Figure 2.11 – Droop control method block diagram for a) *P-f* and b) *Q-E* implementation.

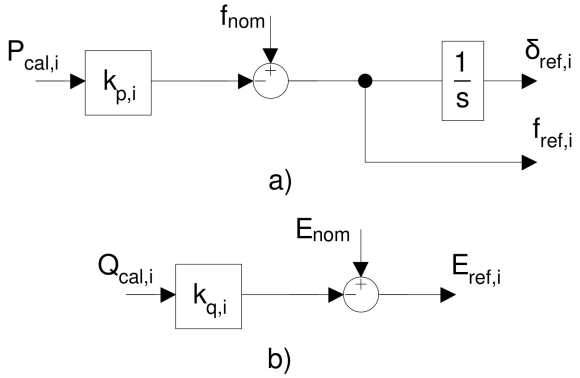

Reference: Adapted from: Young e Bastias (2018)

As the voltage reference parameter would be perceived by all distributed generators at its own connection point, the conventional droop method can be implemented without commu-

nication for proportional power sharing among the local power sources. Therefore, this control strategy presents to be more reliable in comparison to those control strategies based on parallel communication systems (HAN et al., 2017). However, as presented by Han et al. (2016) it has some major drawbacks that needs also to be considered. The main difficulties about implementing the conventional droop technique in an island microgrid as stated by the above mentioned author are:

a) **Mixed resistive and inductive line impedance:** the conventional droop method was developed assuming highly inductive equivalent impedance between the voltage source converters and the common AC busbar. However, this assumption is challenged in microgrid applications since low-voltage distribution lines are typically mainly resistive. Therefore, Equation 2.4 cannot have its validity assured for resistive microgrids (HE; LI, 2012; LI; KAO, 2009). Furthermore, if the line impedance is mixed resistive and inductive, then the active and reactive power will be strongly coupled. According to Rocabert et al. (2012), this case is important in medium-voltage microgrids, in which the power lines R_{eq}/X_{eq} ratio can be close to one;

b) **Multiple control objectives:** since there is only one control variable for each droop characteristic, it is not possible to satisfy multiple control objectives (HE; LI, 2012). Therefore, for power quality management, energy market oscillations, island detection and re-synchronization, and other control information that must be shared among the distributed generator within secondary and tertiary control levels must be necessarily implemented with dedicated communication channels;

c) **Voltage amplitude is not a microgrid global variable:** opposed to frequency, voltage signal amplitude does not have the same value at each converter connection point due grid impedance loses. Thus, the reactive power control is more complex to be shared among parallel units and may result in circulating reactive current. Same problem may occur in highly resistive lines, especially for active current controlled through the voltage (HE; LI, 2012; LI; KAO, 2009);

d) **Nonlinear loads:** in case of nonlinear loads, the conventional droop method is based only on fundamental values and does not consider harmonic current or voltage. Since it only uses P and Q measurements, which are usually average over one line cycle, the

conventional droop method should be modified in order to share harmonic currents (TULADHAR et al., 1997; TULADHAR et al., 2000).

In order to attenuate some of these droop control strategy drawbacks, some assumptions and measures can be taken and will be further discussed.

2.4.2.2 Resistive grid condition

According to Rocabert et al. (2012), the traditional droop scheme is more applicable to predominantly inductive networks, which is a more common condition to high-voltage power lines where resistive impedance can be disregarded. However, as stated by Olivares et al. (2014), the autonomous microgrid is more likely to be developed at the distribution level with low-voltage lines where resistive effects are more significant, due to loads, distributed generation and end user proximity. For low-voltage microgrids with resistive biased lines, active and reactive power coupling issues may occur, which requires the addition of decoupling methods (TULADHAR et al., 1997).

According to Nutkani et al. (2017), Rocabert et al. (2012) and Han et al. (2017), a simple method to decouple the active and reactive power in low-voltage lines is to ensure a purely resistive system, where the lines inductive impedance values can be neglected. As presented by Han et al. (2016) and Dragičević (2018), considering the low power angle approximation and disregarding the effects of the grid inductance, $Z_{Li} \approx R_{Li}$, the Equations 2.1 and 2.2 can be rearranged as:

$$P_i = \frac{E_i \cdot (E_i - V_{PCC})}{(R_i + R_{Li})} \tag{2.10}$$

$$Q_i = \frac{-E_i \cdot V_{PCC} \cdot \delta_i}{(R_i + R_{Li})} \tag{2.11}$$

For the resistive system, the active power P_i delivered by an ideal voltage source is proportional to the amplitude difference between the converter output and the common bus voltage $(E_i - V_{PCC})$, and the reactive power Q_i, in turn, is related to the phase angle δ_i difference between these voltage signals. As presented by Rocabert et al. (2012), the droop *P-E/Q-f* relations are slightly different for a predominantly resistive system once the converter output active power increases as the grid voltage amplitude decrease, and the delivered reactive power increases together with the grid frequency. The resistive droop control behavior can be seen in Figure 2.12

Figure 2.12 – Dominant resistive behavior system voltage and frequency droop characteristics.

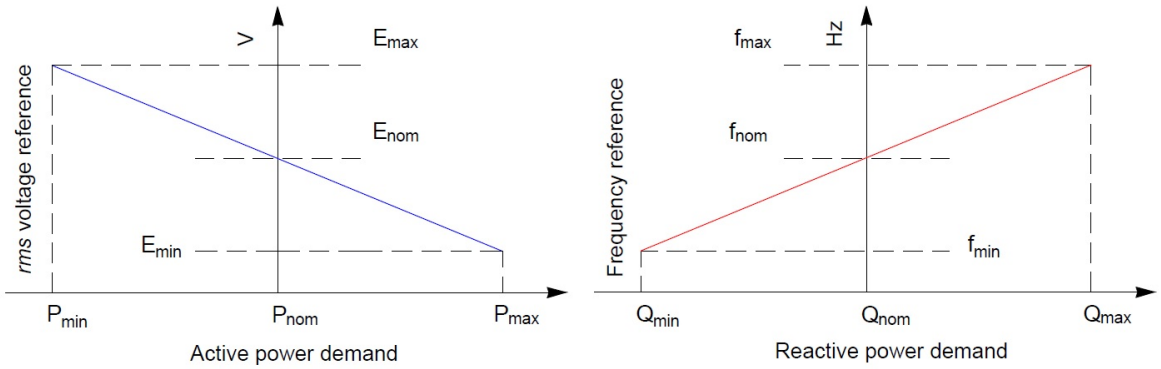

Reference: Adapted from: Rocabert et al. (2012)

Figure 2.13 illustrates the current vectors under a mainly resistive system. Equations 2.12 and 2.13 presents the droop voltage amplitude and frequency references determination for a predominantly resistive circuit (ROCABERT et al., 2012; DRAGIčEVIć, 2018).

Figure 2.13 – Parallel operation of two ideal voltage source under resistive output impedance: a) equivalent circuit and b) circulating current vectors.

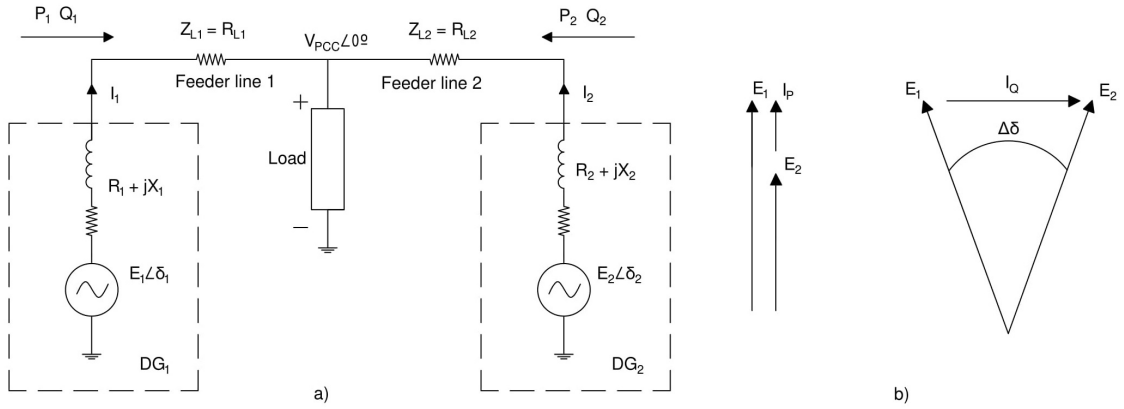

Reference: Adapted from: Guerrero et al. (2005)

$$E_{ref,i} = E_{nom} - k_{p,i} \cdot P_{cal,i} \tag{2.12}$$

$$f_{ref,i} = f_{nom} + k_{q,i} \cdot Q_{cal,i} \tag{2.13}$$

According to Dragičević (2018), the droop control coefficients for mainly resistive power systems are calculated as presented in Equations 2.14 and 2.15.

$$k_{p,i} = \frac{E_{nom} - E_{min}}{P_{nom,i} - P_{max,i}} \tag{2.14}$$

$$k_{q,i} = \frac{f_{nom} - f_{min}}{Q_{nom,i} - Q_{max,i}} \tag{2.15}$$

The block diagram that illustrates the resistive droop concept implementation at the converter primary controller is shown in Figure 2.14.

Figure 2.14 – Droop control method block diagram for a) *P-E* and b) *Q-f* implementation.

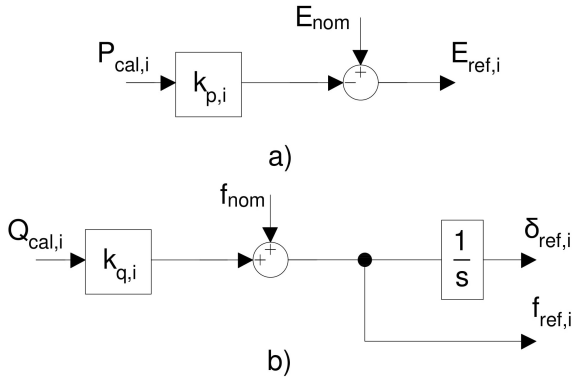

Reference: Adapted from: Young e Bastias (2018)

As stated by Han et al. (2016), the assumption of a purely resistive grid allows the decoupling of active and reactive powers shared between the distributed generators. This fact also aligns with a microgrid implementation at the distribution level network, allowing proper power sharing without the use of a parallel communication system for fast-time signal references control. However, for any kind of grid impedance condition, the droop control technique is only valid among grid-forming or voltage controlled grid-supporting converters, once these units are able to control its own output voltage. This fact allows each grid-forming converter to control its own power dispatch according to the predefined droop curves by adjusting its output voltage signal parameters.

2.5 Economic dispatch scheme

As the microgrid concept involves several distributed generation units which probably will be based on different power source technologies, the hierarchical control must be able to coordinate and optimize the whole system during island operation, especially in terms of voltage regulation and economic power sharing. As stated by Nutkani et al. (2017), the decentralized economic operation schemes have several advantages when compared with the traditional centralized management system for a microgrid. Specifically, according to the above mentioned author the decentralized schemes are more flexible, less computationally intensive, and easier

to implement without relying on communication infrastructure. The purpose of a decentralized strategy is to improve economic operation of the island microgrid using hierarchical control for coordination as a substitute of a traditional centralized controller system.

The traditional droop concept presented by Chandorkar, Divan e Adapa (1993) was developed as a power sharing strategy between close parallel UPS systems. In this system all units shared power proportionally based on their respective power ratings and according to the same droop curve for the whole grid as shown in Figure 2.15. The active power droop curves for the all distributed generator are overwritten, and hence this causes all units to dispatch simultaneously and produce power proportionally to their respective maximum power capacity. Therefore, the microgrid frequency is set to vary from f_{max} to f_{min} when its load demand changes from 0% to 100%, respectively.

To guarantee the microgrid frequency and voltage magnitude operation within acceptable levels, power quality standards must be considered. According to Mumtaz et al. (2016), the IEEE (2009) standard guarantees proper active and reactive power sharing among all distributed generation units in relation to their maximum ratings. Nevertheless, according to Vergara et al. (2019a) this definition disregards any economic information.

Figure 2.15 – Traditional droop control method for distributed generators power dispatch.

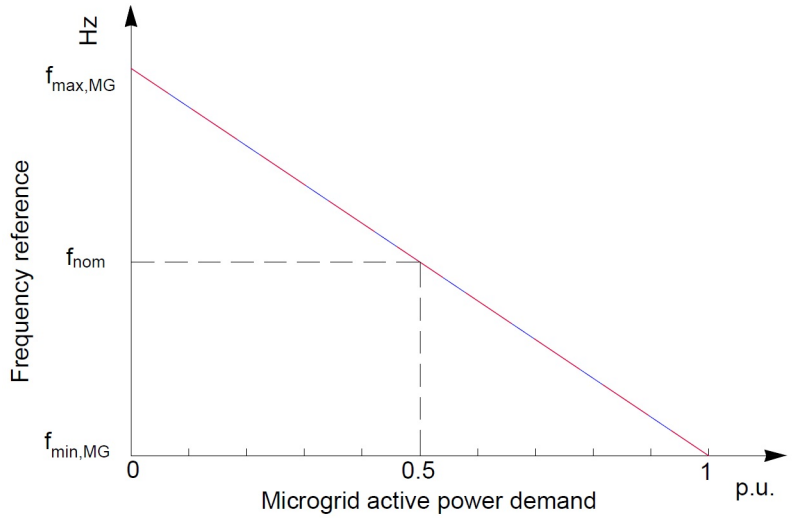

Source: Adapted from: Nutkani et al. (2017)

In order to achieve decentralized economic dispatch within an island microgrid, some variations of the traditional droop control have been proposed. According to Nutkani et al. (2017), economic operation of existing decentralized schemes is usually achieved either by: a) tuning the droop characteristics of distributed generators or, b), prioritizing their dispatch order.

In a preliminary study developed by Nutkani, Loh e Blaabjerg (2013), the dynamic tuning of converters droop characteristics has been proposed to force the less costly units to produce more power, and vice versa. However, it required all droop-controlled distributed generators to operate continuously even at very low-load conditions, during which some units should, ideally, be turned off. The dynamic tuning is, therefore, more suitable for microgrids with high-base loads where all power sources must always operate (NUTKANI et al., 2017). In works like by Vergara et al. (2019b) and Lin et al. (2019), sophisticated algorithms have been developed in order to modify the droop control gains by changing the droop slope inclination, which also considers the economic operation aspects of the microgrid.

Contrary to the traditional/conventional droop power sharing idea, several modified droop schemes have also been proposed using droop principle for power sharing based on distributed generators characteristics such as cost related to energy resource and unit operation. To resolve the load-independent shortcoming of the droop dynamic tuning strategy, a dispatch prioritized scheme has been proposed by Nutkani et al. (2015), where dispatch priorities of distributed generators are defined based on each unity no-load generation costs. In other words, power sources with lower no-load generation costs are given higher dispatch priorities, being the first to enter in operation as the load demand of the island microgrid increases. The dispatch prioritized scheme turns off the costlier generators autonomously during light load, and turns them on only when the microgrid load demand increases significantly.

However, this scheme may not be suitable when some distributed generators have the same no-load generation costs, once this method was thought to assign the same dispatch frequency and overlap droop characteristics to those power sources with the same no-load costs. This may cause an undesirable situation when two or more power sources entering in operation at the same time, regardless of the microgrid load demand conditions. Also, as this scheme relies only on the units no-load costs, the economic operation optimization is limited to a single point, not considering the cost variation as function of the generator output power level. In addition, the scheme proposed by Nutkani et al. (2015) does not allow setting of power dispatch reserves withing the distributed generators power capacity to support sudden microgrid load variations.

To address these concerns, an alternative economic dispatch scheme was proposed by Nutkani et al. (2017) in their latter work. The proposed scheme dispatches the distributed generators in a predefined sequence which prioritizes the participating units after considering multiple

factors, including the number of distributed generators in the microgrid, their power ratings and generation costs, rather than only the no-load generation costs (NUTKANI et al., 2017). This strategy also considers other necessary constraints, such as a minimum online power reserve, ΔP_{online}, within local power sources capacity, and the generator power, voltage, and frequency limits. The key contributions and features of the proposed scheme according to the author can thus be summarized as follows:

a) Distributed generators dispatch priorities and frequencies are determined from multiple factors, including their respective generation costs, power ratings, and number of units participating in the economic operation, which allows the connection or disconnection of participating local power converters autonomously;

b) Desired online power reserves can conveniently be set by microgrid planners for meeting the sudden step-load changes within the island microgrid;

c) Flexible and effective power dispatch strategy even when nondispatchable, or grid-feeding, local distributed generators are included;

d) Simple realization method with all features of the traditional droop scheme retained.

The first step to implement the decentralized economic dispatch strategy proposed by Nutkani et al. (2017) is to obtain a mathematical model of the specific cost curves of each participating power sources, and its relation with the unit active power dispatch. Some distributed generator cost functions based on different technologies are presented next.

2.5.1 Distributed generators operational costs mathematical modeling

Generally, the power source instantaneous operational cost, $C_i(P_i)$, may include maintenance, M_i, fuel, F_i, and emission penalty or incentive, ε_i, costs that can be related to active power production, as expressed in Equation 2.16. Other costs related to distributed generators operation such as feeder losses, equipment overhauling and replacement, and other features can also be included in Equation 2.16 without affecting the subsequently presented scheme.

$$C_i(P_i) = M_i(P_i) + F_i(P_i) + \varepsilon_i(P_i) \tag{2.16}$$

In general, as mentioned by Nutkani et al. (2017), the distributed generator cost factors presented in Equation 2.16 varies with the power source nature, its rated capacity, and instantaneous active power dispatch, P_i.

The economic dispatch strategy proposed by Nutkani et al. (2017) does not relies on a specific cost function model, as it allows the use of generic cost function models for the considered distributed generators. This fact increase versatility to the economic dispatch strategy, allowing its application to a vast range of unique situations where an island microgrid can be planned. According to Nutkani et al. (2017), the proposed scheme does not depend on the specific cost function model presented in Equation 2.16 as it works equally well with other preferred cost functions.

In order to illustrate the considered economic power dispatch capacity in dealing with generic cost function models, two distinct power resources distributed generators operational cost mathematical models are presented next.

2.5.1.1 Combustion engine-based operational cost function mathematical model

As stated by Nutkani et al. (2017), for combustion engine-based power sources such as diesel generators and microturbines, their variable maintenance costs can be represented by a linear function of active power. Also, their fuel and emission costs can also be represented by the quadratic function given in Equation 2.17, as demonstrated in Hetzer, Yu e Bhattarai (2008) and Nutkani, Loh e Blaabjerg (2014).

$$C_i(P_i) = M_i \cdot P_i + F_i \cdot (a_i + b_i P_i + c_i P_i^2) + \varepsilon_i \cdot (\alpha_i + \beta_i P_i + \gamma_i P_i^2 + e_i exp(\rho_i P_i)) \tag{2.17}$$

As presented by Hetzer, Yu e Bhattarai (2008), the a_i, b_i, c_i and α_i, β_i, γ_x, e_i and ρ_i are the quadratic constants of the fuel and emission cost functions. These parameters will change according to the type of equipment, age, condition of use and local legislative position.

2.5.1.2 Renewable-based operational cost function mathematical model

According to Nutkani et al. (2017), solar photovoltaic and wind farms are common renewable distributed generators found in microgrids. These power sources follows a stochastic operational behavior and are, by they nature, nondispatchable and usually operates at its ma-

ximum power points. However, these power sources can be converted to dispatchable units by adding energy storage systems to them, such as battery banks. Nevertheless, as stated by Augustine et al. (2012), Alvarez et al. (2009) and Huang et al. (2011), their operating natures are different from one another, which mean their operational costs should be derived differently and might include recurring maintenance costs and emission incentives as negative fees.

Another factor that needs consideration is battery replacement cost if storage is used, or fuel cost, if fuel cell is used as a green source (EL-SHARKH et al., 2006). According to Driesse, Jain e Harrison (2008), converters power losses should also be included, which under low load conditions are comparably high.

As presented by Nutkani et al. (2017), all the aforementioned factors can be approximated by a linear function of the delivered power for each renewable-based distributed generator. The generic cost functions for fuel-based and storage-based renewable power sources are presented in Equations 2.18 and 2.19, respectively. A more detailed analysis over renewable-base power sources cost modeling can be found in the works of Augustine et al. (2012), Huang et al. (2011), and Driesse, Jain e Harrison (2008).

$$C_i(P_i) = (F_i + M_i \pm \varepsilon_i) \cdot (P_i + \nu_i + \mu_i P_i + \sigma_i P_i^2) \tag{2.18}$$

$$C_i(P_i) = (B_i + M_i \pm \varepsilon_i) \cdot (P_i + \nu_i + \mu_i P_i + \sigma_i P_i^2) \tag{2.19}$$

where M_i, F_i, B_i, and ε_i are cost conversion factors related to maintenance, fuel, battery replacement, and emission fees or incentives, respectively. The other parameters ν_i, μ_i, and σ_i are power loss factors related to the considered power converter itself (NUTKANI et al., 2017).

2.5.2 Decentralized droop-based economic dispatch strategy for island AC microgrids

The first stage to implement the decentralized power dispatch scheme proposed by Nutkani et al. (2017) is to obtain the normalized generation, or operational, costs curves $C_i'(P_i)$ as function of the normalized instantaneous active power dispatch P_i' for all i distributed generators participating in the economic dispatch scheme. Equation 2.20 demonstrates the operational cost function and power dispatch normalization to per-unit system.

$$C_i'(P_i) = \frac{C_i(P_i)}{P_{max,i}} \; and \; P_i' = \frac{P_i}{P_{max,i}} \tag{2.20}$$

were $P_{max,i}$ is the maximum-rated, or nominal, power that distributed generator i can produce, $(i = 1,2,...,i_{max})$, and P_i represents the unit instantaneous active power generation. The $C_i(P_i)$ parameter represent the operational cost function of the distributed generator obtained from mathematical modeling of the energy source in question. For instance, Equations 2.17, 2.18 and 2.19 demonstrates cost function models applicable in the considered power sharing strategy for nonrenewable and renewable sources, respectively. Figure 2.16 illustrates normalized operational cost curves examples and its relations to the distributed generators active power demand in per-unit system.

Figure 2.16 – Normalized operational cost functions of dispatchable distributed generators.

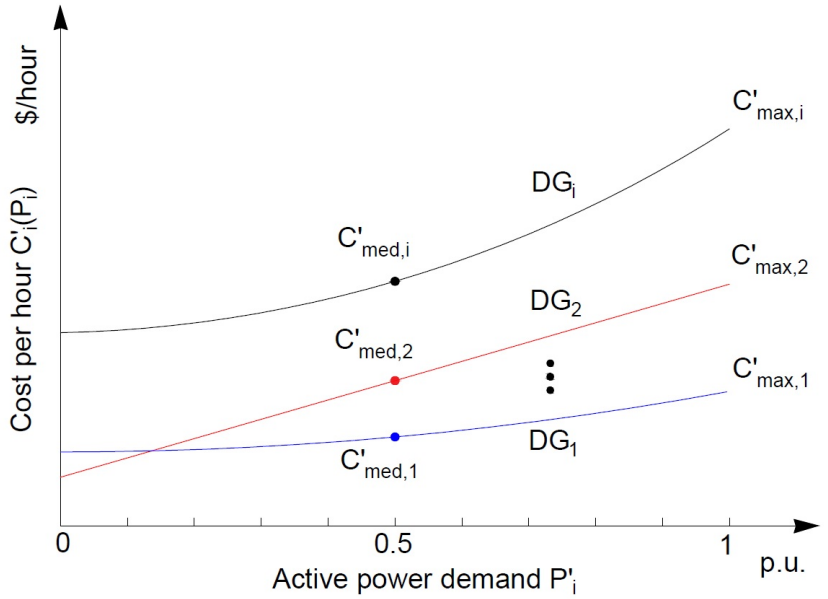

Source: Adapted from: Nutkani et al. (2017)

Therefore, the normalized operational cost curve is used for power sources generation costs comparative analysis of the delivered active power. As normalized per-unit power dispatch is being considered, the operational costs of distinct distributed generators that may be present in a island microgrid system can be compared regardless of constraints such as units power ratings. In the proposed scheme, the average normalized cost $C'_{med,i}$ is embraced for distributed generators coordination, setting ascending higher priorities for local units with relative lower average operational costs in the power dispatch sequencing process.

One benefit of the economic power management strategy proposed by Nutkani et al. (2017) is its capability in considering generic operational cost models, allowing its application for a wide range of distributed generator independently of their primary source nature. Yet, the

effectiveness of microgrid economic optimization is greatly related to the quality and precision of the mathematical modeling process of each power source considered.

The distributed generators no-load operational costs, when $P_i = 0$, can next be subtracted from the respective normalized cost functions, Equation 2.21, as the considered strategy proposes the turning-off of expensive units which are not required to operate given a current status of light load demand condition.

$$C_i''(P_i) = C_i'(P_i) - C_i'(0) \tag{2.21}$$

Instead of just the no-load costs as presented by Nutkani et al. (2015), the proposed economic dispatch scheme considers both cost characteristics and power ratings of the distributed generators, before deciding their dispatch priorities or frequencies at which they should individually be dispatched. Equation 2.22 illustrates the distributed generator dispatch priority N_i determination based on their respective average operational cost C'_{med}.

According to the economic power dispatch strategy proposed by Nutkani et al. (2017), prior to the determination of distributed generators individual droop curve reference frequency range, $f_{max,i}$ and $f_{min,i}$, at which they should individually be dispatched, it is essential to assign dispatch priorities to local generation units which take in consideration inherent economic aspects. Equation 2.22 demonstrate the distributed generator dispatch priority N_i determination process based on the average normalized operational cost C'_{med}.

$$C'_{med,1} < C'_{med,2} < \cdots < C'_{med,i} \rightarrow N_1 = 1,\ N_2 = 2,\ \cdots,\ N_{max} = i \tag{2.22}$$

After the definition of units dispatch priorities, the frequency range at which each distributed generator are set be dispatched can then be determined. According to the droop control logic for inductive grid condition presented in section 2.4.2, as the island microgrid load demand gradually increases, the droop control proportionally reduce the overall system frequency. Each prioritized distributed generator maximum frequency, $f_{max,i,N}$, determine the reference set-point at which each generator starts its operation within the island microgrid. The distribute generators individual maximum operation frequency can be calculated as presented in Equation 2.23.

$$f_{max,i,N} \;=\; max\left\{ \underbrace{f_{max,MG} - \Delta f_{max} \cdot \frac{N_i - 1}{N_{max} - 1}}_{Calculated\ based\ on\ priority\ order},\quad \underbrace{f_{min,i,N-1} + k_{p,i,N-1} \cdot \Delta P_{online}}_{Calculated\ based\ on\ online\ reserve} \right\} \tag{2.23}$$

were N_i indicates the distributed generator i priority and ΔP_{online} is the microgrid selected online power reserve. The $f_{min,i,N-1}$ and $k_{p,i,N-1}$ parameters represents the individual minimum droop frequency and droop curve gradient of the immediately lower priority generator, $N_i - 1$, respectively. Other factors that also must be taken into consideration in Equation 2.23 are the defined microgrid maximum frequency, $f_{max,MG}$, the defined generators maximum dispatch frequency range, Δf_{max}, and the highest-cost generator priority, N_{max}.

The online power reserve, ΔP_{online}, establishes the quantity of nominal active power capacity the close-priority generators must share together in order to damp sudden load variations. As stated by Nutkani et al. (2017), a trade-off occur for high values of ΔP_{online} as it increases the microgrid reliability, yet reducing the economic benefits of the proposed strategy.

According to Nutkani et al. (2017) economic power sharing strategy, the highest value between the one based on the generator priority N_i and the other obtained considering the online power reserve to be maintained must be considered for each generators maximum dispatch frequency definition as demonstrated in Equation 2.23.

Distributed generators minimum droop frequency and their respective droop curve gradients can be obtained as presented in Equations 2.24 and 2.25.

$$f_{min,i,N} = f_{min,MG} + \Delta f_{min} \cdot \frac{max(C''_{i,N}) - C''_{i,N}}{max(C''_{i,N}) - min(C''_{i,N})} \tag{2.24}$$

$$k_{p,i,N} = \frac{f_{max,i,N} - f_{min,i,N}}{P_{max,i,N}} \tag{2.25}$$

where highest mean generation cost among the distributed generators, $max(C''_{i,N})$, is defined as distributed generators maximum average value of the normalized no-load generation cost curves, obtained as: $max(C''_{i,N}) = max(C''_{1,N_1}, C''_{2,N_2}, \cdots, C''_{i,N_i})$. Similarly, the average minimum cost of the no-load normalized curve, $max(C''_{i,N})$, is defined as: $min(C''_{i,N}) = min(C''_{1,N_1}, C''_{2,N_2}, \cdots, C''_{i,N_i})$. Other considered parameters are the microgrid minimum allowed frequency, $f_{min,MG}$, and generators minimum dispatch frequency range Δf_{min}.

The economic dispatch strategy proposed by Nutkani et al. (2017) activate and deactivate the distributed generators autonomously according to the system power demand. When two or more units are required to operate simultaneously, they are set share the demanded active power proportionally according to each unit inherent droop curve. The power management strategy logic is presented in Equation 2.26, where P_i represents the instantaneous active power provided

by generator i and $f_{ref,i,N}$ indicates the immediate converter output voltage signal frequency reference.

$$f_{ref,i,N} = \begin{Bmatrix} f_{max,i,N} - k_{i,N} \cdot P_i & f_{MG} \leq f_{max,i,N} \\ DG\ off, & f_{MG} > f_{max,i,N} \end{Bmatrix} \tag{2.26}$$

The sequence for the decentralized economic dispatch strategy implementation proposed by Nutkani et al. (2017) is described as follows:

1º. Identification of the dispatchable generators that will participate in the economic dispatch scheme;

2º. Determination of the operational cost mathematical models for all participating distributed generators;

3º. Assign distributed generators priorities and dispatch sequence order based on the normalized average operational costs without unit priority repetition, setting higher priorities to less-expensive units. According to Nutkani et al. (2017), no two or more generators should be assigned the same priority. If their average generation costs are equal, their priorities should be set as N_i and N_{i+1};

4º. Determine the microgrid main parameters such as microgrid overall maximum and minimum frequencies, voltage amplitude maximum variation and online power reserve value;

5º. Definition of the maximum operational frequency value for every local dispatchable distributed generator considering the unit dispatch priority and the selected online power reserve by the use of Equation 2.23;

6º. Definition of the distributed generators minimum operational frequency values considering the units average generation cost by the use of Equation 2.24;

7º. Implementation of the generators droop curves for the decentralized droop-based economic dispatch strategy as presented in Equations 2.25 and 2.26 in distributed generators primary control level according to microgrid hierarchical control strategy.

Figure 2.17 illustrates the decentralized droop-based economic dispatch strategy proposed by Nutkani et al. (2017), where the distributed generators are gradually activated from

the lowest operation cost to the most expensive unity according to a decrease in grid frequency caused by an active power demand rise. Other constraints such as voltage and frequency limits, generators power rating and minimum online power reserves are also considered, which are all directly or indirectly responsible for power sources droop gradient tuning. As stated by Nutkani et al. (2017), the grid-forming distributed generators can then be activated and deactivated autonomously without the use of any parallel communication channel other than the islanded power grid parameters itself.

Figure 2.17 – Decentralized economic dispatch strategy *P-f* droop-characteristic control curve for predominantly inductive island microgrids.

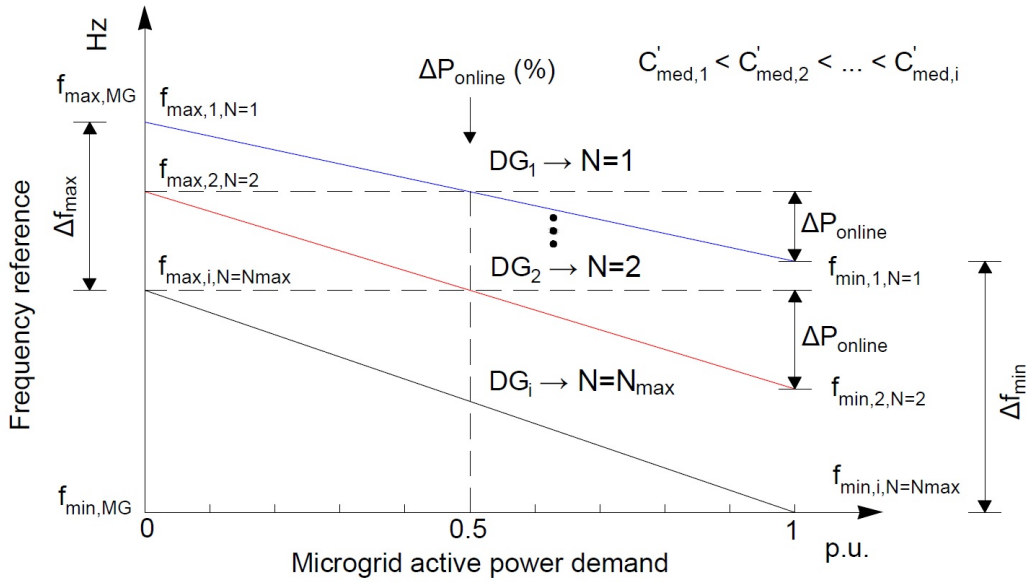

Source: Adapted from: Nutkani et al. (2017)

According to Nutkani et al. (2017), the proposed methodology also can be adapted for economic reactive power sharing and harmonic compensation, however, this capabilities are not considered in the present work. For the reactive power, the scheme proposed by Nutkani et al. (2017) adopt the traditional *Q-V* droop control method, where the reactive power is shared with equal rate among all participating distributed generators.

The decentralized economic dispatch strategy can integrate the tertiary control level of an island microgrid hierarchical control methodology, providing the local distributed generators primary controller with the dispatch priority information, the online power reserve and the maximum and minimum operational frequencies. Therefore, economic and decentralized active power sharing among grid-forming distributed generators can be achieved without the use of parallel communication systems between local power sources and hence, improving system

reliability during island operation. Notwithstanding, for resistive biased systems, such as low-voltage microgrids, Nutkani et al. (2017) stated that Equations 2.23, 2.24, 2.25 and 2.26, can be adapted for *P-V/Q-f* droop control method. The low-voltage adaptation of the described economic power sharing strategy will be further investigated in the present study.

3 METHODOLOGY

The methodology applied for the decentralized economic dispatch strategy implementation for a resistive biased microgrid in island operation is presented in this chapter. The following topics are presented: microgrid topology definition and general aspects; microgrid primary control level with FCS-MPC control technique proposed for economic and conventional droop-based power sharing strategies as converters local control; resistive biased microgrid tertiary control implementation of traditional *P-V/Q-f* droop power dispatch and adapted economic droop-based power sharing strategy; low-voltage island microgrid software simulations for adapted control strategy validation.

3.1 Microgrid general description

The microgrid topology selected to test the adapted economic power sharing strategy is presented in Figure 3.1. The selected system consisted of a single-phase circuit with two distributed generators, DG_1 and DG_2, based on electronic converters for DC-AC transformation. Both converters were set to share local loads variable power demand based on the resistive droop control method, simulating a typical condition for a possible low-voltage distribution level island microgrid.

The designed microgrid composed by two distributed generation units was selected as it was the minimum necessary quantity of parallel power sources to test the adapted power sharing strategy. A third parallel distributed generator was later considered during software simulation to test the expandability of the adapted strategy in this study.

The single-phase system was selected as it have a relative lower complexity for software implementation. According to Guimaraes (2019), the single-phase H-bridge converter can be used for low-power systems and in single-phase microgrids. Additionally, this model can be applied to a three-phase system with individual compensation per phase (GUIMARAES, 2019).

The single-phase microgrid with two parallel converters considered for software simulations is presented in Figure 3.1.

Figure 3.1 – Island microgrid topology.

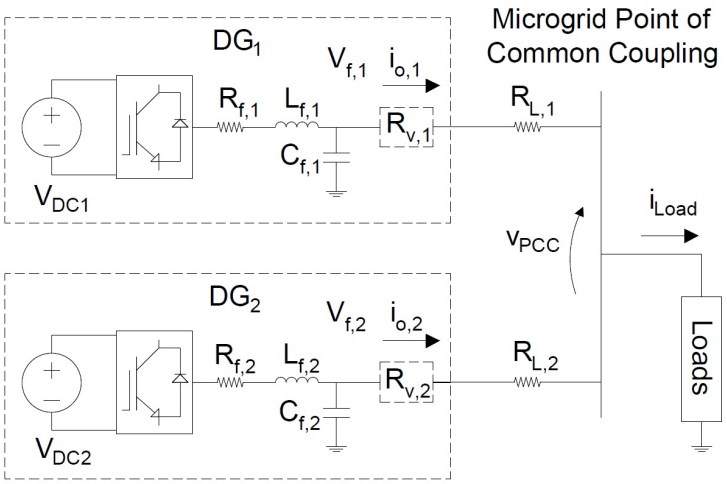

Source: From author (2021)

where DG_1 and DG_2 represents the distributed generators participating on the island microgrid power sharing strategy. V_{DC1} and V_{DC2} indicates the respective converters DC link voltages. $L_{f,1}$, $L_{f,2}$, $C_{f,1}$, $C_{f,2}$, $R_{f,1}$ and $R_{f,2}$ typify the passive elements associated with the output LC filters of each converter. The filters output voltages are represented by $V_{f,1}$ and $V_{f,2}$, while $i_{o,1}$ and $i_{o,2}$ are the filter output currents of each distributed generator. V_{PCC} and i_{Load} indicates the microgrid common busbar voltage and load current, respectively. Finally, $R_{L,1}$ and $R_{L,2}$ represents the feeders resistance, while $R_{V,1}$ and $R_{V,2}$ designates the virtual resistance used to ensure the microgrid resistive behavior and improve power sharing capacity.

As the microgrid is designed to operate in island condition, it is essential to generate locally the grid voltage reference. Thus, the distributed generators are configure to operate as grid-forming converters and control their respective output voltage amplitudes, V_{f1} and V_{f2}, and signal frequencies when sharing power. This references will be set according to the active and reactive load demand by the use of the resistive droop control methodology as presented in Equations 2.12 and 2.13. Therefore, the instantaneous load demand condition is used to set the microgrid point of common coupling voltage amplitude, V_{PCC}, and frequency, f_{MG}, within previously established limits.

The block diagram in Figure 3.2 presents the integration of both primary and tertiary control levels over a generic distributed generator *i* and the operational sequence for the adapted economic based control strategy implementation. The scheme presents the integration of the FCS-MPC with the droop control and virtual impedance adjustment, which are implemented

in MATLAB/*Simulink s-function* code block environment for software simulation validation of the adapted power sharing strategy.

The control variables required for the system short-time operation are measured locally at each converter output, namely the converter output current, i_i, load currents, i_0 and filter output voltage, v_f. The reference voltage, v^*_{ref}, is calculated internally in the control algorithm and will follow the droop curves references provided by the tertiary control.

The secondary control was not implemented in parallel with the primary and tertiary hierarchical levels, since compensation of problems related to power quality and nominal values recovery at microgrid PCC are not being addressed in the present work.

Figure 3.2 – Adapted power sharing strategy control diagram.

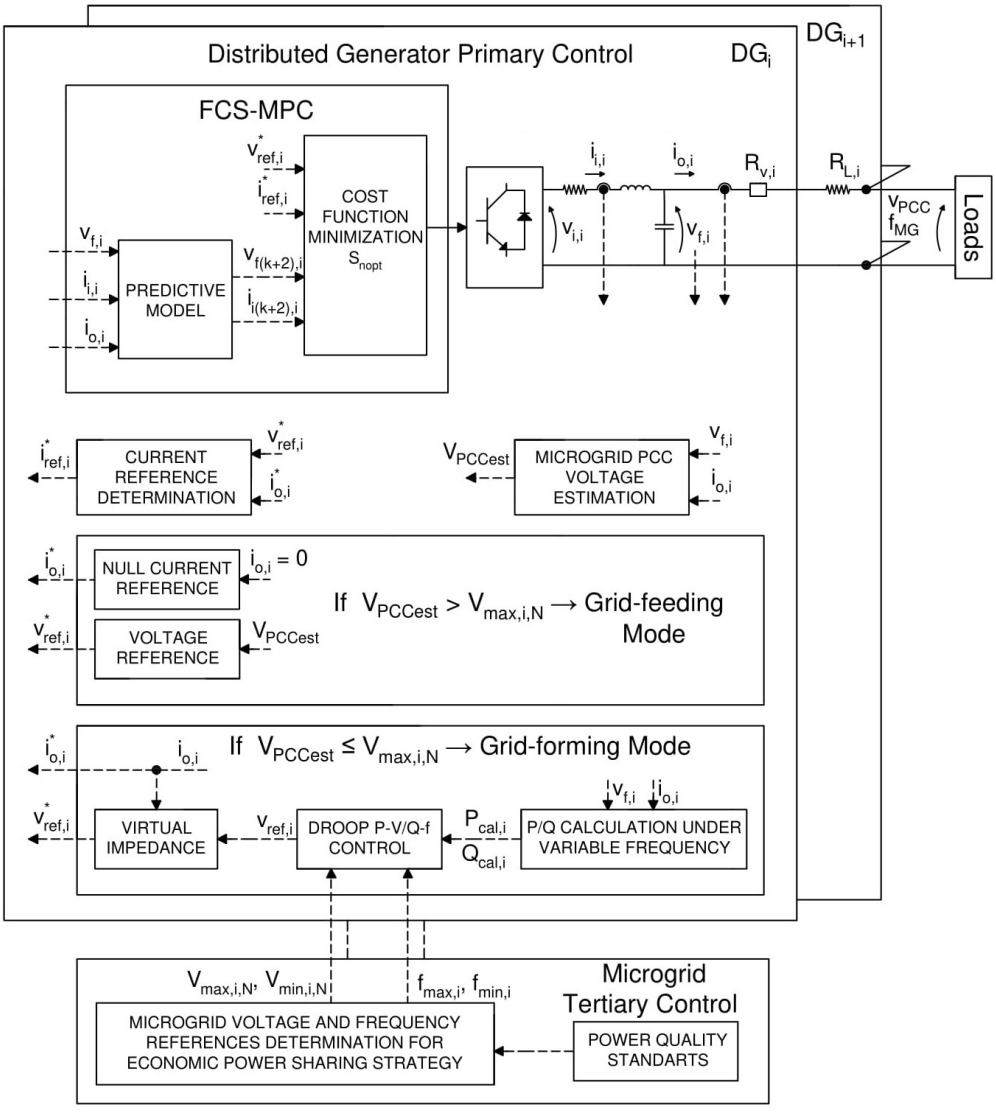

Source: From author (2021)

3.2 Distributed generators primary control definition

The primary controllers were individually implemented for each converter i with the objective of coordinating the semiconductors switching states in order to follow a dynamic voltage signal reference. The given voltage reference amplitude and frequency allows the instantaneous active and reactive powers to be shared among the distributed generators within the proposed island microgrid. Figure 3.3 illustrates the block diagram of the primary control level for the adapted droop-based power sharing strategy implemented in this work.

Figure 3.3 – Primary control block diagram for adapted droop-based economic power sharing strategy

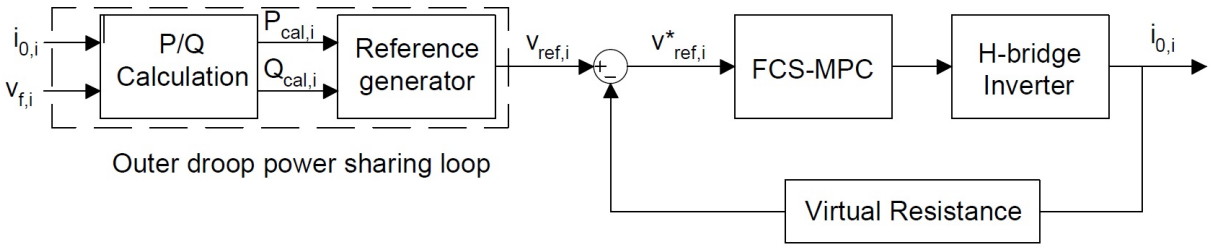

Source: Adapted from Guerrero et al. (2005)

where $v_{f,i}$ and $i_{o,i}$ are the respective converter i LC filter capacitor voltage and output load current. $P_{cal,i}$ and $Q_{cal,i}$ are the active and reactive power delivered to supply the system demand which are calculated for a fundamental varying frequency condition. Finally, $v_{ref,i}$ and $v^*_{ref,i}$ are the droop and the virtually adjusted FCS-MPC sinusoidal voltage references.

The converters primary controllers receives unit individual operational limits information from tertiary control and sets the voltage signal reference, $v^*_{ref,i}$ using droop relations according to the instantaneous load demand conditions, $P_{cal,i}$ and $Q_{cal,i}$. The FCS-MPC control loop then use the droop voltage reference to adjust the converter output signal by selecting a switching state that minimizes a determined quality cost function. In order to prevent active and reactive power coupling issues, and also add harmonic resonances damp, a virtual impedance loop was implemented. The primary control proposed in this study will be further detailed in this section.

3.2.1 Active and reactive power calculation under variable grid frequency

In order to implement the resistive droop control, Equations 2.12 and 2.13, a fast and accurate fundamental frequency active and reactive power measurement technique is required to obtain the distributed generators dispatched powers $P_{cal,i}$ and $Q_{cal,i}$ used to establish the grid

voltage and frequency references in a system were the signal frequency and amplitude normally varies.

For three-phase systems, the power calculation using $\alpha\beta$ or dq synchronous reference frame methods are commonly applied and can be found in the works of Guerrero et al. (2013), Young e Bastias (2018) and Dragičević (2018). For power measurements in single-phase systems, Ferreira (2012) impelemented a methodology proposed by Yazdani et al. (2009) based on adaptive filters which enables the active and reactive power to be calculated using two orthogonal signal similarly to the power measurement using the $\alpha\beta$ reference which will be presented in the following.

3.2.1.1 Adaptive notch filter with frequency estimator

The adaptive notch filter tuned with frequency estimator, or simply ANF-FE, is a type IIR (*Infinite Impulse Response*) filter, with an algorithm to estimate the input signal frequency (FARHANG-BOROUJENY, 1998). This filter was initially proposed in the time domain by Bodson e Douglas (1996), and modified by Hsu, Ortega e Damm (1999) to solve the instability problems. After that, it was extended to an arrangement capable of individually extracting the sinusoidal components of a signal (YAZDANI; BAKHSHAI; JAIN, 2010). According Ferreira (2012), one of the advantages in using the ANF-FE is the unnecessity of complex control PLL algorithms when compared to other techniques.

As presented by Ferreira (2012), the ANF-FE can be defined by the following set of equations:

$$\dot{\omega}_1(t) = -\gamma\omega_1(t)x_1(t)e(t) \tag{3.1}$$

$$\ddot{x_1}(t) = 2\zeta\omega_1(t)e(t) - \omega_1^2(t)x_1(t) \tag{3.2}$$

$$e(t) = d(t) - \dot{x_1}(t) \tag{3.3}$$

In this structure, *d(t)* is the signal to be filtered and $x_1(t)$ is the filter output. The signal fundamental frequency, $\omega_1(t)$, is estimated from Equation 3.1 and then used to adjust the notch frequency in the filter Equation 3.2. The error signal, *e(t)*, is used in the frequency estimator, Equation 3.1. The parameters γ and ζ are the adaptation coefficient and the damping factor,

respectively. These parameters determine the behavior of the frequency and filter adaptation, in terms of speed and accuracy.

According to Ferreira (2012), if becomes necessary to estimate the signal harmonic components, other sub-filters can be syntonized just by adding a multiplier h in Equation 3.4, proportional to the harmonic order of interest.

$$\dot{x_h}(t) = 2\zeta\omega(t)e(t) - h^2\omega^2(t)x_h(t) \rightarrow h = 3,5,...,N \tag{3.4}$$

$$e(t) = d(t) - \dot{x_1}(t) - \sum_{h=3}^{N} \dot{x_h}(t) \tag{3.5}$$

To implement this filter digitally, these equations are divided into two state variables (x_i and $\dot{x_i}$), and Equations 3.1 and 3.2 are rewritten as follows:

$$\dot{x_1}(t) = \int 2\zeta_1\omega(t)e(t) - \omega^2(t)x_1(t) \cdot dt \tag{3.6}$$

$$x_1(t) = \int \dot{x_1}(t) \cdot dt \tag{3.7}$$

The two state variables of the filter applied to the current, x_1 and $\dot{x_1}$, represent two orthogonal vectors proportional to the amplitude of the fundamental voltage, v_1 and $v_{1_{90^o}}$, and can be calculated as presented in Equations 3.8 and 3.9, respectively.

$$v_1 = V_1 \sin(\omega_1 t) \tag{3.8}$$

$$v_{1_{90^o}} = V_1 \cos(\omega_1 t) \tag{3.9}$$

Similarly to the voltage signal, the current orthogonal vectors, i_1 and $i_{1_{90^o}}$, can be determined as shown in Equations 3.10 and 3.11, respectively.

$$i_1 = I_1 \sin(\omega_1 t + \theta_1) \tag{3.10}$$

$$i_{1_{90^o}} = I_1 \cos(\omega_1 t + \theta_1) \tag{3.11}$$

where ω_1 is the signal estimated frequency and θ_1 is the phase angle between current and voltage signals.

The amplitude of the fundamental voltage, V_1, and current, I_1, can be calculated as presented in Equations 3.12 and 3.13, respectively:

$$V_1 = \sqrt{v_1^2 + v_{1_{90^o}}^2} \tag{3.12}$$

$$I_1 = \sqrt{i_1^2 + i_{1_{90^o}}^2} \tag{3.13}$$

Once implemented, the calculation of the fundamental instantaneous active and reactive powers can be done similarly to the $\alpha\beta$ and pq theories. Thus, according to Ferreira (2012) the active and reactive instantaneous powers delivered by the power converters were obtained as presented in Equations 3.14 and 3.15.

$$P_{cal} = v_1 i_1 + v_{1_{90^o}} i_{1_{90^o}} \tag{3.14}$$

$$Q_{cal} = v_1 i_{1_{90^o}} - v_{1_{90^o}} i_1 \tag{3.15}$$

The block diagram in Figure 3.4 summarizes the steps for power calculation using the ANF-FE.

Figure 3.4 – Block diagram of active and reactive current part extraction using adaptive notch filter with frequency estimation technique.

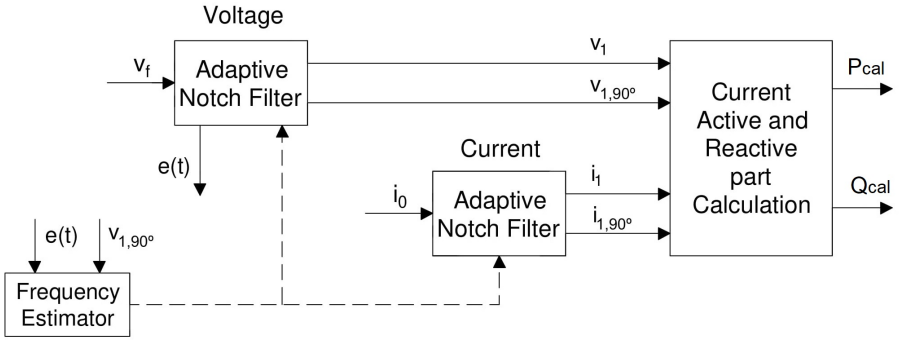

Source: Adapted from: Ferreira (2012)

In the present work, the ANF-FE were implemented at each converter primary control in order to execute the calculation of the single-phase active, P_{cal}, and reactive, Q_{cal}, output powers. Both powers were calculated according to Equations 3.14 and 3.15, respectively.

However, the Forward Euler method was necessary for time-discrete algorithm implementation of the adaptive notch filter technique. The time-discrete filter equations are not presented here, but can be seen in the work of Ferreira (2012).

3.2.2 Grid-forming power converter voltage reference determination

When the microgrid load demand level requires the proportional power sharing among the local distributed generators as determined by the considered power management strategy, such units must operate as grid-forming converters in order to control their respective output voltage signal, v_f. Each converter internal voltage reference, v_{ref}, was obtained in accordance to the respective distributed generator droop curves and the microgrid instantaneous active and reactive load demand as described next.

With the definition of each converter operational limits and, as result, the respective droop curve coefficients, the converters individual voltage amplitude, V_{ref}, and frequency, f_{ref}, instantaneous references were calculated in relation to the active, P_{cal}, and reactive, Q_{cal}, power demanded. These references were obtained according to the droop Equations 2.12 and 2.13 for the resistive microgrid as previously defined in section 2.4.2.2.

The converter time-continuous sinusoidal voltage reference, v_{ref}, was obtained as presented in Equation 3.16 and is doubly related to the instantaneous delivered active, P_{cal}, and reactive, Q_{cal}, powers.

$$v_{ref} = V_{ref}\sqrt{2}\sin(2\pi f_{ref}t) \tag{3.16}$$

3.2.2.1 Virtual resistance methodology for microgrid impedance adjustment

Even with the assumptions of purely inductive or purely resistive grid conditions for achieving proper active and reactive power sharing using droop strategy, in practical terms, it is barely likely to occur such situations. According to Guerrero et al. (2005), the inverter output impedance is considered usually to be inductive due to both the high inductive component of line impedance and large inductance of converters output filter.

A possible solution to the line impedance problem consists of adding an inductor in series with the inverter output in order to adjust the output impedance. Nevertheless, this inductor is heavy and bulky, increasing the size and the cost of the equipment. With the objective of phy-

sically avoiding this inductor, several fast control loops emulating the desired output impedance have been proposed (GUERRERO et al., 2005).

According to Guerrero et al. (2013), there are two main approaches to address the effects of interconnection lines impedance on droop-based control. The first approach decouples the voltage and frequency droop controls by analyzing and compensating for the effect of the line impedance on active and reactive power flows. The second procedure introduces the effects of a virtual impedance at the converter output through a closed-loop control. The virtual impedance method is insensitive to the nature of the line impedance (GUERRERO et al., 2013).

The virtual impedance method to address the line impedance mismatch is presented by Guerrero et al. (2005), Young e Bastias (2018) and Dragičević (2018), in which a virtual output impedance Z_v is introduced by modifying the converter voltage reference v_{ref} based on the respective output current i_o feedback. To achieve a predominantly resistive grid, Z_v can be assumed containing only the virtual resistive part, R_v, which effects ensure the *P-V/Q-f* droop relations applicability.

Considering the fundamental component of the converter output current signal, i_o, the adjusted voltage reference, v^*_{ref}, can be determined as shown in the Equation 3.17.

$$v^*_{ref} = v_{ref} - R_v i_o \tag{3.17}$$

To implement the virtual resistive loop for grid impedance adjustment described in section 3.2.2.1, Equation 3.16 is modified as presented below.

$$v^*_{ref} = V_{ref}\sqrt{2}\sin(2\pi f_{ref} t) - R_v i_o \tag{3.18}$$

As stated by Rocabert et al. (2012), for a proper R_v value selection, the selected virtual impedance value should be larger than the actual feeder line impedance, otherwise it will not have a predominant effect in power flow equations. Nevertheless, output voltage level drop should be carefully put in balance by microgrid planners as virtual reference adjustments are introduced at converters primary level controllers.

3.2.3 Grid-feeding power converter voltage reference determination

During low load conditions, when the total power demand can be fully supplied by less costly power sources, the other non-operating units should be ideally deactivated. This

strategy developed by Nutkani et al. (2017) was proposed in order to avoid no-load operational costs among the distributed generators. However, short-time load variations could induce the activation and deactivation of several microgrid converters within a short period of time.

As some distributed generation units can take time lengths of several seconds to minutes in order to re-synchronize to the existing grid, a full stop for short-time load variations should be avoided. In this sense, the present work adopted a hybrid power converter operation scheme, which changes the lowest dispatch priority distributed generator operational mode of grid-forming to grid-feeding control instead of switching off the unit.

In order to operate in grid-feeding mode, the voltage reference provided to the FCS-MPC controller must be based on the converter local voltage measured at the LC filter output, v_f. The v_f signal amplitude, V_f, and frequency, f_{PLL}, were obtained using a PLL algorithm based on the ANF-FE methodology as described in Section 3.2.1.1. Equation 3.19 demonstrate the voltage reference determination for the converter while on grid-feeding control mode.

$$v^*_{ref} = V_f\sqrt{2}\sin(2\pi f_{PLL}t) \tag{3.19}$$

3.2.4 Finite-control-set model predictive control implementation

After the droop control sets the converters voltage and frequency references and the virtual impedance adjusts the output signals to the grid conditions in order to decouple the delivered active and reactive powers in grid-forming mode, or while following the local voltage signal as operating as grid-feeding units, the next stage consists in controlling the switching states of the converter itself. The converter control performs the DC-AC conversion while following the previously established references, being this the core of the primary level of the microgrid hierarchical control.

For the implementation of the FCS-MPC, it is initially necessary to identify the converters possible switching states and to determine the relationship between then and the filter output voltage. The second step is to obtain a discrete model of the system according to the derivative of the control variable aiming to predict its future value. Finally, it is necessary to define a quality cost function that represents nonlinearities and system restrictions, allowing control variable optimization.

As demonstrated by Guimaraes (2019), to take the processing time into account for the FCS-MPC implementation, the control algorithm must be designed according to the following steps:

1º. Measure the control variables $v_{f(k)}$ and $i_{i(k)}$;

2º. Apply the switching state calculated in the previous sampling period;

3º. Estimate the control variable for the instant $k+1$;

4º. Predict the control variable for instant $k+2$ for all converter possible switching states;

5º. Evaluate the quality cost function;

6º. Choose the optimum switching state that minimizes the quality cost function and which will be applied in the next sampling period.

Figure 3.5 presents a single-phase grid-forming converter with a output LC filter. $i_i(t)$ and $i_o(t)$ represents the converter filter delivered and load output currents, respectively, while $v_f(t)$ indicates the filter output voltage. According to Queiroz et al. (2017), this converter topology has been widely used for renewable sources integration with the grid.

Figure 3.5 – Grid-forming converter topology with equivalent LC filter.

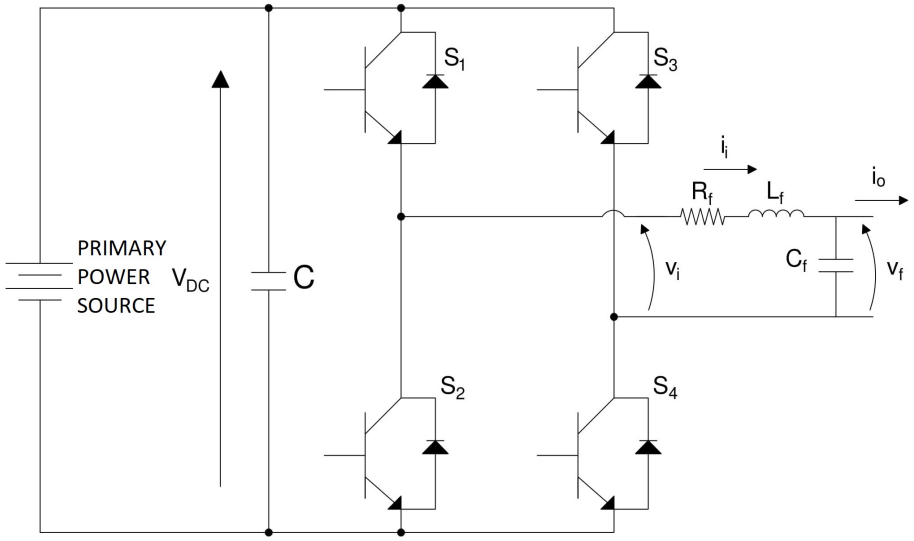

Reference: Adapted from: Guimaraes (2019)

In opposition to the L filter, LC filters can be used for grid-connected applications and also for stand-alone voltage source converters. For both cases, the converter circuit with the

output LC filter can be modeled by the application of Kirchoff's law (YOUNG; BASTIAS, 2018; GUIMARAES, 2019). The dynamics of the output voltage $v_f(t)$ and the filter inductor current $i_i(t)$ are given by the differential Equations 3.20 and 3.21:

$$L\frac{\mathrm{d}i_i(t)}{\mathrm{d}t} = v_i(t) - v_f(t) - R_f i_i(t) \tag{3.20}$$

$$C_f\frac{\mathrm{d}v_f(t)}{\mathrm{d}t} = i_i(t) - i_o(t) \tag{3.21}$$

The LC filter can be represented as a state-space matrix as shown in Equation 3.22. However, in this case the state variables are $i_i(t)$ and $v_f(t)$ and the control variables are $v_i(t)$ and $i_o(t)$ (GUIMARAES, 2019).

$$\begin{bmatrix} \dot{i_i} \\ \dot{v_f} \end{bmatrix} = \begin{bmatrix} \frac{-R_f}{L_f} & \frac{-1}{L_f} \\ \frac{1}{C_f} & 0 \end{bmatrix} \begin{bmatrix} i_i \\ v_f \end{bmatrix} + \begin{bmatrix} \frac{1}{L_f} & 0 \\ 0 & \frac{-1}{C_f} \end{bmatrix} \begin{bmatrix} v_i \\ i_o \end{bmatrix} \tag{3.22}$$

For implementing the FCS-MPC output voltage control, a discrete-time model of the system is required. This ensures that the output of the system will react to the input in the next sampling instant (YOUNG; BASTIAS, 2018). Using a discretization method based in Forward Euler theorem, the system above can be presented as a state-space model ($x_{(k+1)}$=$\mathbf{A}x_{(k)}$+$\mathbf{B}u_{(k)}$) as demonstrated in Equation 3.23 (GUIMARAES, 2019).

$$\begin{bmatrix} i_{i(k+1)} \\ v_{f(k+1)} \end{bmatrix} = \begin{bmatrix} (1-\frac{T_s R}{L_f}) & \frac{-T_s}{L_f} \\ \frac{T_s}{C_f} & 1 \end{bmatrix} \begin{bmatrix} i_{i(k)} \\ v_{f(k)} \end{bmatrix} + \begin{bmatrix} \frac{T_s}{L_f} & 0 \\ 0 & \frac{T_s}{C_f} \end{bmatrix} \begin{bmatrix} v_{i(k)} \\ i_{o(k)} \end{bmatrix} \tag{3.23}$$

According to Cortes et al. (2008), a quality cost function is responsible for minimizing the error between control and reference variables, thus choosing the best possible switching state. In this application, the variable to be controlled is the output filter voltage, v_f. The quality cost function is evaluated two time steps ahead, k+2, Equation 3.24, in order to compensate for the computation delay in digital implementation of the FCS-MPC (YOUNG; BASTIAS, 2018).

$$\begin{bmatrix} i_{i(k+2)} \\ v_{f(k+2)} \end{bmatrix} = \begin{bmatrix} (1-\frac{T_s R}{L_f}) & \frac{-T_s}{L_f} \\ \frac{T_s}{C_f} & 1 \end{bmatrix} \begin{bmatrix} i_{i(k+1)} \\ v_{f(k+1)} \end{bmatrix} + \begin{bmatrix} \frac{T_s}{L_f} & 0 \\ 0 & \frac{T_s}{C_f} \end{bmatrix} \begin{bmatrix} v_{i(k+1)} \\ i_{o(k+1)} \end{bmatrix} \tag{3.24}$$

The FCS-MPC was implemented for the considered distributed generators converter 1 and 2 according to the methodology developed in the work of Guimaraes (2019). Further details and control specifications can be found there. The main steps used in the present work are described next.

3.2.4.1 Switching states definition

For converters 1 and 2 there are four n possible switching states which are presented in Table 3.1. These states allows to vary the converter output voltage, v_i, from $+V_{DC}$, $-V_{DC}$ and $0V$. The converters DC busbar voltage, V_{DC}, was set with a fix value of 310V$_{DC}$ in accordance with the model predictive control capacity to follow a sinusoidal 127V$_{rms}$ Brazilian phase-neutral voltage standard reference for low-voltage distribution level systems as defined in ANEEL/PRODIST (2018).

Table 3.1 – Switching states for the adopted H-bridge converter topology.

n	S_1	S_2	S_3	S_4	v_i
0	0	1	0	1	0
1	1	0	0	1	V_{DC}
2	0	1	1	0	-V_{DC}
3	1	0	1	0	0

The adopted converters H-bride topology and semiconductors switches S_1, S_2, S_3 and S_4 arrangement for both considered distributed generator units can be seen in Figure 3.5.

3.2.4.2 Cost function definition

The FCS-MPC cost function main objective is to seek the smallest error between the predicted voltage by the converter mathematical model, $v_{f(k+2)}$, and a given voltage reference, v_{ref}, thus obtaining the optimal switching state, $S_{n_{opt}}$, so that the converter output voltage is closer to the instantaneous given reference. The aimed sinusoidal voltage reference, v^*_{ref}, can be provided either from the droop controller in grid-forming operation, or from a PLL while following the microgrid voltage measured at the converter filter output during grid-feeding control mode.

The conventional cost function used for converters with LC output filter takes into account only the filter predicted and reference voltages as demonstrated in Equation 3.25, where v_{ref} represents the converter internal reference and $v_{f(k+2)}$ indicates the predicted value from system discrete model.

$$J = (v_{ref} - v_{f(k+2)})^2 \tag{3.25}$$

As stated by Dragičević (2018) and Panten, Hoffmann e Fuchs (2016), the conventional cost function application can be seen as a satisfactory solution when it comes to a first-order system. However, as in this work the studied models are second-order systems, the control becomes more complex, since the output voltage, v_f, is directly related to the converter current, i_i. Therefore, it is required to control both the above mentioned variables simultaneously with the inclusion of a converters reference current, i^*_{ref}, and its respective predicted value, $i_{i(k+2)}$, at the FCS-MPC cost function.

Also, in order to avoid converters misbehavior, a switching state restriction k_e was incorporated within the cost function at the present study, resulting in Equation 3.26.

$$J = \lambda_v(v^*_{ref} - v_{f(k+2)})^2 + \lambda_i(i^*_{ref} - i_{i(k+2)})^2 + k_e \tag{3.26}$$

The above defined cost function was applicable for the converters while in grid-forming mode as for during grid-feeding operation, with the respective changes in the voltage and current references for each operational mode and on the weighting factors, λ_v and λ_i, which defines the influence of each control variable to be observed by the FCS-MPC.

3.2.4.3 Converter reference current determination

The reference current, i^*_{ref}, definition is set to change based on the distributed generator current mode of operation and, therefore, is directly related to the instantaneous microgrid load demand.

During grid-forming operation, the reference current i^*_{ref} is calculated from the system mathematical model and the previously defined reference voltage v^*_{ref} (GUIMARAES, 2019). From nodal current analysis over the circuit presented in Figure 3.5, it can be written:

$$i_f = i_i - i_o \tag{3.27}$$

As the filter capacitor current, i_f, can be determined by Equation 3.28:

$$i_f = \frac{v_f}{jX_C} \tag{3.28}$$

Hence:

$$\frac{v_f}{jX_C} = i_i - i_o \tag{3.29}$$

Also, as the converter current, i_i, is the model control variable, therefore it can be replaced by the predicted current reference, i^*_{ref}, once the filter output voltage v_f also receives the model reference voltage v^*_{ref}. Rearranging Equation 3.29 and replacing the capacitor reactance X_C by $\frac{1}{2\pi f C_f}$, the reference current can be obtained as presented in Equation 3.30:

$$i^*_{ref} = i_o - jv^*_{ref}(2\pi f_{ref} C_f) \tag{3.30}$$

were i^*_{ref} is the converter current reference, i_o represents the filter output, or load current, C_f is the filter capacitance and v^*_{ref} and f_{ref} are the internally generated droop references for voltage and frequency, respectively.

The non-real term *-j(v^*_{ref})* can be given by:

$$-jv^*_{ref} = V^*_{ref}\cos(2\pi f_{ref} t) \tag{3.31}$$

Differently, during low demand conditions, the converter will operate as a grid feeder, but with a zero current internal reference, $i_o = 0$. In contrast to the original power dispatch strategy proposed by Nutkani et al. (2017), the zero value current reference adopted in this work avoids power to be delivered or absorbed by the distributed generator during short-time load variations instead of fully deactivating the respective unit.

3.2.4.4 Switching states operation restriction

According to Guimaraes (2019), as the FCS-MPC selects an optimal switching state, there is a possibility of repeatedly selecting the same state several times. For this reason, it was necessary to apply a security restriction that prevented a state from being chosen several times in a row. Therefore, the restriction term k_e was responsible for representing the state repetition limiter at the cost function, which operates as demonstrated in Equation 3.32:

$$k_e = \begin{cases} \infty & \text{if } S \geq x \\ 0 & \text{if } S < x \end{cases} \tag{3.32}$$

In case of limit violation during the prediction process, k_e receives a extremely high value after x defined repetitions, forcing the FCS-MPC to select a new switching state. The details of this coefficient implementation can be found in the work of Guimaraes (2019).

3.3 Microgrid tertiary control definition

The tertiary hierarchical control level, as described in section 2.3.3, was developed in order to implement an island microgrid power management strategy related to local distributed generators inherent economic aspects and which is based on grid signal parameters for converters intercommunication. The microgrid tertiary controller sets the active and reactive droop curves for each converter by defining the respective units voltage amplitude and frequency operational limits.

Subsequently, the droop curves information are provided to every distributed generator primary control participating in the power-sharing strategy within the island microgrid, which will be used to set the system voltage signal and share cost-proportional active and reactive powers. The grid-forming converters follows the dynamic droop-defined voltage amplitude and frequency references, which are proportionally set according to the microgrid instantaneous active and reactive load demand. The voltage signal parameters serve as instantaneous operational references for every island microgrid distributed generators, indicating the respective instantaneous proportional power dispatch and on or off unit status.

Figure 3.6 shows the control relation between the tertiary and the primary controllers established in the present work. $V_{max,i}$, $V_{min,i}$, $f_{max,i}$ and $f_{min,i}$ represents the maximum and minimum operational *rms* voltage amplitude and frequency reference values defined for each distributed generator i, respectively. These parameters are defined by the microgrid tertiary control and sent to the distributed generators 1 and 2 local primary controllers. The active and reactive powers dispatched individually by the distributed generators, $P_{cal,i}$ and $Q_{cal,i}$, are responsible to set the microgrid instantaneous sinusoidal voltage reference according to the droop curves defined within the microgrid tertiary control.

Figure 3.6 – Tertiary control block diagram for the adapted droop-based economic power sharing strategy.

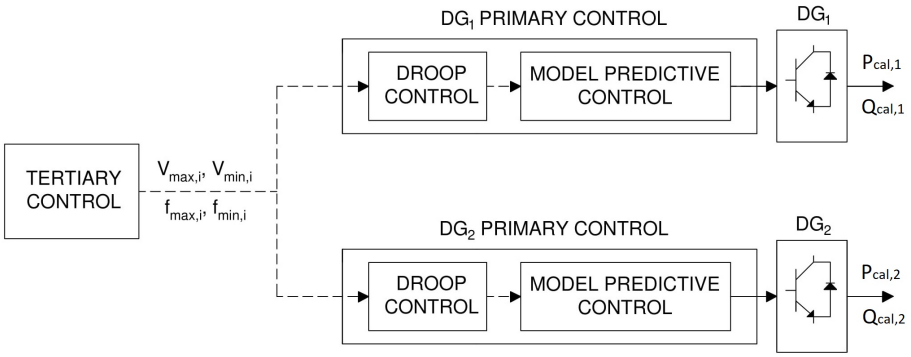

Source: From author (2021)

The economic power sharing strategy, adapted in this work to operate in a mainly resistive microgrid, and also the traditional resistive droop approach were both implemented at the tertiary control level. The traditional resistive droop control was implemented for comparison purposes to verify the cost reduction efficiency of the modified strategy. Other functionalities generally attributed to the tertiary control level, such as long-term costs variations and main power system disconnection and re-synchronization, were not considered in this moment.

3.3.1 Power-quality parameters definition for island operation

The nominal *rms* voltage, V_{nom}, established by ANEEL/PRODIST (2018) Brazilian standard for low-voltage distribution systems is 127V$_{rms}$. To ensure the microgrid operation withing the aforementioned standard range of 133V$_{rms}$ to 117V$_{rms}$ for maximum and minimum acceptable *rms* voltage amplitude, respectively, a narrower range was selected in order to accommodate voltage oscillations. Equation 3.33 and 3.34 demonstrates the microgrid new allowable maximum, $V_{max,MG}$, and minimum, $V_{min,MG}$, voltage limits definitions applied at the present work. A safety factor, ζ, was considered to avoid standard threshold overrun during steady-state operation under nominal conditions.

$$V_{max,MG} = V_{max,standart} - \zeta \cdot V_{nom} \tag{3.33}$$

$$V_{min,MG} = V_{min,standart} + \zeta \cdot V_{nom} \tag{3.34}$$

According to ANEEL/PRODIST (2018) standard, the distribution system and the generation facilities connected to it must, under normal conditions and in steady-state operation,

operate within the frequency limits between 59.9Hz and 60.1Hz. Outside the predefined range, the standard establishes a time period to recover to nominal condition range, or even considers the disconnection of loads and generation units until system is able to restore normal operation. However, the ANEEL/PRODIST (2018) does not deal specifically with island operation and the established limits are suitable for main power system operation.

In order to implement a droop-based control, a wider and flexible frequency range must be considered. The upper and lower frequency limits are suggested by IEEE (2014) standard for microgrids under island operation. According to the aforementioned standard, the frequency normal operating range, $f_{max,MG}$ to $f_{min,MG}$, are 60.5Hz and 59.3Hz, respectively. According to Nutkani et al. (2017), the selected voltage and frequency ranges should not be too narrow to avoid degrading the power sharing accuracy and also not be too wide to avoid large frequency variations that may eventually lead to system instability.

3.3.2 Traditional power-sharing droop control for resistive grid

The traditional resistive droop tertiary control sets all power sources with the same maximum and minimum voltage and frequency reference values, which, as described in section 2.4.2.2, establishes all the microgrid distributed generator to dispatch simultaneously according to the same P-V and Q-f droop curves. The maximum and minimum microgrid voltage amplitude and frequency, $V_{max,MG}$, $V_{min,MG}$, $f_{max,MG}$, and $f_{min,MG}$, respectively, were selected based on national and international power-quality standards and security factor chosen by the microgrid planner as presented in section 3.3.1.

For the conventional resistive droop control method implementation, the converters common maximum and minimum voltage amplitude and frequencies were set as: $V_{max,1} = V_{max,2} = V_{max,MG}$; $V_{min,1} = V_{min,2} = V_{min,MG}$; $f_{max,1} = f_{max,2} = f_{max,MG}$ and $f_{min,1} = f_{min,2} = f_{min,MG}$, respectively. The distributed generator 1 and 2 active and reactive power droop curves for a predominantly resistive grid are presented in Figures 3.7 and 3.8.

Figure 3.7 – Traditional resistive P-V droop curve.

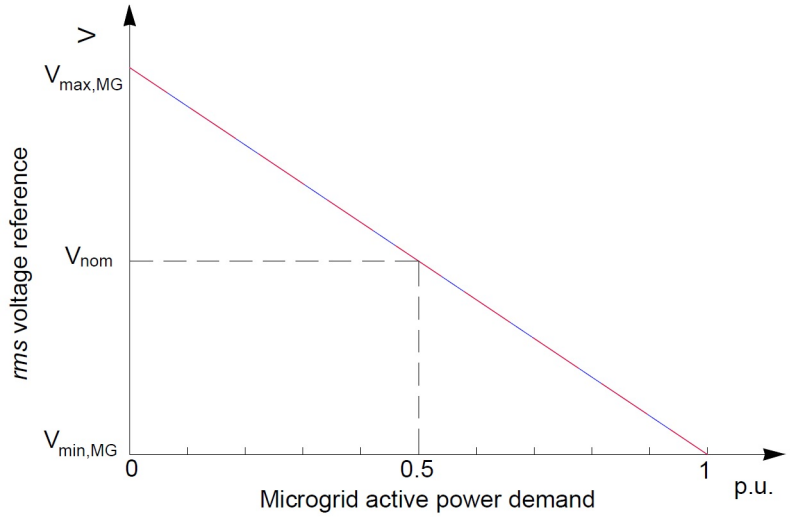

Source: From author (2021)

Figure 3.8 – Traditional resistive Q-f droop curve.

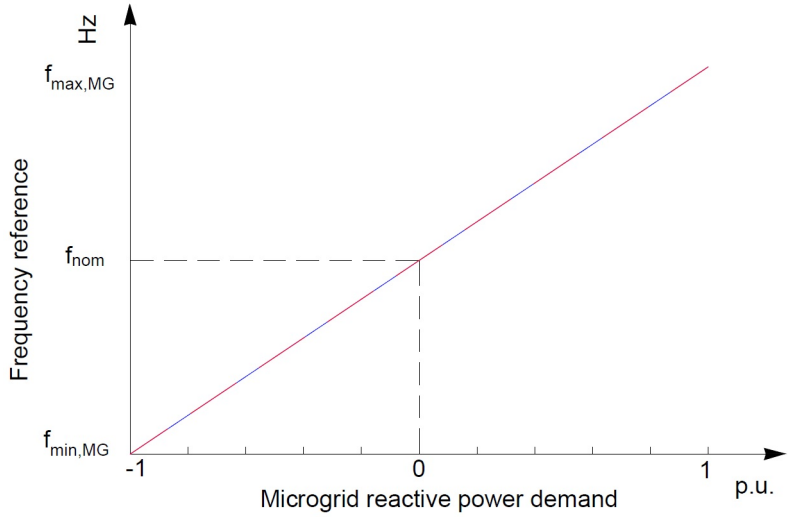

Source: From author (2021)

The defined droop curves causes both distributed generators to dispatch simultaneously and produce powers proportionally to their respective power ratings, regardless of the generators specific operational costs and load demand level. Equations 3.35 and 3.36 presents the converters internal voltage and frequency reference determination.

$$V_{ref,i} = V_{max,MG} - \frac{P_{cal,i}}{P_{max,i}} \cdot (V_{max,MG} - V_{min,MG}) = V_{max,MG} - P_{cal,i} \cdot k_{p,i} \tag{3.35}$$

$$f_{ref,i} = f_{min,MG} + \frac{Q_{cal,i}}{Q_{max,i}} \cdot (f_{max,MG} - f_{min,MG}) = f_{min,MG} + Q_{cal,i} \cdot k_{q,i} \tag{3.36}$$

where, $V_{ref,i}$ and $f_{ref,i}$ are the conventional resistive *rms* voltage amplitude and frequency droop references calculated internally at all microgrid grid-forming converters i. $P_{cal,i}$ and $Q_{cal,i}$ represents the converters instantaneous output active and reactive powers, obtained as presented in section 3.2.1. $P_{max,i}$ and $Q_{max,i}$ are the distributed generator rated powers and indicates the nominal maximum active and reactive power dispatch capacity of each converter. Lastly, $k_{p,i}$ and $k_{q,i}$ represents each distributed generator active and reactive droop curves inclination coefficients.

The microgrid *rms* voltage amplitude and frequency was, therefore, simultaneously defined by the local grid-forming converters as the active and reactive load demand changes from 0% to 100% of microgrid total capacity.

3.3.3 Adapted decentralized droop-based economic dispatch strategy for low-voltage island microgrids

Unlike the traditional scheme, distributed generators controlled by the cost-prioritized droop strategy described in section 2.5.2 shares power proportionally to its instantaneous operational cost and are turned on and off automatically based on the microgrid load demand. The purpose is to reduce the island microgrid total generation cost autonomously and without the use of secondary communication channels, rather than simply share power among its distributed generator based on units power ratings.

However, in practical terms the process of turning on and off of a distributed generator may take several seconds to minutes to complete, being inadequate for short-time load variations. In this sense, the present work proposes an adaptation for the strategy presented by Nutkani et al. (2017), where instead of turning off an unit during a short-time low-load condition, the converter operational mode switches from grid-forming to grid-feeding with null output current reference.

To include economic aspects to the conventional droop power-sharing strategy, a cost-based dispatch scheme was described in section 2.5.2, where dispatch priorities were set to the distributed generators according to the units specific operational cost functions. However, the economic dispatch strategy proposed by Nutkani et al. (2017) was designed for highly inductive microgrids with *P-f/Q-V* droop relations. This model is more appropriate for high-voltage systems where impedance are typically inductive.

For low-voltage distribution level microgrids, where the resistive component are significantly higher, power coupling issues emerge as described by Young e Bastias (2018), Guerrero et al. (2013) and Han et al. (2017). To overcome this drawback, Equations 2.23, 2.24, 2.25 and 2.26 were rewritten in order to incorporate the resistive *P-V/Q-f* droop relations and avoid active and reactive power coupling in a resistive low-voltage microgrid. The adapted equations are presented next in this section.

The adapted economic dispatch strategy also considered the cost characteristics of the distributed generators before deciding their dispatch priority order and voltage amplitude at which they should individually be dispatched. Other constraints such as generators power ratings, voltage and frequency limits and online power reserves were also considered, which upon realized, indirectly tuned the droop curve gradients of the microgrid dispatchable distributed generators. The adapted strategy, as in Nutkani et al. (2017), allows the integration of several units to the economic dispatch scheme by the use of the rewritten equations.

If an unity is added or removed from the microgrid operated under the proposed economic dispatch strategy, the tertiary control will, therefore, recalculated the maximum and minimum operational parameters of each operating unit. This information is then sent to each distributed generator by a proper tertiary control communication channel, indicating the new microgrid droop curves and dispatch order priorities. Thus, the proposed strategy allows plug-and-play capability for different types of generators, with the operation parameters being revised by the microgrid tertiary control in case there is any change in the standard microgrid configuration.

The adapted resistive droop economic dispatch scheme, like the conventional droop power-sharing strategy, does not require any secondary communication channel for primary control besides the instantaneous estimated grid voltage amplitude, $V_{PCC_{est}}$, and frequency, which increases the microgrid reliability and fast-time response capacity for the primary control level.

Figure 3.9 – Adapted economic dispatch strategy *P-V* droop-characteristic control curve for predominantly resistive island microgrids.

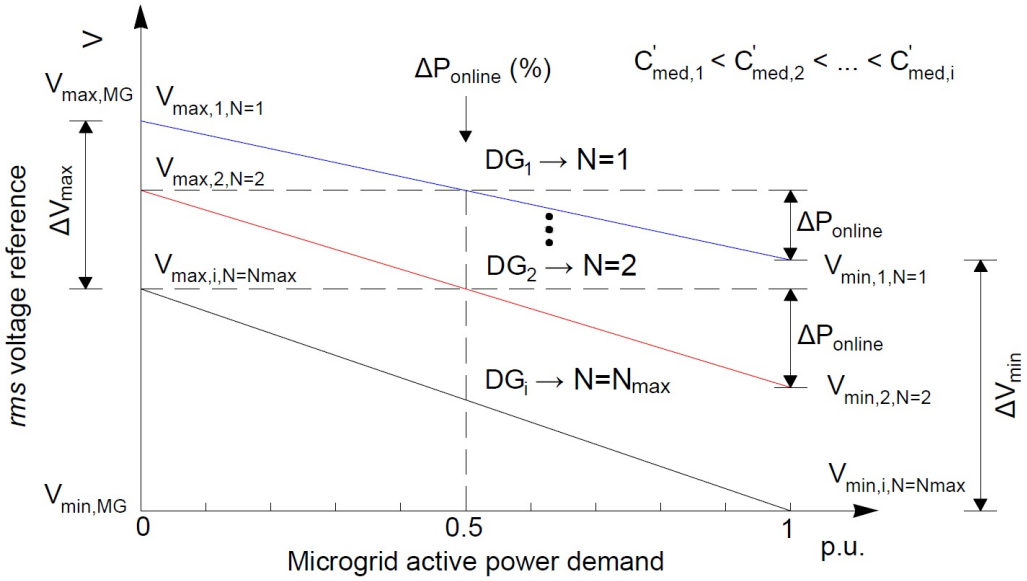

Reference: Adapted from: Nutkani et al. (2017)

A general view of the adapted droop-based economic power sharing strategy is presented in Figure 3.9, where ΔV_{max} and ΔV_{min} are the maximum and minimum defined dispatch voltage range, respectively. N_i represents the dispatch priority attributed to every power-sharing participating distributed generator i. Lastly, ΔP_{online} indicates the online power reserve chosen by the microgrid planner in order to include a secure power dispatch margin allowing the next priority generator start its grid-forming operational mode face a sudden load variation.

The core aspect of the adapted economic power sharing strategy was to attribute prioritized singular cost-proportional droop curves to each microgrid distributed generator. For each unit i, the tertiary control was responsible for the determination of a maximum and minimum *rms* voltage amplitude reference as function of the generator dispatch priority N_i. The generators dispatch priorities were attributed according to the respective unit average operational cost as presented in Equation 2.22. The maximum *rms* voltage amplitude $V_{max,i,N}$ for which the respective distributed generator must start its operation as a grid-forming unit was defined according to Equation 3.37.

$$V_{max,i,N} = max\left\{ \underbrace{\frac{V_{max,MG} - \Delta V_{max} \cdot \frac{N_i - 1}{N_{max} - 1}}{Calculated\ based\ on\ priority\ order}}, \underbrace{\frac{V_{min,i,N-1} + k_{p,i,N-1} \cdot \Delta P_{online}}{Calculated\ based\ on\ online\ reserve}} \right\} \tag{3.37}$$

In order to guarantee the desired online power reserve and, at same time, considers the distributed generators dispatch priority, Equation 3.37 selects the highest *rms* maximum voltage value calculated over these two parameters. Other points with regard to Equation 3.37 are summarized as follows:

a) ΔV_{max} represents the dispatch voltage range marked in Figure 3.9. A similar recommendation as made by Nutkani et al. (2017), this parameter must be chosen carefully, together with ΔV_{min}, to give reasonable droop gradients for all distributed generators. In general, wider ΔV_{max} and ΔV_{min} give rise to more gradual droop gradients, and hence affect the generating units power sharing accuracy. Narrower ΔV_{max} and ΔV_{min}, in contrast, lessen the cost saving advantage expected from the proposed economic dispatch scheme;

b) $V_{max,MG}$ is the maximum *rms* voltage amplitude permitted in the microgrid. Its selection was similar as for the traditional droop scheme described in section 3.3.1;

c) N_i represents the dispatch priority of DG_i, and N_{max} is the priority of the most expensive DG unit. Value of N_{max} is, therefore, equal to the total number of distributed generators participating in the economic dispatch;

d) $V_{min,i,N-1}$ is the minimum droop voltage and $k_{p,i,N-1}$ is the droop curve inclination of the N_i*-1* prioritized generator, computed using Equations 3.38 and 3.39, respectively;

e) ΔP_{online} is the online power reserve to be maintained within the microgrid. Its value must be selected based on the expected load dynamics or sudden switching of one or more loads at the same time. This parameter dictates the voltage amplitude where the converters switches its primary control as grid-forming or grid-feeding operational mode.

In the present work, initially a microgrid comprising two distributed generator was considered, DG_1 and DG_2, to test the main power-sharing aspects of the adapted economic dispatch strategy in software simulations. Then, a third distributed generator was added to the simulated microgrid to verify the scalability of the adapted strategy in a predominantly resistive system.

As in the original economic dispatch scheme, for the highest priority unit, N_i*=1*, the maximum dispatch voltage equals the microgrid maximum global voltage set reference, $V_{max,i,1} = V_{max,MG}$. In the considered two distributed generator microgrid, for DG_1 was assumed a renewable fuel-based cost function with a lower average cost in relation to a nonrenewable

fuel-based power source considered for DG_2. Both primary power sources are assumed to be interconnected to the AC microgrid by power electronic converters as in the work of Nutkani et al. (2017), where the operational cost function mathematical models of the considered sources can also be found. Therefore, for the considered microgrid the dispatch priority assignment is set as: $C'_{med,1} < C'_{med,2} \rightarrow N_1=1,\ N_2=2$. This resulted in the continuous operation of DG_1 even during low-load conditions.

The maximum dispatch voltage for DG_2, $V_{max,2,2}$, was obtained according to Equation 3.37, where the maximum value between the one calculated based on priority order and the other calculated based on the selected online power reserve was adopted. For the present work, it was considered an online power reserve ΔP_{online} of 50% as in the work of Nutkani et al. (2017).

The distribute generators individual minimum dispatch voltages, $V_{min,i,N}$, were calculated according to Equation3.38. This parameter indicate the voltage amplitude where a given unit reaches its maximum dispatch capacity. For the lowest priority unit in this work, $N_{max} = N_2 = 2$, the minimum dispatch voltage was set equal to the microgrid minimum global voltage. Therefore, $V_{min,2,2} = V_{min,MG}$.

$$V_{min,i,N} = V_{min,MG} + \Delta V_{min} \cdot \frac{max(C''_{i,N}) - C''_{i,N}}{max(C''_{i,N}) - min(C''_{i,N})} \tag{3.38}$$

Where, similarly to Nutkani et al. (2017):

a) ΔV_{min} represents the minimum voltage dispatch range;

b) $V_{min,MG}$ is the minimum voltage amplitude permitted by the microgrid. Selection of $V_{min,MG}$ is similar as the traditional scheme described in section 3.3.1;

c) The highest mean generation cost among the distributed generator, $max(C''_{i,N})$, was defined as in section 2.5.2 as the maximum average value of the normalized no-load generation cost curves of the distributed generators, obtained as: $max(C''_{i,N}) = max(C''_{1,N_1}, C''_{2,N_2}, \cdots, C''_{i,N_i})$. Similarly, the lowest average generation cost of the no-load normalized curve, $max(C''_{i,N})$, was defined as: $min(C''_{i,N}) = min(C''_{1,N_1}, C''_{2,N_2}, \cdots, C''_{i,N_i})$;

d) $C''_{i,N}$ represents the distributed generator average generation cost with priority N_i-1.

The tertiary control provide the previous determination of the maximum and minimum dispatch voltage, $V_{max,i,N}$ and $V_{min,i,N}$ of every adapted power sharing strategy participating

distributed generation unit i. It was then feasible to obtain each converter individual droop curve inclination coefficient, $k_{p,i,N}$, as presented in Equation 3.39.

$$k_{p,i,N} = \frac{V_{max,i,N} - V_{min,i,N}}{P_{max,i,N}} \tag{3.39}$$

The reactive power curve coefficients, $k_{q,i,N}$, were obtained identically as for the conventional droop strategy in relation to the microgrid frequency operational limits, where all participating distributed generator shared reactive power according to similar Q-f droop curves. For the adapted power sharing strategy, each participating converter instantaneous frequency reference, $f_{ref,i}$, were calculated according to Equation 3.36 as described in section 3.3.2.

The distributed generators operational mode and their respective voltage amplitude references, $V_{ref,i,N}$, were given depending on the instantaneous estimated microgrid voltage amplitude, $V_{PCC_{est}}$, as perceived at each units connection point. The distributed generators were able to switch its mode of operation between grid-forming and grid-feeding autonomously and without any secondary communication according to the logical relations presented in Equation 3.40.

$$V_{ref,i,N} = \begin{Bmatrix} V_{max,i,N} - k_{p,i,N} \cdot P_{cal,i} & if\ V_{PCC_{est}} \leqslant V_{max,i,N} & \rightarrow Grid{-}forming\ mode \\ V_{PCC_{est}};\ i^*_{ref} = 0 & if\ V_{PCC_{est}} > V_{max,i,N} & \rightarrow Grid{-}feeding\ mode \end{Bmatrix} \tag{3.40}$$

where $V_{ref,i,N}$ represents the instantaneous defined *rms* voltage amplitude. $k_{p,i,N}$ is the active power droop curve inclination coefficient. $P_{cal,i}$ is the active power provided by the respective distributed generator. Lastly, $V_{PCC_{est}}$ represents the estimated microgrid PCC *rms* voltage amplitude from every participating distributed generator perspective obtained as presented in Equation 3.41:

$$V_{PCC_{est}} = V_{f,i} - I_{1,o,i} \cdot (R_{L,i} + R_{V,i}) \tag{3.41}$$

were $V_{f,i}$ represents the filter capacitor voltage measured at the converter output, $I_{1,o,i}$ the output fundamental current and $R_{L,i}$ and $R_{V,i}$ the real feeder line and virtual resistances for the respective converter i.

Therefore, the converter primary control level was able to dynamically define the FCS-MPC cost function sinusoidal voltage reference, v^*_{ref} and set the distributed generator operati-

onal mode according to the microgrid active and reactive load demand. A closed-loop control was established, where every distributed generator adjusts its own delivered active and reactive powers, $P_{cal,i}$ and $Q_{cal,i}$, proportion as the voltage signal parameters perceived over the island microgrid varies.

3.4 MATLAB/*Simulink* software implementation

The software implementations were developed over two main stages in this study. The first part consisted in the adapted droop-based economic power sharing strategy and traditional droop implementation as microgrid tertiary control level in a *.m* MATLAB programming language. The purpose of this algorithm was obtaining for each considered microgrid distributed generator its respective droop curves according to predefined power quality standards for further instantaneous reference determination by converters primary control. The second stage consisted in performing software simulations of the formerly described low-voltage island microgrid on MATLAB/*Simulink* platform using *s-function* block with C programming language to run the proposed primary control level algorithm, implemented independently for each distributed generator. The block diagram presented in Figure 3.2 demonstrated the operation sequence of the adapted droop-based economic power sharing strategy.

The first part of primary control algorithm was responsible for the definition of the operational mode of the converter as grid-forming or grid-feeding according to the unit predetermined maximum dispatch voltage amplitude, $V_{max,i,N}$, and the estimated voltage amplitude at the microgrid PCC, $V_{PCC_{est}}$. For the adapted power-sharing strategy, $V_{max,i,N}$ served as a threshold between each converter mode of operation. If the microgrid estimated voltage amplitude was higher than the distributed generator designated maximum value ($V_{PCC_{est}} > V_{max,i,N}$), it was considered, similarly to the original economic power-sharing strategy, that the microgrid power demand could be supplied by the N_i-*1* higher priority distributed generators. The unit *i* with dispatch priority N_i should in this circumstances operate in grid-feeding mode with no power being delivered to the system.

While in grid-feeding operational mode, the converter voltage reference, $v^*_{ref,i}$, was obtained from a internal PLL within the ANF-FE algorithm, and the current reference, $i^*_{ref,i}$ was calculated based on a null reference value. The only exception was given for the highest dispatch priority distributed generator, N_i=*1*, which was set to operate continuously in grid-forming

mode for any load condition, providing the microgrid with a voltage reference even during no power demand situations.

This adaptation of the original economic power sharing strategy was implemented in order to improve the system dynamic response for short-time low load demand situations. However, as stated by Nutkani et al. (2017), for the island microgrid during longer periods in low demand conditions the lower priority generators should ideally be turned off. This last condition was not considered in the present study, which focus was given to short-time load variations.

When the microgrid estimated voltage amplitude equals or lower the distributed generator maximum dispatch voltage, $V_{PCC_{est}} \leq V_{max,i,N}$, the grid-forming mode is activated and the converter is then able to control its respective output voltage, $v_{f,i}$ and the delivered active and reactive powers, $P_{cal,i}$ and $Q_{cal,i}$. Within this operational mode, the distributed generators participate in the adapted economic power sharing strategy, and the active power dispatch becomes proportional to the unit average operational cost.

The primary control level for each microgrid converter were implemented considering the FCS-MPC technique as control method. The first part of the primary level algorithm consisted in measuring locally each converter i output current, $i_{i,i}$, filter output current, $i_{o,i}$, and voltage $v_{f,i}$ with sensors. Next, the converter delivered active and reactive powers, $P_{cal,i}$ and $Q_{cal,i}$, were calculated for a system under variable fundamental frequency using the ANF-FE technique. Then, the voltage amplitude and frequency references, $V_{ref,i}$ and $f_{ref,i}$, could be set dynamically according to the predefined tertiary control droop curves equations and the instantaneous power demand.

Virtual impedance technique was applied to adjust the feeder impedance as perceived by each converter, enhancing virtually resistive grid behavior in order to guarantee droop power-sharing capacity and avoid active and reactive power coupling issues for the considered low-voltage system. The converter output reference, current $i^*_{ref,i}$, was also calculated based on the adjusted voltage reference, $V^*_{ref,i}$, frequency reference, $f_{ref,i}$, and the filter output current, $i_{o,i}$. The adjusted sinusoidal voltage and current references served then as input reference signals to be observed by the FCS-MPC quality cost function for switching state optimized selection.

The semiconductors optimal switching state, $S_{n_{opt}}$, was obtained from the decisions made by the forecasting algorithm implemented in the FCS-MPC block. This block received both the converter current $i_{i,i}$ and the filter voltage, $v_{f,i}$ and calculated the predicted voltage $v_{f(k+2),i}$ and current $i_{i(k+2),i}$ for $k+2$ discrete time instant. Lastly, the predicted and refe-

rence voltage and current were used to minimize the converters quality cost function and set the optimal n switching state. Figure 3.10 presents the procedures flowchart of a converter primary control used to implement the adapted droop-based economic power sharing dispatch strategy.

In accordance to Olivares et al. (2014), the hierarchical control method have a very distinct time bases response, being of hours to days for tertiary control level and fractions of seconds for primary one. Therefore, for the present study, the microgrid tertiary control was implemented separately from the primary and considered time-fixed operational cost parameters for all distributed generators, being the units operational costs only dependent of the units instantaneous active power dispatch as described in section 2.5.1. Thus, the converter droop curves inclination, $k_{p,i}$ and $k_{q,i}$, and distributed generators priories, N_i, did not change over time.

As the microgrid tertiary control provided the maximum and minimum dispatchable voltage *rms* amplitudes, $V_{max,i,N}$ and $V_{min,i,N}$, and frequencies, $f_{max,i}$ and $f_{min,i}$, and hence, each individual distributed generator droop curve and primary control references operational range, it was necessary to be previously executed. Figure 3.11 illustrates the procedures flowchart of the tertiary control to implement the adapted economic dispatch strategy.

Figure 3.10 – Adapted droop-based economic power sharing strategy primary control procedures flowchart.

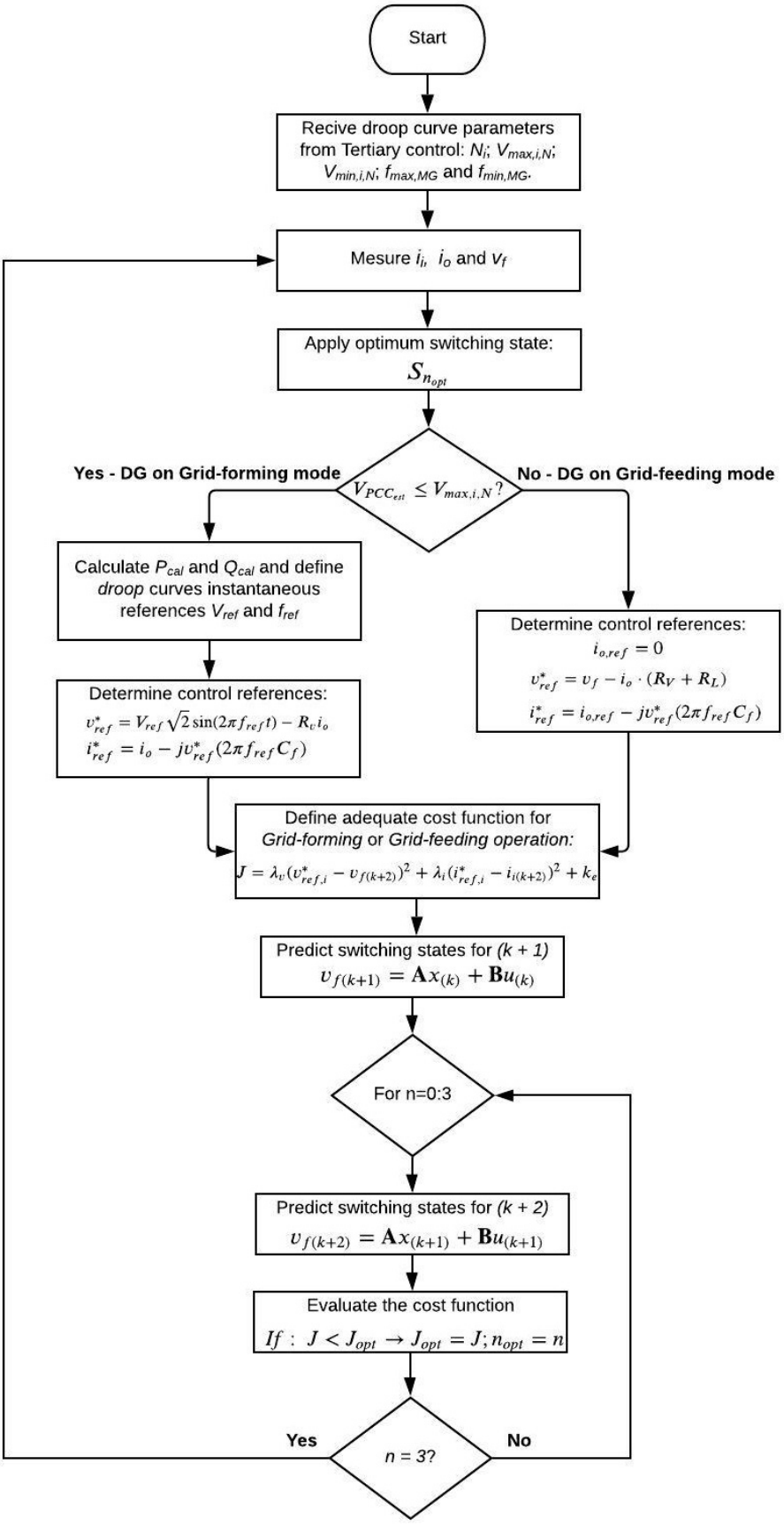

Source: From author (2021)

Figure 3.11 – Adapted droop-based economic power sharing strategy tertiary control procedures flowchart.

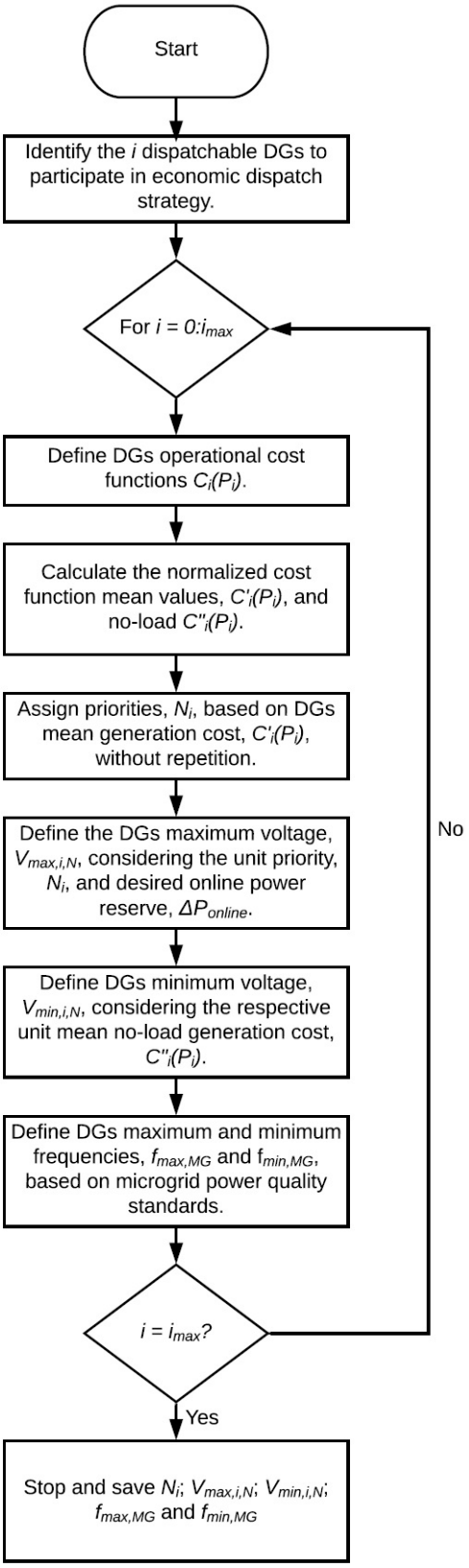

Source: From author (2021)

3.5 Adapted droop-based economic power sharing strategy software validation

To validate the adapted droop-based economic power sharing strategy operation, software simulations were performed considering the proposed microgrid as described in Section 3.1. The developed tests are presented in the following sections.

3.5.1 Virtual resistance parameter determination

The virtual resistance analysis developed in this study serves to demonstrate the capacity of the aforementioned technique to adjust system impedance characteristics for further proper application of the adapted droop-based economic power sharing strategy in a low-voltage island microgrid. The virtual resistance, R_v, control parameter are selected considering a mathematical model of the proposed electrical system. The R_v value is gradually incremented and the Thevenin equivalent circuit theorem is applied to verify the R_{eq}/X_{eq} grid impedance ratio from the converters perspective, and, simultaneously, the feeder overall electrical loss is observed.

As feeder lines impedance mismatch compensation is not the focus of the present study, to represent the low-voltage distribution system all feeder lines resistance are considered to be similar, R_L=$R_{L,1}$ = $R_{L,2}$ = $\cdots$ = $R_{L,i}$. And also, as converters power ratings are being considered to be equal, the selected R_v value is applied for every considered converter virtual resistance control loop, R_v=$R_{v,1}$ = $R_{v,2}$ = $\cdots$ = $R_{v,i}$.

A 0.5Ω value is considered for feeder $R_{L,i}$ resistance, which, together with the converter LC filter impedance, indicates a typically inductive system. Therefore, to adjust the grid impedance characteristic, the R_v value is defined on the basis of which a typically resistive behavior can be guaranteed and, consequently, a proper power sharing condition for the island low-voltage microgrid can be achieved.

A trade-off occurs between the system virtual resistivity enhancement and the voltage drop from the converter output and the microgrid point of common coupling. Therefore, the selection of and adequate R_v value for the simulated microgrid will also take into consideration the value which presents the lowest voltage drop possible in feeder lines.

3.5.2 Adapted droop-based economic power sharing strategy for low voltage microgrids validation

To perform software simulations in order to validate the adapted droop-based economic power sharing strategy, it is first necessary to implement a tertiary control level for the considered island microgrid, which based on the operational cost functions of each unit will dynamically set the individual voltage amplitude and frequency for every converter. The adapted power sharing strategy as microgrid tertiary control requires two input parameters sets: the operational cost function of local distributed generators and the considered power-quality standards for the low-voltage microgrid island operation.

As economic aspects are been considered for microgrid power sharing optimization, it is necessary to attribute distinct cost function models and parameter prices for the local power sources. Therefore, it is considered for converters 1 and 2 distinct primary power sources responsible for providing stable DC voltage to converters DC link. A renewable fuel-based cost function is present in Equation 3.42 which is considered for DG_1. In the same manner, a nonrenewable fuel-based cost function demonstrated in Equation 3.43 is assumed for DG_2. Both the operational cost function adopted here are based in the work of Nutkani et al. (2017).

Renewable fuel-based operational cost function model considered for distributed generator 1:

$$C_1'(P_{cal,1}) = [(F_1 + M_1 + \varepsilon_1) \cdot (P_{cal,1} + 0.05 + 0.01P_{cal,1} + 0.12P_{cal,1}^2)]/P_{max,1} \cdot 6.93^{-7} \quad (3.42)$$

Nonrenewable fuel-based operational cost function model considered for distributed generator 2:

$$C_2'(P_{cal,2}) = [M_2 \cdot P_{cal,2} + F_2 \cdot (4 + 12P_{cal,2} + 2P_{cal,2}^2) +$$
$$+\varepsilon_2 \cdot (1 - 2P_{cal,2} + 6.5P_{cal,2}^2 + 0.0002exp(3P_{cal,2}^2))]/P_{max,2} \cdot 6.93^{-7}$$

where $C_1(P_{cal,1})$ and $C_2(P_{cal,2})$ are the normalized operational cost per hour of distributed generators 1 and 2, calculated in relation to the instantaneous active power delivered by each converter, $P_{cal,1}$ and $P_{cal,2}$, respectively. $P_{max,1}$ and $P_{max,1}$ represents the distributed generators active power maximum rated capacity, which is considered of 500W for both units. Power loss, fuel and emission quadratic constants and other equipment-related parameters were obtained from the work of Nutkani et al. (2017). The adopted fuel, maintenance and emission cost va-

lues are presented in Table 3.2, where a generic monetary unit is assumed. The defined cost parameters are considered to be constant in time for the software simulations performed.

Table 3.2 – Fuel, maintenance and emission operational costs of distributed generators 1 and 2.

PARAMETERS	DG_1	DG_2
Fuel cost (F_i)	0.1 \$/kW	0.01 \$/kW
Maintenance cost (M_i)	0.01 \$/kW	0.02 \$/kW
Emission cost (ε_i)	0.005 \$/kW	0.01 \$/kW

Power quality parameters are defined in the following for the microgrid island operation as the second input parameters necessary to the adapted economic power dispatch strategy tertiary control implementation. The power quality parameters are selected considering a low-voltage distribution level power system, and the adopted values are based on national and international references for voltage and frequency ranges, respectively.

The reference values for voltage amplitude and frequency for the island microgrid operation were based on standard references for low-voltage distribution systems defined by the Brazilian national electricity agency (ANEEL), in the standard ANEEL/PRODIST (2018), Module 8: Power Quality. According to the aforementioned standard, the acceptable voltage *rms* values for a low-voltage distribution network must be within the range of $133V_{rms}$ to $117V_{rms}$, being 127_{rms} the nominal voltage value, V_{nom}. The maximum and minimum microgrid voltage reference values will then be considered among this standardized limits in order to analyze the system behavior in comparison with the low-voltage power quality parameters defined for the main power system.

In order to avoid any voltage limit violation, a narrower operation range for the microgrid island operation is considered. A security margin ζ of 3.5% was adopted, resulting in a strict voltage operational range of 128.555V to 121.445V for the microgrid maximum and minimum *rms* voltage values, $V_{max,MG}$ and $V_{min,MG}$, respectively. However, the microgrid PCC voltage amplitude is expected to experience below established threshold values due to virtual resistance impedance adjustment, once a secondary control with voltage amplitude recovery algorithm is not being considered in this study. The security margin value was selected in order to accommodate voltage signal oscillations while in stand-by operation.

As established by the IEEE (2013) standard, the frequency normal operational range is 59.3Hz to 60.5Hz for a microgrid while on island operation. Based on the aforementioned standard frequency operational range, to equalize the reactive-inductive and reactive-capacitive

droop power sharing capacity the values of 60.5Hz and 59.5Hz are adopted as the respective maximum and minimum operational frequencies, $f_{max,MG}$ and $f_{min,MG}$, for the island microgrid simulation. According to the resistive droop relations presented in section 2.4.2.2, a 60Hz reference is considered for the system under purely active power demand. Table 3.3 summarizes the considered voltage and frequency operational limits considered for all simulation tests performed.

Table 3.3 – Microgrid defined operational limits reference values.

PARAMETERS	
Microgrid maximum *rms* voltage ($V_{max,MG}$)	128.555 V
Microgrid minimum *rms* voltage ($V_{min,MG}$)	121.445 V
Microgrid maximum frequency ($f_{max,MG}$)	60.5 Hz
Microgrid minimum frequency ($f_{min,MG}$)	59.5 Hz

With the operational cost function definition for both distributed generators and with power quality parameters range definition for the island microgrid operation, the microgrid tertiary control can, therefore, set each unit respective droop curves by calculating the individual maximum and minimum operational voltage amplitude and frequency values.

To verify the adapted economic dispatch strategy power sharing capacity, four tests were elaborated considering distinct load natures and demand levels varying over time. The first three tests considered active and active-reactive demand steps for the proposed island microgrid with linear loads, being the first with purely resistive, Case 1: R, the second with resistive-inductive, Case 2: RL, and the third with resistive-capacitive, Case 3: RC, loads. The fourth test evaluated the microgrid operation with nonlinear load demand conditions, Case 4: NL, where single-phase rectifiers with RL loads were considered. Figure 3.1 presented previously in section 3.1 shows the microgrid location where each of the described load types were connected for tests purposes.

Three decreasing identical load steps connected in parallel with an interval of one second between them are considered for the microgrid power demand simulations. To simulate the demand of a purely resistive load, each step was considered with a resistance of 50Ω. For simulations with active-reactive demand, the identical resistance value of 50Ω was also considered for each of the three steps, being each load bank connected in series with a 50mH inductor for RL demand simulation and with a 150μF capacitor for RC load simulation. For the nonlinear loads test, a resistance of 50Ω and an inductance of 100mH are adopted, connected to single-phase rectifiers in each of the three steps considered.

For each demand condition considered, the active, P_i, and reactive, Q_i, powers shared by each distributed generator within the island microgrid can be analyzed simultaneously. Also their relations with the instantaneous voltage amplitudes, $V_{ref,i,N}$, and frequencies, $f_{ref,i}$, references defined by each converters primary control can be verified.

As the proposed strategy uses the FCS-MPC control technique where signal references are dynamically being set by the droop control according to instantaneous load condition, the sinusoidal output current, $i_{o,i}$, and voltage, $V_{f,i}$, of each unit will be observed as well.

3.5.3 Adapted droop-based economic power sharing strategy total generation costs comparative analysis

To verify the cost reduction efficiency of the adapted economic droop-based dispatch strategy, the microgrid TGC (*Total Generation Cost*) is calculated based on distributed generators 1 and 2 individual instantaneous operational costs, $C_1(P_{cal,1})$ and $C_2(P_{cal,2})$ respectively, for every power demand condition considered. As each distributed generator is assumed with a distinct cost function, the system operational cost will normally vary according to the each unit inherent droop-defined instantaneous power dispatch.

The total generation cost is calculated as presented in Equation 3.43, where the insertion of more distributed generators units are being considered as it will be further necessary for the proposed adapted strategy expandability verification.

$$TGC = \sum_{t=0}^{t_{max}} \sum_{i=1}^{i_{max}} C_{i,t}(P_{cal,i,t}) = \sum_{t=0}^{t_{max}} [C_{1,t}(P_{cal,1,t}) + C_{2,t}(P_{cal,2,t}) + \cdots + C_{i,t}(P_{cal,i,t})] \tag{3.43}$$

where $C_i(P_{cal,i})$ represents a distributed generator generic instantaneous operational cost based on the delivered active power $P_{cal,i}$. t_{max} represents total simulation time considered.

The obtained TGC values are compared with the total generation costs calculated from a tertiary control implemented with a conventional resistive droop method over equal microgrid demand conditions, allowing comparative cost reduction performance analysis.

3.5.4 Converters control mode transient analysis

To analyze the dynamic transition response of the adapted economic power sharing strategy in changing the distributed generators operational control mode, a short-time low-load demand is simulated.

A step-down RL load demand transitory event is considered for this test, which allows the analysis of both *P-V* and *Q-f* relations of droop control simultaneously. The control systems experiences an increase in droop voltage amplitude references as the active power demand drop from approximately 75% of the microgrid total capacity to a nearly no-load condition, resulting in a sudden change in the system overall voltage. After short period, the load demand is set to recover to its initial condition, causing a sudden drop in the microgrid voltage amplitude in accordance to the converters resistive droop inner controller.

The grid voltage amplitude variation is perceived locally at the connection point of the lowest dispatch priority distributed generator participating in the microgrid economic scheme, which will take action whether it is necessary to provide power to the system or remain in grid-feeding stand-by operation tracking a null output current reference as a short-time transitory measure.

As the adapted economic strategy is implemented for parallel distributed generators using the FCS-MPC method as converters switching state control technique, the controller inner dynamic references tracking capacity is verified. Both quality cost function reference signals, converter current $i^*_{ref,i}$ and filter capacitor output voltage $v^*_{ref,i}$, and the converter output reference current, $i_{o,i}$ are observed during converter control mode transition simulation.

The distributed generator control mode switching decision process will rely only in the simulated grid parameters measured locally at each convert output, sparing the use of other communications channels between local converters. With this test it will be possible to evaluate the adapted economic strategy transition algorithm performance during short-time low power demand conditions.

3.5.5 Adapted economic power sharing strategy expandability verification

As the economic dispatch strategy presented by Nutkani et al. (2017) was developed to allow the inclusion of several distributed generator in the power dispatch scheme, the adapted strategy expandability capacity is also verified. A third similar distributed generator is connected in the simulated island microgrid. The new unity is considered with the same power ratings

as the other two participating distributed generator, however with a distinct nonrenewable fuel-based operational cost function as presented in Equation 3.44.

$$C_3'(P_{cal,3}) = [M_3 \cdot P_{cal,3} + F_3 \cdot (2 + P_{cal,3} + 2P_{cal,3}^2) +$$
$$+\varepsilon_3 \cdot (1 - P_{cal,3} + 5.5P_{cal,3}^2 + 0.0002exp(3P_{cal,3}^2))]/P_{max,3} \cdot 6.93^{-7}$$

The new distributed generator cost function is considered with the system lowest operational cost, imposing an overall rearrangement in tertiary control assigned dispatch priorities of the local converters. The system configuration for this test is presented in Figure 3.12. Table 3.4 presents the adopted fuel, maintenance and emission costs related to the simulated distributed generators 1, 2 and 3.

Figure 3.12 – Microgrid topology for adapted economic power sharing strategy expandability verification.

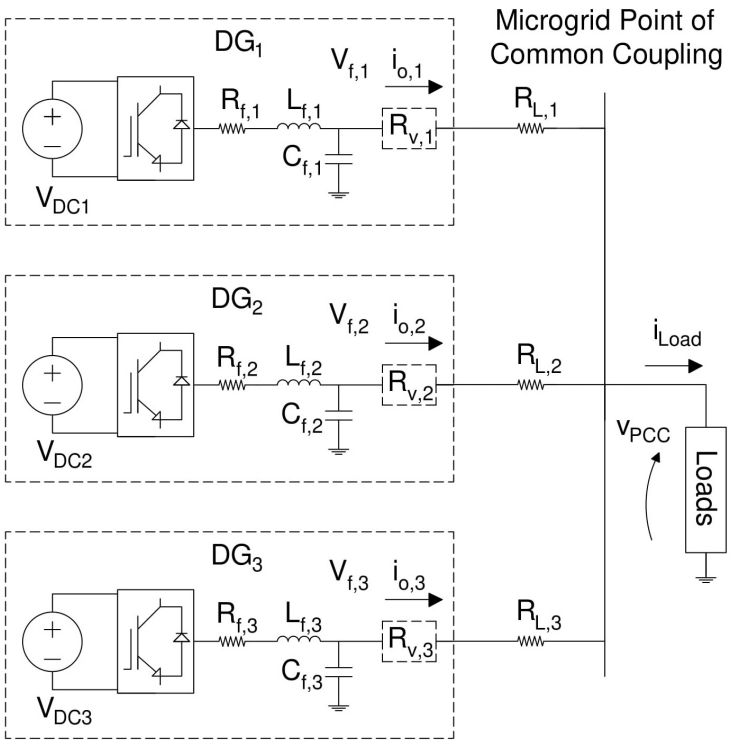

Source: From author (2021)

Table 3.4 – Fuel, maintenance and emission operational costs of distributed generators 1, 2 and 3.

PARAMETERS	DG_1	DG_2	DG_3
Fuel cost (F_i)	0.1 \$/kW	0.01 \$/kW	0.01 \$/kW
Maintenance cost (M_i)	0.01 \$/kW	0.02 \$/kW	0.02 \$/kW
Emission cost (ε_i)	0.005 \$/kW	0.01 \$/kW	0.001 \$/kW

Simulations are executed considering the same loads-banks demand conditions as previously performed for a two distributed generator system. Tertiary control dispatch priorities reassignment, active and reactive power sharing redistribution, Total harmonic distortions of microgrid voltages THD_V, and currents THD_I, and system overall cost reductions are observed.

4 RESULTS

For the adapted economic dispatch strategy validation, a single-phase low-voltage microgrid comprised by two distributed generators feeding a time-varying R, RL, RC and non-linear load banks was simulated using MATLAB/*Simulink* software environment. Table 4.1 presents the microgrid and distributed generators general parameters that are considered during the execution of software simulations for all the evaluated conditions.

Table 4.1 – Microgrid and distributed generators general parameters adopted for software simulations.

PARAMETERS	
Frequency reference ($f_{nom,MG}$)	60 Hz
DC link voltage ($V_{DC,1\ and\ 2}$)	310 V_{DC}
Converters maximum rated active power ($P_{max,1\ and\ 2}$)	500 W
Converters maximum rated reactive power ($Q_{max,1\ and\ 2}$)	500 VAR
Filters inductance ($L_{f,1\ and\ 2}$)	2.0 mH
Filters capacitance ($C_{f,1\ and\ 2}$)	60 μF
Internal filters resistance ($R_{f,1\ and\ 2}$)	0.1 Ω
Feeder lines resistance ($R_{L,1\ and\ 2}$)	0.5 Ω
Simulation sampling time (T_s)	2.5 μs

For each distributed generator is assumed a rated active power of 500W, $P_{max,1}$ and $P_{max,2}$, resulting in a 1000W microgrid total generation capacity. Also, a maximum reactive power dispatch of 500VAR is considered for each unit.

The distributed generators primary sources are considered to be providing a stable DC voltage signal to the converters DC link. For the simulated conditions, each converter DC-link are considered to be fed from an ideal DC power source providing a constant 310V_{DC} voltage signal, $V_{DC,1}$ and $V_{DC,2}$. This DC voltage amplitude is selected in order to eliminate the necessity of DC/DC converters or voltage step-up transformers as presented in the work of Guimaraes (2019). Also, single-phase H-bridge electronic converters with LC output filters are being considered as the integration element between the DC-link to the microgrid AC busbar, adding proper voltage reference controllability and fast-time response capacity to the system. As result, the considered distributed generators can be controlled as fully dispatchable units, providing power continuously to the island microgrid according the instantaneous power demand.

A 2.0mH inductor and a 60μF capacitor are considered for the converters output LC filters. The respective filter inductance, L_f, and capacitance, C_f, were selected considering proper FCS-MPC operation in regulating converters output voltage. More details considering

LC filter design procedures can be found in the work of Guimaraes (2019). For the considered converter LC filter, the cutoff frequency is approximately 460 Hz. Also, an electric resistance of 0.5Ω is considered for both feeder lines, $R_{L,1}$ and $R_{L,2}$, connecting distributed generators 1 and 2 to the microgrid PCC.

An adaptation coefficient γ of 0.09 and a damping factor ζ of 1.414 were considered in this study based on the ANF-FE speed and accuracy optimization achieved in the work of Silva (2019). In order to avoid switching states to be repeatedly selected, a restriction k_e was considered whiting the FCS-MPC cost function. Also, a weighting factor λ_i was adopted to enhance current reference tracking performance while on grid-feeding operation. The cost functions defined for converters simulations on grid-forming and grid-feeding operation modes are presented in Equations 4.1 and 4.2, respectively.

$$J = (v^*_{ref} - v_{f(k+2)})^2 + (i^*_{ref} - i_{i(k+2)})^2 + k_e \tag{4.1}$$

$$J = (v^*_{ref} - v_{f(k+2)})^2 + 100 \cdot (i^*_{ref} - i_{i(k+2)})^2 + k_e \tag{4.2}$$

Prior to the software simulations of the adapted economic dispatch strategy, it is firstly necessary to determine the primary control virtual resistance values, $R_{v,1}$ and $R_{v,2}$, to ensure proper power sharing capability within the low-voltage microgrid. Once the virtual resistance values are defined, the following tests are performed to validate the adapted economic dispatch strategy:

- Microgrid linear and nonlinear load demand variations considering purely active, active-reactive inductive and capacitive, and nonlinear three power demand steps: R, RL, RC and NL;
- Adapted economic dispatch strategy and conventional resistive droop method operational costs comparative analysis;
- Converters control mode transient analysis for sudden short-time RL load variation;
- Adapted economic power sharing strategy expandability verification with the addition of a third cost-distinct distributed generator in the considered system.

The MATLAB/*Simulink* simulation diagrams developed can be seen in Appendix A. The implemented algorithms for primary and tertiary control considering traditional droop method and the adapted economic power sharing strategy are presented in Appendix B.

4.1 Virtual resistance parameter determination

To determine an adequate virtual resistance R_V value to ensure the effectiveness of *P-V/Q-f* resistive droop power sharing capacity by emulating the presence of a real resistance between converters output and the microgrid PCC, a system impedance model based on Thevenin equivalent circuit theorem was elaborated in MATLAB.m software environment. The aforementioned algorithm can be visualized in Appendix C.

For the virtual resistance impact analysis over the considered microgrid impedance, the predefined impedance values for converter LC filter, $\mathrm{L}_{f,i}$, $\mathrm{C}_{f,i}$ and $\mathrm{R}_{f,i}$, and feeder resistance, $\mathrm{R}_{L,i}$, between the power source i and the microgrid PCC were considered to be constant. Therefore, the R_V influence over the system overall impedance condition could be analyzed. Figure 4.1 presents the system behavior for a $R_{V,i}$ parameter variation from 0 to 6Ω, where a trade-off between $R_eq,i/X_eq,i$ ratio and the estimated microgrid PCC voltage drop can be visualized.

Without a virtual resistance adjustment, $R_V = 0$, the system $R_{eq,i}/X_{eq,i}$ ratio is 0.27. In this scenario, the estimated voltage drop percentage is 1.7% and occurs mainly due to converter LC filter and feeder impedance. In accordance to the work of Rocabert et al. (2012), this ratio value is commonly observed in high voltage system, where highly inductive behavior is expected.

To improve the resistive behavior of the considered microgrid in order to simulate a low-voltage distribution system, a virtual resistance, R_V, of 4.0Ω is considered. The R_V iterative determination process assumed the lowest value in which the system resistive behavior could be guaranteed, therefore avoiding active and reactive power coupling while keeping the lowest microgrid PCC estimated voltage drop.

Figure 4.1 – Estimated converter voltage drop for system Thevenin equivalent impedance ratio variation.

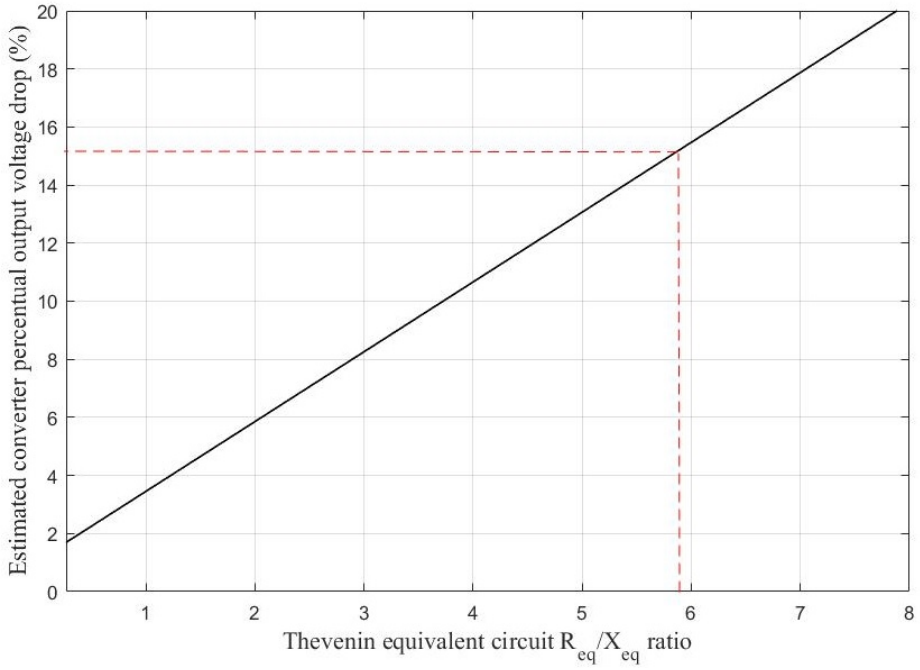

Source: From author (2021)

The adopted virtual resistance value is assumed for both distributed generators, $R_{V,1} = R_{V,2} = 4.0\Omega$, as feeders impedance, $R_{L,1}$ and $R_{L,2}$, and converters LC filters are considered to be equal. As illustrated in Figure 4.1, the resulting $R_{eq,i}/X_{eq,i}$ impedance ratio is 5.91 with a maximum microgrid PCC estimated voltage drop of 15.3% while the system operates under maximum power demand condition. Hence, the maximum estimated voltage drop occurs when the system requires the distributed generator rated output current, $i_{o,i,max}$, while operating at reference-defined minimum voltage amplitude, $121.445\text{V}_{min,MG}$.

According to Rocabert et al. (2012), the selected virtual impedance value adjust the system impedance behavior to a predominantly resistive biased circuit, imitating a typical low-voltage distribution system. With the virtual impedance adjustment value definition, the microgrid resistive behavior can be guaranteed and the adapted economic power sharing strategy for low-voltage systems software simulations can be performed next.

4.2 Adapted droop-based economic power sharing strategy validation

For validation process of the adapted droop-based economic power sharing strategy, an ordered hierarchical control structure must be implemented for the considered island microgrid. The first part consist in the implementation of the proposed strategy as microgrid tertiary control level, which is set to determine from time invariant generators operational cost models and

from power quality parameters the distributed generators dispatch sequence. Consequently, the operational limits and respective droop curves equations for each considered distributed generator are also determined.

In sequence, proper primary level controllers are implemented for each dispatchable distributed generators. The local controllers considers the FCS-MPC control method to coordinate the switching states optimization selection process for the H-bridge single-phase converters, while following a dynamic droop-defined voltage signal reference. As the system resistive behavior could be enhanced using virtual resistance technique, the active and reactive power sharing capacity within the considered low-voltage microgrid can then be analyzed.

4.2.1 Tertiary control implementation - Two distributed generation units microgrid

Initially, the tertiary control algorithm implementing the adapted droop-based economic power sharing strategy is executed for the considered island microgrid comprised of two cost-distinct distributed generators. The algorithm for the adapted droop-based economic power sharing strategy implementation as microgrid tertiary control level can be visualized in Appendix .2.1.

The distinct power sources operational cost functions parameters adopted and also the considered island microgrid power quality parameters used as algorithm inputs are described in section 3.5.2, Tables 3.2 and 3.3, respectively.

The considered distributed generators normalized cost functions presented in Equations 3.42 and 3.43 are illustrated in Figure 4.2. From the normalized cost curves, the average operational costs, $C'_{med,1}$ and $C'_{med,2}$, and the dispatch priority sequencing could be obtained for DG_1 and DG_2, respectively. The considered cost function normalized average values and distributed generators dispatch priorities are presented in Table 4.2.

Figure 4.2 – Normalized operational cost functions of distributed generators 1 and 2.

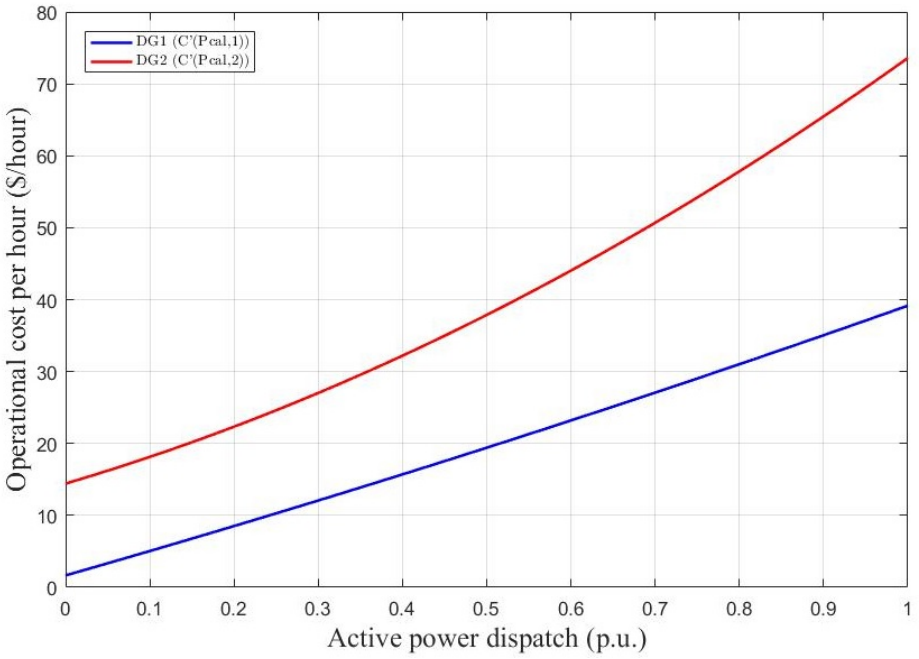

Source: From author (2021)

Table 4.2 – Average operational costs and power dispatch priority for distributed generators 1 and 2.

PARAMETERS	DG_1	DG_2
Average normalized cost ($C'_{med,i}$)	19.76 $/hour	39.92 $/hour
Power dispatch priority order (N_i)	1	2

Considering the power quality parameters defined in Table 3.3 for the island microgrid operation and assuming a maximum and minimum dispatch voltage range, ΔV_{max} and ΔV_{min}, of 5V and 3V, respectively, and an online power reserve, ΔP_{online}, of 50%, the adapted strategy characteristic active power droop curves could be determined. Figure 4.3 presents the obtained adapted economic strategy *P-V* droop-characteristic control curve for the considered two DG microgrid.

As can be visualized in Figure 4.3, the adapted strategy sets the lowest cost unit, DG_1, with the highest dispatch priority, $N_1 = 1$, thus enhancing the amount of active power shared by the respective generator by setting high voltage amplitude references over the system operation, and also allowing this unit functioning even in low-demand conditions.

Figure 4.3 – Adapted decentralized economic power sharing strategy P-V droop curves for distributed generator 1 and 2.

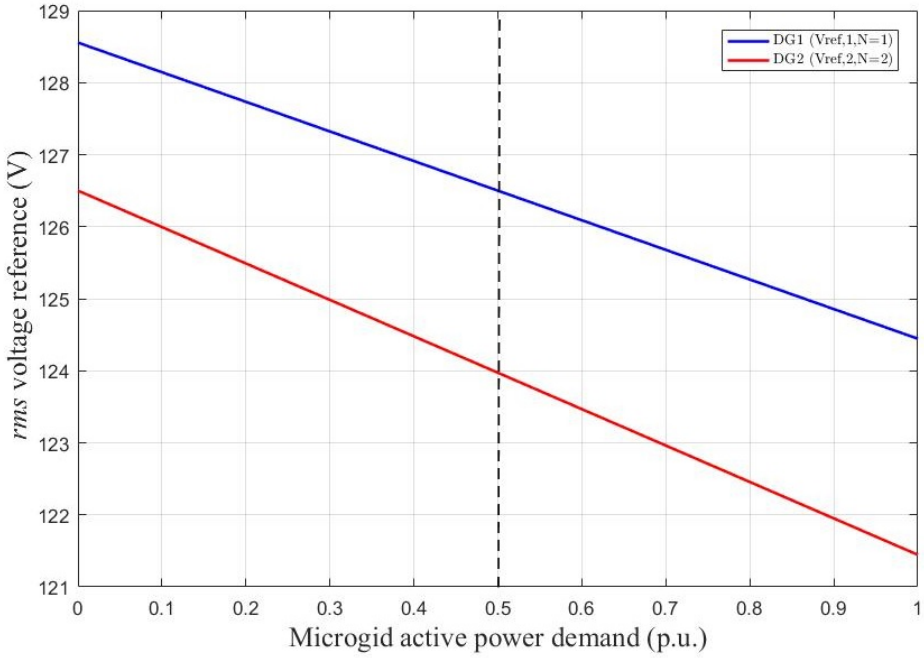

Source: From author (2021)

Figure 4.4 – Adapted decentralized economic power sharing strategy Q-f droop curves for distributed generator 1 and 2.

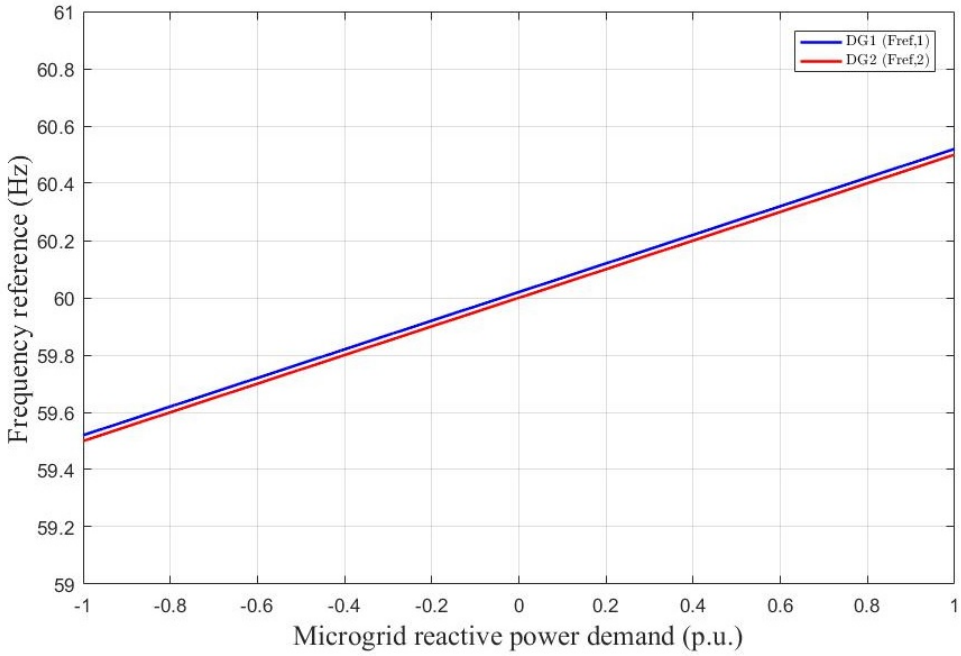

Source: From author (2021)

The *Q-f* adapted economic strategy droop-characteristic curves for both units are also determined by the tertiary control algorithm and are illustrated in Figure 4.4. As can be seen,

both converters droop curves are overwritten, and hence the microgrid reactive power demand is equally shared among the same rate units as in traditional droop scheme.

Table 4.3 summarizes the obtained maximum and minimum voltage and frequency operational references, and the droop curves inclination coefficients. These parameters were calculated in relation to the generators average operational cost, the selected online power reserve and the power quality parameters assumed for the low-voltage island microgrid as defined in the adapted Equations 3.37 and 3.38.

Table 4.3 – Adapted droop-based power sharing strategy tertiary control parameters definition for distributed generators 1 and 2.

PARAMETERS	DG_1	DG_2
Maximum operational *rms* voltage ($V_{max,i,N}$)	128.555 V	126.50 V
Minimum operational *rms* voltage ($V_{min,i,N}$)	124.445 V	121.445 V
Maximum operational frequency ($f_{max,MG}$)	60.5 Hz	60.5 Hz
Minimum operational frequency ($f_{min,MG}$)	59.5 Hz	59.5 Hz
Droop voltage curve coefficient ($k_{p,i,N}$)	4.11 $V/P_{1p.u.}$	5.055 $V/P_{2p.u.}$
Droop frequency curve coefficient ($k_{q,i,N}$)	1 $V/Q_{1p.u.}$	1 $V/Q_{2p.u.}$

Therefore, with the parameters presented in Table 4.3, it is possible for the distributed generators primary controllers to dynamically set their respective output voltage signal references related to the instantaneous delivered active and reactive power demand, $P_{cal,i}$ and $Q_{cal,i}$, hence controlling the converter output current without the use of parallel communication systems.

Also, the maximum operational voltage amplitude defined for DG_2, $V_{max,i,N} = 126.50V$, servers as threshold between grid-forming and grid-feeding mode of operation definition. As DG_2 presented the highest average operational cost $C'_{med,i} = 39.92\$/hour$, and hence, the microgrid lowest dispatch priority, $N_2 = 2$, the unity control logic is set as presented in Equation 3.40 for the low-voltage adapted economic power sharing strategy. As DG_1 is evaluated with the microgrid highest dispatch priory, $N_1 = 1$, this unity is set to operate always as grid-forming unit, hence providing voltage reference for the microgrid system even in low-demand conditions.

As in the original economic dispatch strategy proposed by Nutkani et al. (2017), the adapted strategy sets the highest dispatch priority to the relative operational less expensive distributed generator, setting proper cost-defined droop curves to the system. Therefore, the adaptation for a low-voltage mainly resistive microgrid with *P-V/Q-f* droop relations was correctly

related to the original *P-f/Q-V* decentralized economic dispatch strategy for predominantly inductive system.

With dispatch priorities definition for DG_1 and DG_2, and with the respective droop curves determination for primary control inner reference setting, power sharing software simulations for time-varying R, RL, RC and nonlinear loads and further tests can be performed. The tertiary control defined parameters presented in Table 4.3 are sent to each considered distributed generator local controller allowing the analysis of power sharing capacity of the two parallel converter using FCS-MPC primary controllers in order to validate the adapted economic strategy over the proposed low-voltage island microgrid. The algorithm implemented in converters primary control is presented in Appendix B and the microgrid simulation and load-banks schematics can be seen in Appendix A.

4.2.2 Two DG units microgrid under active power demand - Case 1: R loads demand

Initially the defined low-voltage microgrid was simulated considering a purely active power demand. The simulated load-bank consisted of three 50Ω parallel resistors connected to the microgrid PCC, being simulated in sequential step disconnection considering a time interval of 1 second between them. Each parallel R load was considered with a nominal power demand of 320VA, considering nominal voltage of 127V/60Hz.

Figure 4.5 – Adapted economic strategy software simulation for two DG units microgrid - Case 1: R loads demand: a) Active power sharing; b) Microgrid *rms* voltages.

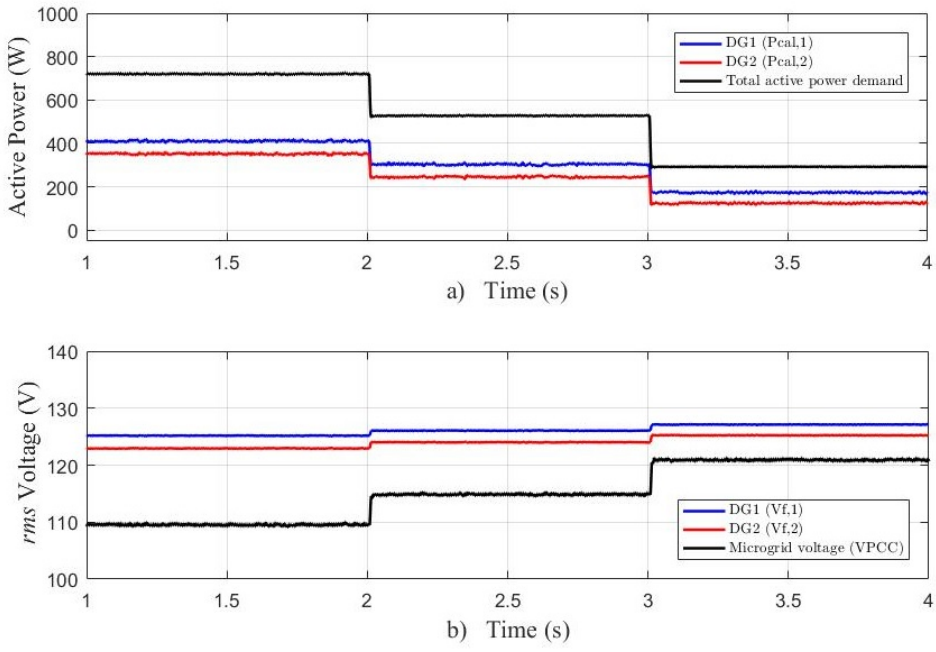

Source: From author (2021)

The active power sharing and the instantaneous droop *rms* voltage reference are presented in Figure 4.5. From this, it is possible to observe the DG_1 active power share represents a larger proportion in relation to the microgrid total demand, as in accordance to the adapted economic strategy priority designation and the respective droop curve proportionality, Figure 4.3.

Figure 4.6 demonstrates the microgrid reactive power sharing and the instantaneous droop frequency reference. It is possible to notice that no reactive power is shared among the distributed generators in accordance to the simulated load nature, despite some minor transitory events during load demand variations. Therefore, the converters inner frequency references are set to the nominal standard reference of 60Hz in accordance to the adapted economic strategy control logic.

Figure 4.6 – Adapted economic strategy software simulation for two DG units microgrid - Case 1: R loads demand: a) Reactive power sharing; b) Microgrid frequencies.

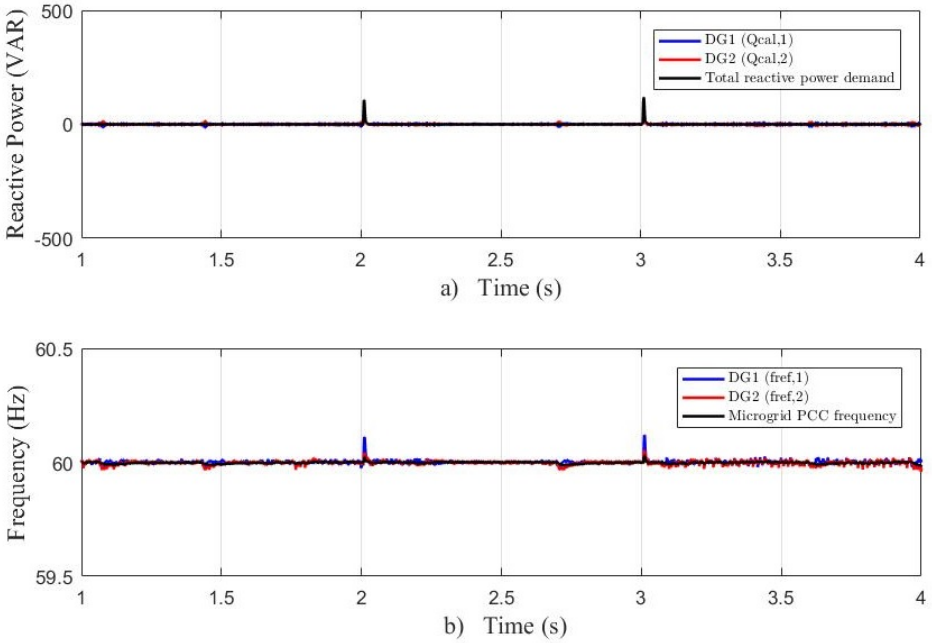

Source: From author (2021)

When comparing Figures 4.5 and 4.6, it is possible to visualize that virtual resistance selection was satisfactory in adjusting the system resistive behavior and, therefore, avoiding active and reactive power coupling issues, even when DG_1 and DG_2 shares different proportions of active power within the simulated low-voltage system.

The voltage and current signals for the simulated load demand condition are presented in Figure 4.7. It is possible to observe the FCS-MPC capacity in following the dynamically set voltage reference, providing proper sinusoidal voltage to the island system. Converter output current signal are identified to be sharing harmonic components as no active compensation

system or virtual harmonic damping are implemented as microgrid secondary control. However, load current signal presented typical sinusoidal behavior as purely resistive loads are being considered.

Figure 4.7 – Adapted economic strategy software simulation for two DG units microgrid - Case 1: R loads demand: a) Voltage signals; b) Current signals.

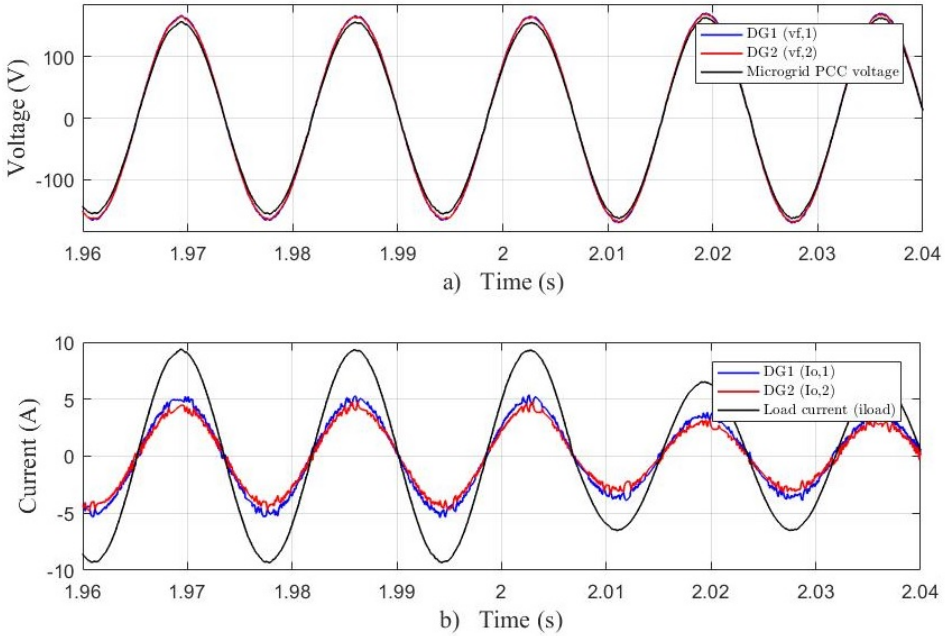

Source: From author (2021)

Observing Figures 4.5 and 4.7 a), it is possible to identify the voltage drop between the microgrid PCC voltage level and converters 1 and 2 output voltages. Feeder resistance and the considered R_V virtual resistance adjustment parameter are responsible for the effect, thus reducing the system power sharing capacity and degrading the microgrid PCC voltage amplitude level. Nevertheless, the adopted primary control structure prove effective in sharing proportional power among parallel connected converter while keeping proper sinusoidal voltage signal within the simulated system.

4.2.3 Two DG units microgrid under active and inductive-reactive power demand - Case 2: RL loads demand

To validate the performance of the adapted droop-based economic strategy in sharing active and reactive power simultaneously, an RL load bank power demand were considered. The RL load bank is composed of three parallel 50Ω resistors in series with 50mH inductors. The RL load demand test were conducted similarly as done in previous R load simulation.

Each RL load represented an equivalent nominal power demand of approximately 300VA to the island system while considering a nominal voltage of 127V/60Hz.

Figure 4.8 presents the active power shared and the respective converters *rms* voltage inner droop-defined references. Also, the microgrid PCC *rms* voltage and the total active power demand for the considered case are shown. The presence of reactive load component lessened the system active power sharing capacity when comparing the results obtained in previous simulation, (FIGURE 4.5). Nevertheless, similar system control behavior could be identified while sharing active power as the highest priority unit participates in a larger proportion of the total active demand.

Figure 4.8 – Adapted economic strategy software simulation for two DG units microgrid - Case 2: RL loads demand: a) Active power sharing; b) Microgrid *rms* voltages.

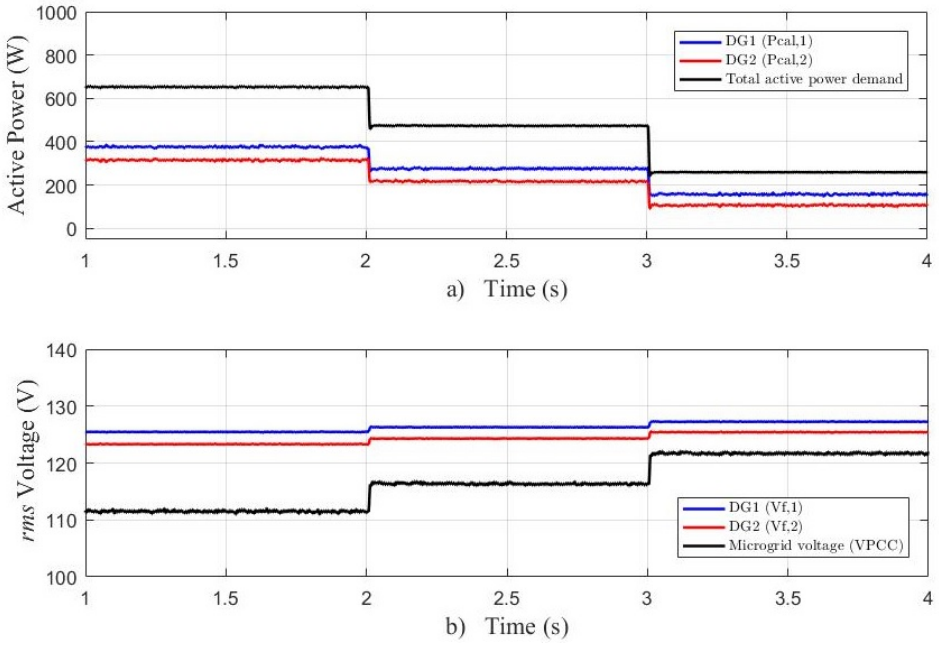

Source: From author (2021)

Figure 4.9 presents the reactive power sharing and primary controlled internal droop-defined frequency references for the RL load demand simulation test. The converters reactive power, $Q_{cal,1}$ and $Q_{cal,2}$, were equally shared among both units, Figure 4.9 a), in accordance to the respective predefined droop *Q-f* control curve. As the adapted economic strategy only considers cost-related aspects to active power sharing, the reactive power must be shared among the distributed generators considering only their respective power ratings. As stated by Nutkani et al. (2017), reactive power sharing may be more appropriate to be managed by a higher level controller when considering island microgrids, as power quality aspects must be also considered.

As reactive-inductive loads are being considered, voltage and current circulating harmonic components increases over the system, and the ANF-FE presented an oscillatory response while calculating reactive power. This effect can be observed as oscillatory behavior in the definition of converters frequency references as presented in Figure 4.9 b). Nevertheless, the microgrid overall frequency reference increases in accordance to the adopted droop control logic, indicating the presence of reactive-inductive power demand in the system as can be visualized in Figure 4.9 b).

Figure 4.9 – Adapted economic strategy software simulation for two DG units microgrid - Case 2: RL loads demand: a) Reactive power sharing; b) Microgrid frequencies.

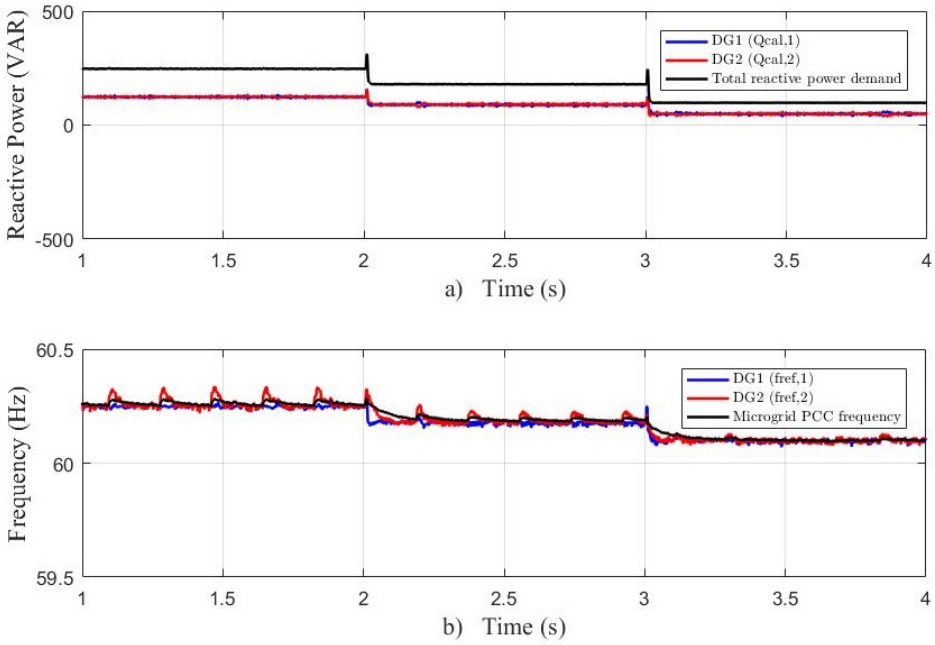

Source: From author (2021)

Figure 4.10 presents both converters and microgrid voltage and current signals for the simulated active and reactive-inductive load demand condition. As can be observed, the parallel connected FCS-MPC controlled converters were able to keep following the internal droop-set voltage reference signals while providing the system with active and reactive-inductive currents. Both voltage and current signals are seen to be predominantly sinusoidal, however converters output current signals are perceived to be sharing higher amounts of harmonic distortion components. Similarly as identified in the work of Guimaraes (2019) for a single FCS-MPC controlled converter, a smooth transition during RL load transients can be observed for the parallel connected FCS-MPC controlled units.

Figure 4.10 – Adapted economic strategy software simulation for two DG units microgrid - Case 2: RL loads demand: a) Voltage signals; b) Current signals.

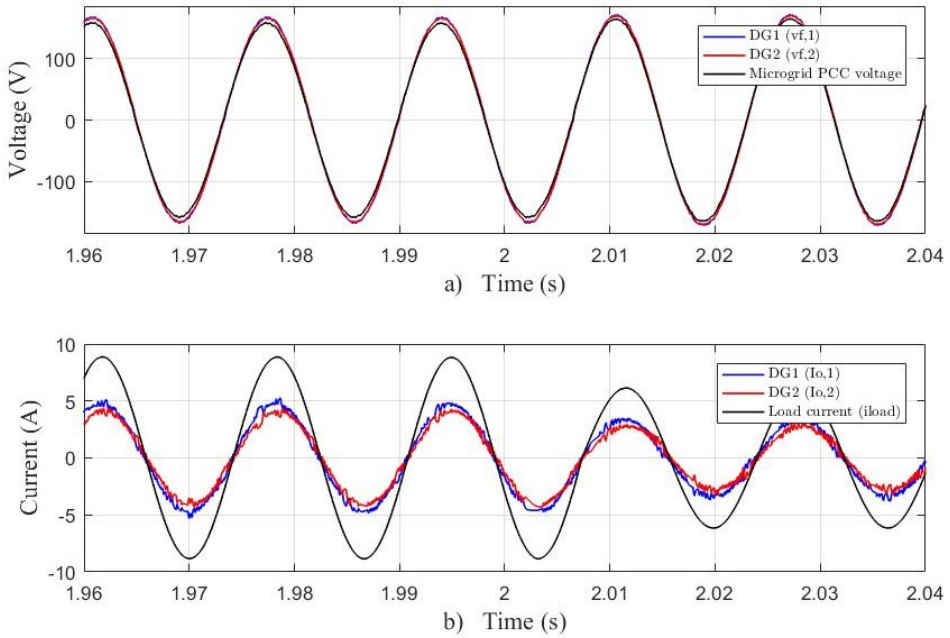

Source: From author (2021)

In Figure 4.10, an angular displacement between voltage and current signals can be observed with a relative delay in current signal, indicating the self-regulating capacity of the parallel primary controlled in sharing active and reactive-inductive components.

4.2.4 Two DG units microgrid under active and capacitive-reactive power demand - Case 3: RC loads demand

The adapted droop-based economic strategy primary control response is also analyzed for active and reactive-capacitive load demand condition. Similarly to the previous simulations, three parallel RC loads are considered. The simulated loads comprises three sets of 1.5μF capacitor connected with 50Ω resistors, resulting for each load set an equivalent power demand of approximately 300VA considering the nominal voltage of 127V/60Hz.

Figure 4.11 presents the active power shared among the converter and the respective units *rms* voltage inner droop-defined references for the active and reactive-capacitive load demand simulation. As perceived in previous RL load demand simulation, the reactive-capacitive load component downgrades the primary controller active power sharing capacity. However, the control system also acted according to the adapted economic strategy droop proportion definition, imposing DG_1 to provide a larger active power portion to supply the overall system demand.

Figure 4.11 – Adapted economic strategy software simulation for two DG units microgrid - Case 3: RC loads demand: a) Active power sharing; b) Microgrid *rms* voltages.

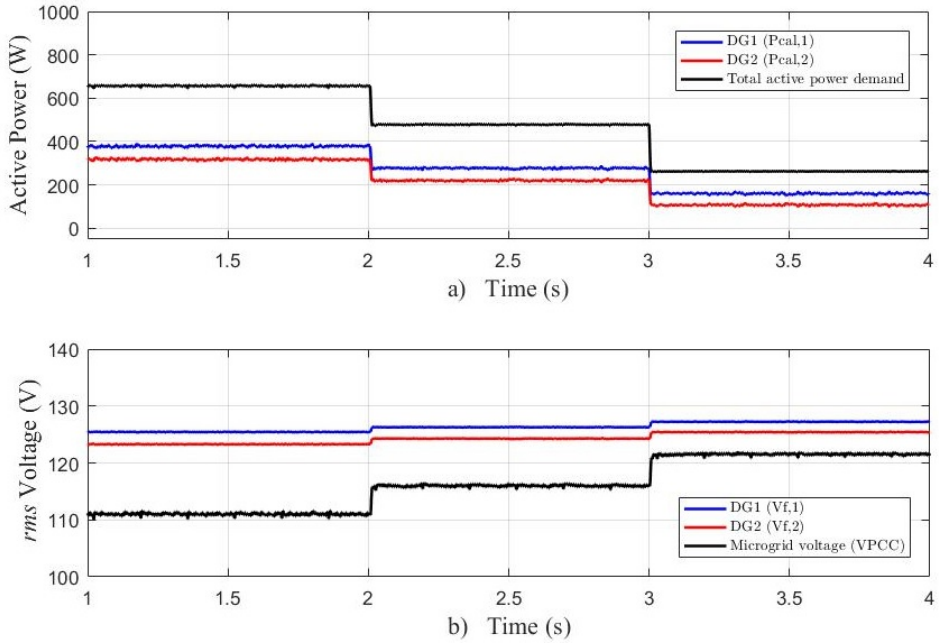

Source: From author (2021)

Figure 4.9 presents the reactive power sharing and primary controlled internal droop-defined frequency references for the RC load demand simulation. As can be noticed, the converters reactive powers, $Q_{cal,1}$ and $Q_{cal,2}$, were also equally shared among both units, Figure 4.9 a), according to the tertiary control defined *Q-f* droop curve.

In opposition to the RL load demand condition, the microgrid overall frequency reference decreases when RC loads are concerned. This behavior indicated the converters defined primary controllers capacity in correctly follow the adapted economic strategy *Q-f* droop control curve reference presented in Figure 4.4. Also in this simulation test, the ANF-FE presented a oscillatory response while calculating reactive power. This effect can be observed as the oscillatory behavior in the definition of converters frequency references as presented in Figure 4.12 b).

Figure 4.12 – Adapted economic strategy software simulation for two DG units microgrid - Case 3: RC loads demand: a) Reactive power sharing; b) Microgrid frequencies.

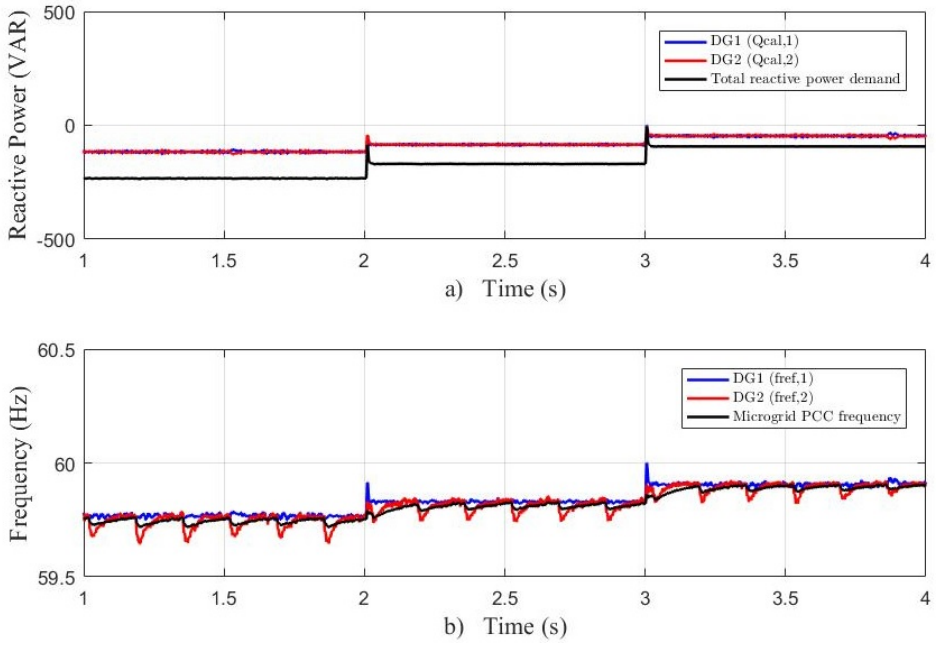

Source: From author (2021)

Figure 4.13 presents both converters and microgrid voltage and current signals for the simulated active and reactive-capacitive load demand condition. Also in this simulation, the parallel connected FCS-MPC controlled converters were able to keep following the internal droop-set voltage reference signals while providing the system with active and reactive-capacitive currents. Both voltage and current signals also proved to be predominantly sinusoidal, with a smooth transition during load transients, similarly as observed in the previous RL load demand simulation.

As observed in the previous RL power demand simulation, an angular displacement between voltage and current signals is also noticeable, occurring with a negative current signal displacement in relation to voltage in this case. Therefore, the parallel converters primary control system self-regulating capacity in managing proportional sharing of both active and reactive-capacitive load demand is also validated in this simulation

Figure 4.13 – Adapted economic strategy software simulation for two DG units microgrid - Case 3: RC loads demand: a) Voltage signals; b) Current signals.

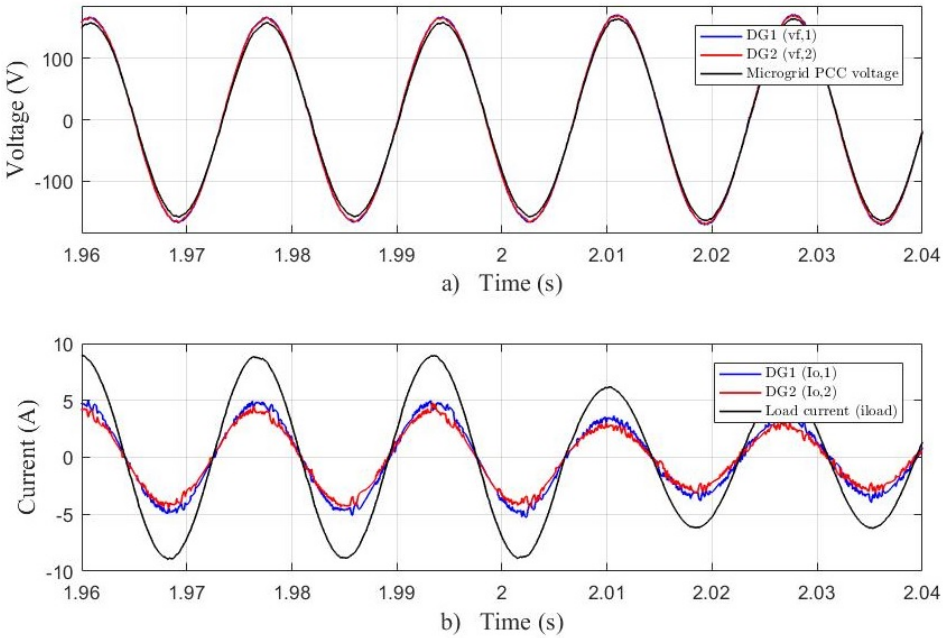

Source: From author (2021)

4.2.5 Two DG units microgrid under nonlinear loads power demand - Case 4: NL loads demand

The parallel converters primary controller behavior are also verified in attending nonlinear loads while implementing the adapted droop-based economic strategy in the simulated system. A three set of single-phase rectifiers connected to RL loads with 50Ω resistance and 100mH inductance are considered to simulate the nonlinear load demand steps. Each nonlinear load set represented a system power demand of approximately 280VA under nominal voltage of 127V/60Hz.

Figure 4.14 presents the active power sharing among the parallel connect FCS-MPC converter simulating nonlinear load demand condition. Oscillations are perceived in active power measurement ANF-FE algorithm response as currents are considerably distorted. Therefore, the droop-set voltage amplitude references also indicated oscillatory behavior. However, the controller where able to follow the power dispatch priority as DG_1 can be seen providing relative higher portion of active power to the simulated system as defined in the adapted economic strategy characteristic *P-V* droop control curve.

Figure 4.14 – Adapted economic strategy software simulation for two DG units microgrid - Case 4: NL loads demand: a) Active power sharing; b) Microgrid *rms* voltages.

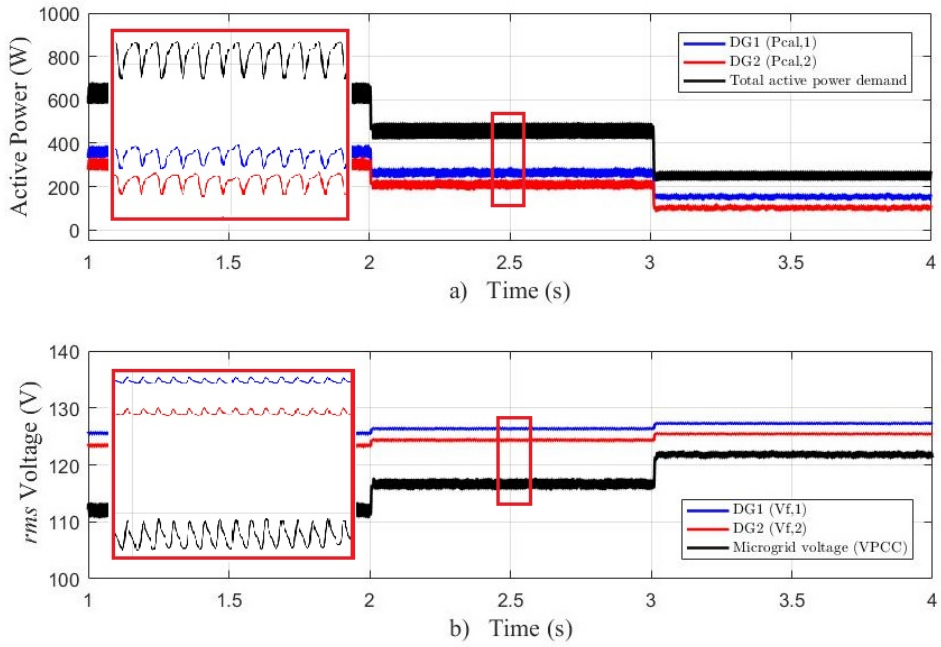

Source: From author (2021)

Figure 4.15 – Adapted economic strategy software simulation for two DG units microgrid - Case 4: NL loads demand: a) Reactive power sharing; b) Microgrid frequencies.

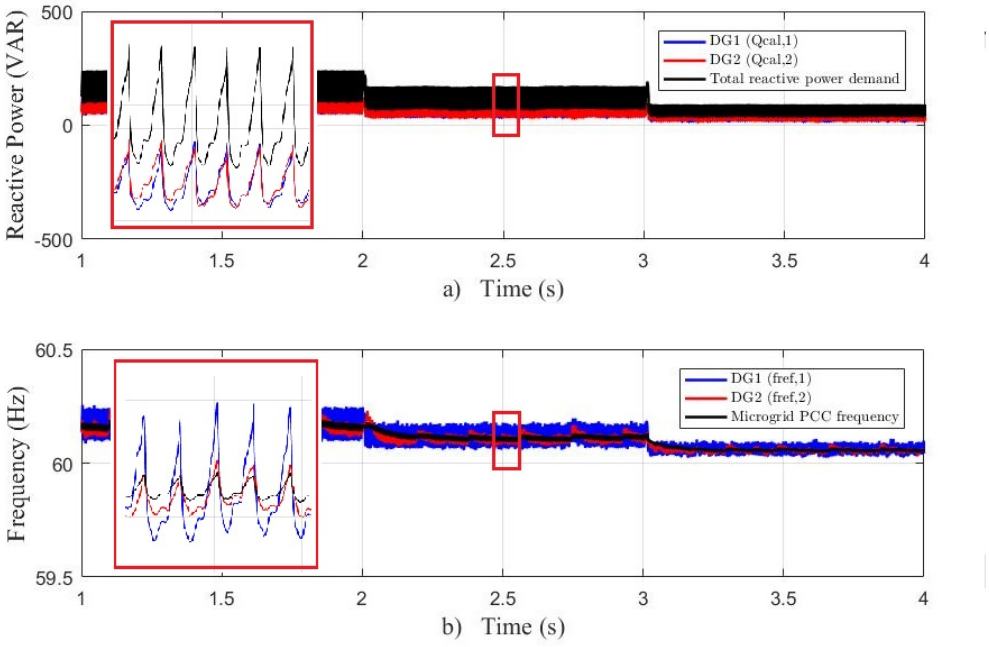

Source: From author (2021)

Also in Figure 4.15, the presence of harmonic distortions caused oscillatory effects over the reactive power measurement and, therefore, in the converters internal frequency reference definition. The reactive power observed while simulating nonlinear loads occur mainly due

to non-ideal diode switching, causing an angular displacement between voltage and current signals. Nevertheless, the primary control system demonstrated its capacity to share active and reactive powers according to the adapted economic strategy even in the presence of harmonic oscillatory effects over the power calculation algorithms as demonstrated in Figure 4.14 a).

The presence of nonlinear harmonic distortions in the current signal illustrated in Figure 4.16, b), causes oscillatory effects in the ANF-FE signal filtering and, consequently, in the converters active and reactive power calculations, $P_{cal,i}$ and $Q_{cal,i}$. Therefore, the droop-calculated voltage and frequency references are set by oscillatory power measurement inputs, leading to a FCS-MPC tracking of oscillatory references signals.

Figure 4.16 – Adapted economic strategy software simulation for two DG units microgrid - Case 4: NL loads demand: a) Voltage signals; b) Current signals.

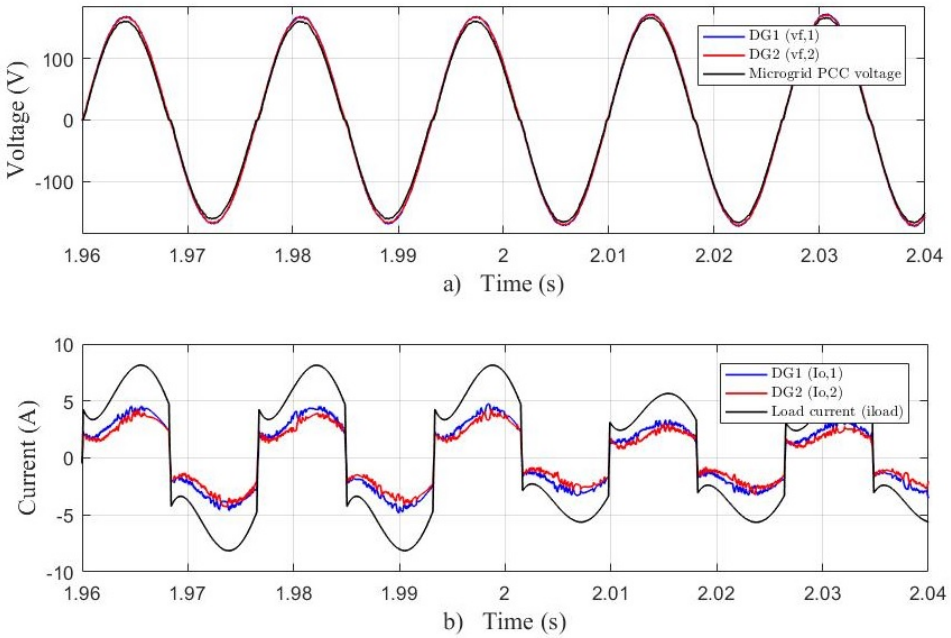

Source: From author (2021)

As stated by Guimaraes (2019), it is difficult to maintain a purely sinusoidal voltage when nonlinear loads are connected to the converter due to current signal harmonics. Circulation of current harmonic components can cause resonances and increase the voltage THD. However, a predominately sinusoidal converters 1 and 2 output voltage, $V_{f,1}$ and $V_{f,2}$, and microgrid PCC voltage signal, v_{PCC}, can be observed in Figure 4.16 a) on the considered simulation test. Therefore, the parallel connected FCS-MPC controlled converters implementing the adapted economic power sharing strategy proved effective in maintaining a typically sinusoidal voltage signal over the simulated microgrid while attending nonlinear loads

4.2.6 Total harmonic distortion analysis - Two distributed generation units microgrid

Tables 4.9 and 4.10 presents the total harmonic distortion for voltage, THD_V, and current, THD_I, calculated for the considered R, RL, RC and nonlinear load demand conditions in the simulated two distributed generator microgrid. The THD_V and THD_I results were obtained from simulations using the MATLAB/ *Simulink* FFT (*Fast Fourier Transform*) tool.

Table 4.4 – Voltage signals THD analysis - Two distributed generator microgrid.

PARAMETERS	Total Harmonic Distortion - THD_V			
	Case 1: R	Case 2: RL	Case 3: RC	Case 4: NL
Filter output voltage ($v_{f,1}$)	0.66 %	6.47 %	4.77 %	3.59 %
Filter output voltage ($v_{f,2}$)	0.7 %	6.48 %	4.78 %	3.63 %
Microgrid PCC voltage (v_{PCC})	0.61 %	6.47 %	4.78 %	4.47 %

Table 4.5 – Current signals THD analysis - Two distributed generator microgrid.

PARAMETERS	Total Harmonic Distortion - THD_I			
	Case 1: R	Case 2: RL	Case 3: RC	Case 4: NL
Filter output current ($i_{o,1}$)	5.05 %	8.11 %	7.2 %	27.69 %
Filter output current ($i_{o,2}$)	5.93 %	8.66 %	7.98 %	33.4 %
Load current (i_{load})	0.61 %	6.31 %	4.66 %	29.81 %

When comparing the total harmonic distortion simulations results obtained for parallel connected FCS-MPC controlled grid-forming converters and the results observed by Guimaraes (2019) for a single FCS-MPC grid-forming converter, it is verified an increase in THD_V and THD_I values when the parallel connected systems are concerned. From Tables 4.4 and 4.5 it is possible to observe that, despite the presence of relative higher harmonic components in the converters output current signal, the THD_V maintained relative lower values in all considered situation. Therefore, both considered parallel primary control systems were able to control autonomously their respective voltage output signal correctly while sharing proportional active and reactive power to the simulated microgrid.

4.3 Adapted droop-based economic power sharing strategy total generation costs comparative analysis - Two DG units microgrid

To perform a comparative analysis of the adapted droop-based economic power sharing strategy cost reduction performance, the traditional resistive droop control is also implemented as tertiary control level for the considered low voltage microgrid. The software simulations

for the same R, RL, RC and nonlinear load demand situation were repeated considering the traditional resistive droop control, and the microgrid total generation costs are calculated for both tertiary control strategies.

Figure 4.17 presents the traditional *P-V* droop curves for distributed generators 1 and 2. In this system, the converters sets their inner voltage reference from overwritten curves inclination coefficients, which are obtained considering only the microgrid maximum and minimum permitted voltage, $V_{max,MG}$ and $V_{min,MG}$ and the respective unit power rating. The considered microgrid operational limits are specified in Table 3.3. Therefore, the distributed generator will dispatch power regardless of the respective unit operational cost. The *Q-f* traditional droop curves are similar to the ones obtained for the adapted economic strategy and can be visualized in Figure 4.4. Appendix B presents the algorithm used for traditional resistive droop implementation for the simulated low-voltage microgrid.

Figure 4.17 – Traditional resistive *P-V* droop curve for the considered low-voltage microgrid.

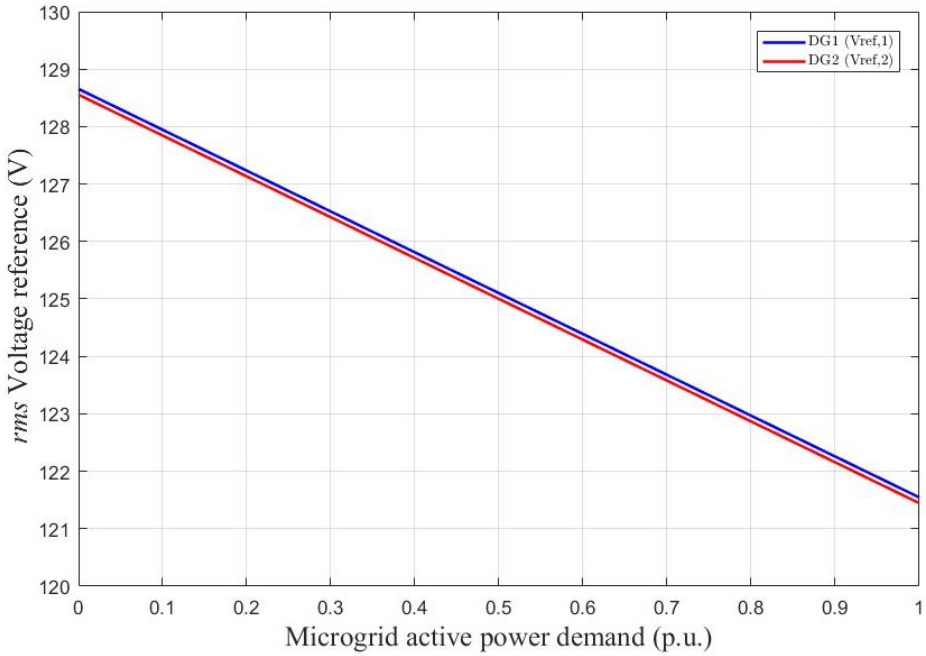

Source: From author (2021)

As the total generation cost is a cumulative function over time, Figure 4.18 illustrates the TGC evolution over the considered software simulation execution time for every load demand considered for both the adapted and traditional droop strategy.

Figure 4.18 – Microgrid total generation cost for the considered R, RL, RC and NL for the adapted economic and traditional droop strategies - Two distributed generation units microgrid.

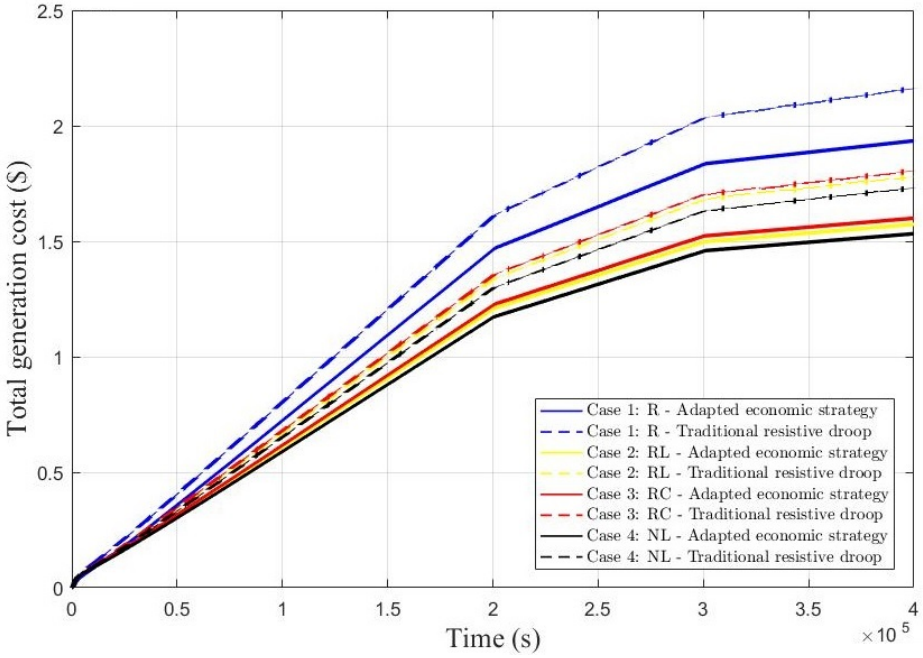

Source: From author (2021)

Table 4.6 – Total generation cost for the simulated two distributed generator microgrid system comparative analysis.

Power demand	Traditional droop strategy	Adapted economic strategy	TGC reduction
Case 1: R loads	2.16 $	1.94 $	10.5%
Case 2: RL loads	1.78 $	1.57 $	11.6%
Case 3: RC loads	1.81 $	1.60 $	11.4%
Case 4: NL loads	1.73 $	1.53 $	11.4%

As informed in Table 4.6, the adapted droop-based economic power sharing strategy presented cost reductions of 10.5%, 11.6%, 11.4% and 11.4% for the simulated R, RL, RC and NL load sets in comparison to the result obtained for the microgrid under equal power demand conditions using the traditional resistive droop control strategy.

4.4 Converters control mode transient analysis

The adapted economic strategy control mode transition analysis was observed for the lowest dispatch priority distributed generator control mode response over a sudden power demand drop event. Also, the unit reintegration to the system as a power-sharing participating element after a sudden microgrid load demand increase was analyzed.

When the grid voltage amplitude overpass the lowest priority unit predefined maximum dispatch voltage, $V_{max,i,N}$, the distributed generator performs autonomously a change in its operational control mode from grid-forming to grid-feeding unity (*Control Mode = 1 to 0*). At this condition, the lowest priority generators is not providing power to the microgrid as the converter output current reference, $i^*_{ref,i}$, is calculated from a null current output reference, $i^*_{o,ref} = 0$. Yet, the converter is still following the microgrid local voltage signal reference, allowing a fast time recovering to grid-forming mode in case of a short-time load demand increase. Thereafter, the opposite scenario is evaluated (*Control Mode = 0 to 1*), where a sudden increase in microgrid active demand causes a decrease in the microgrid overall voltage amplitude, causing the grid-feeding distributed generators to return its control mode to grid-forming units and to share power proportionally according to its respective average operational cost.

According to the adapted economic strategy implemented tertiary control of the considered microgrid, the DG_2 unit is given the lowest dispatch priority, $N_2 = 2$. Therefore, when the microgrid active power demand drop, DG_2 unit change its control mode from grid-forming to grid-feeding, (*Control Mode 1 to 0*). Also, when the microgrid power demand suddenly increases, DG_2 restore to normal power-sharing operation as grid-forming unity, (*Control Mode 0 to 1*). The control mode voltage threshold is equal to the respective unit set maximum operational voltage, which for the considered DG_2 unit is 126.50V as presented in Table 4.3.

Figures 4.19 and 4.20 demonstrates the considered island microgrid response to software simulated sudden power demand step-down variation. The considered RL load represents 75% of the microgrid total active power capacity, being disconnected at 0.5s simulation-time instant. After, the RL load is reconnected in 1.0s time instant, allowing the transition analysis of the simulated system recovery from a short-time low load demand event.

Figure 4.19 – Adapted economic strategy operational control mode transition analysis: *P-V* microgrid system response.

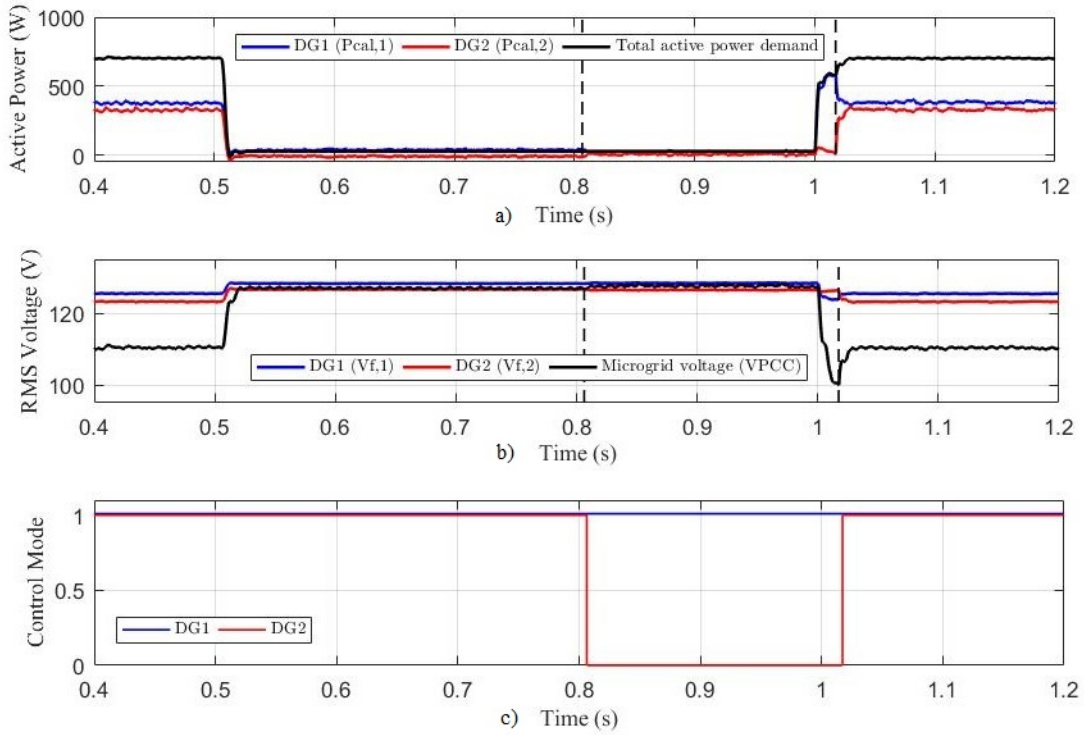

Source: From author (2021)

Figure 4.20 – Adapted economic strategy operational control mode transition analysis: *Q-f* microgrid system response.

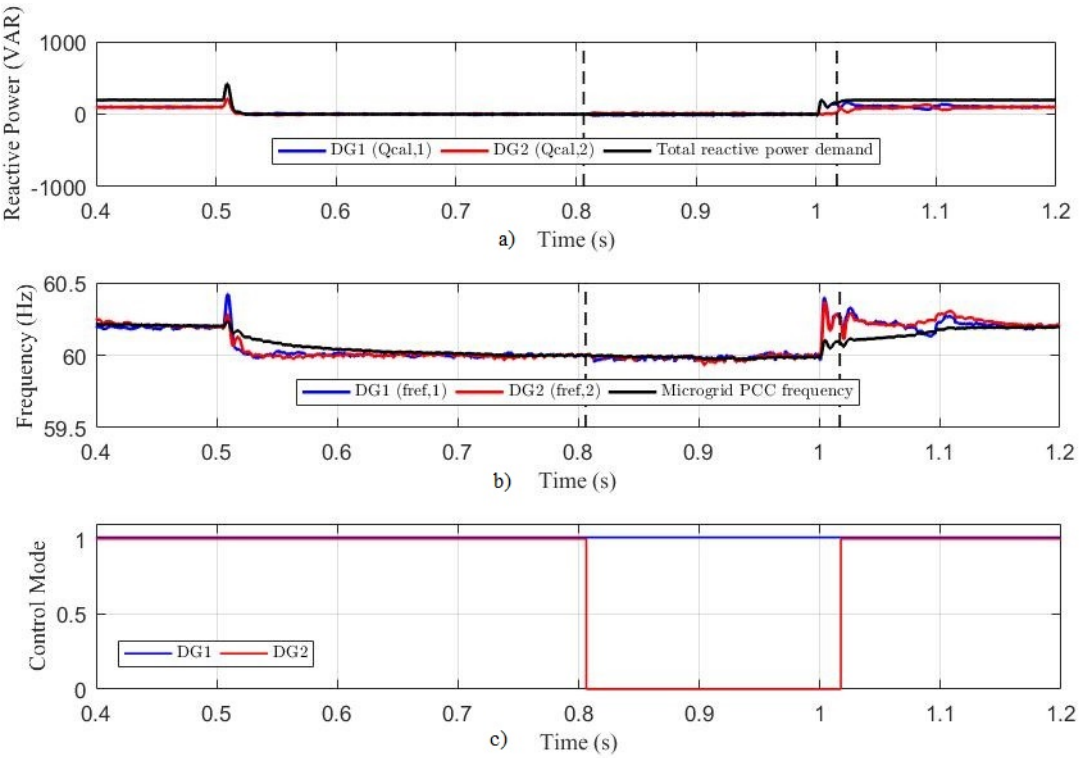

Source: From author (2021)

Initially, as can be observed in Figure 4.19 c), from the RL load disconnection event to the DG_2 control mode change from grid-forming to grid-feeding control, a time length of 0.31s is required for the control mode change. As can be observed in the aforementioned figure, a single change is performed in the converter operational mode as the time-delay security factor is observed, avoiding therefore unnecessary control modes transitions.

While on grid-feeding mode, it can be visualized in Figures 4.19 a) and 4.20 a) that no active or reactive power are being delivered to the system, as the FCS-MPC quality cost function follows a converter current reference, $i^*_{ref,2}$, determined in relation of a null output current, $i^*_{o,2} = 0$. It can also be verified in Figures 4.19 b) and 4.20 b) that DG_2 in grid-feeding operation keeps following the microgrid voltage signal reference measured locally at its respective LC filter output, $v_{f,2}$, which is being provided by DG_1 as it keeps operating as grid-forming unity.

As the RL load increases suddenly at 1.0s simulation time, the DG_2 is then required to return is operation as grid-forming unit and to share power proportional within the island microgrid. In Figures 4.19 c) it can be identified a time length inferior to 0.018s from the RL load reconnection and DG_2 control mode logic change form grid-feeding to grid-forming control. A time duration inferior to 0.02s can be visualized from figures 4.19 a) and b) for both distributed generator recovery to its active power sharing steady-sate condition. Similarly, from Figure 4.20 a) and b), a time length inferior to 0.17s is observed for both distributed generator to recover its original reactive power sharing steady-sate condition.

As observed in the works of Alhasheem et al. (2018) and Panten, Hoffmann e Fuchs (2016), the total time length for active and reactive powers transitory events within an island microgrid with parallel grid-forming converters using the FCS-MPC method as control technique and also implementing a droop-based control method varies from 0.01s to 0.4s. Therefore, the transitory time length achieved in the considered simulation are within common limits identified in related technical literature.

Figure 4.21 – DG_1 converter FCS-MPC control quality cost function references: a) Filter output voltage; b) Filter output current; c) Converter current.

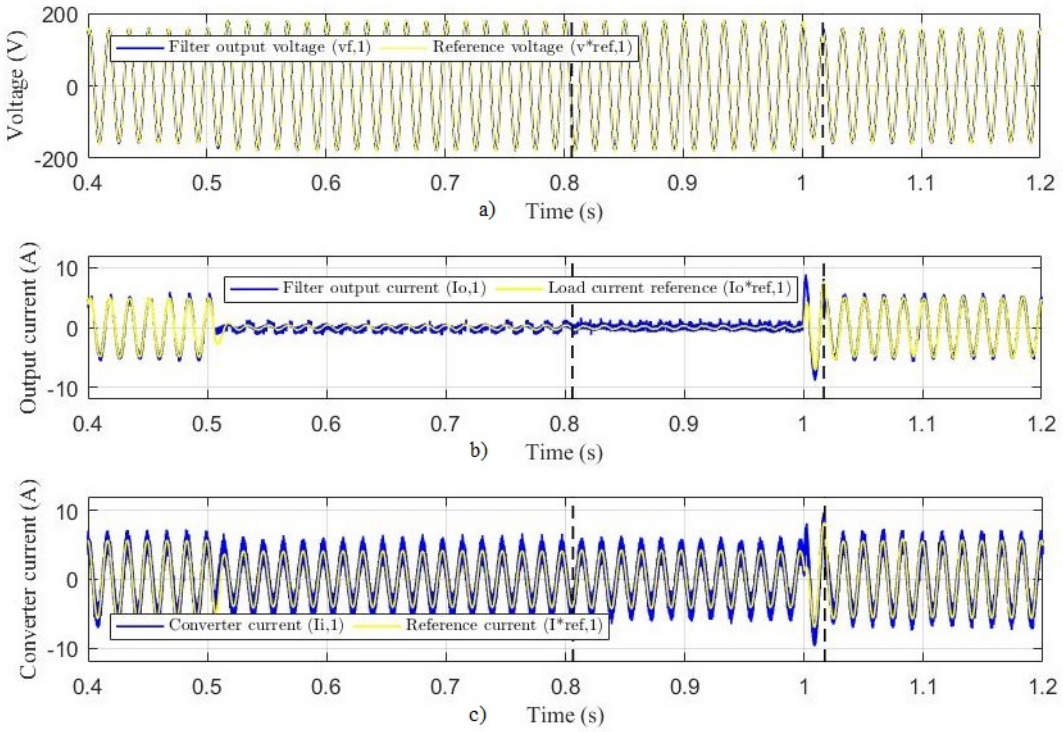

Source: From author (2021)

Figure 4.22 – DG_2 converter FCS-MPC control quality cost function references: a) Filter output voltage; b) Filter output current; c) Converter current.

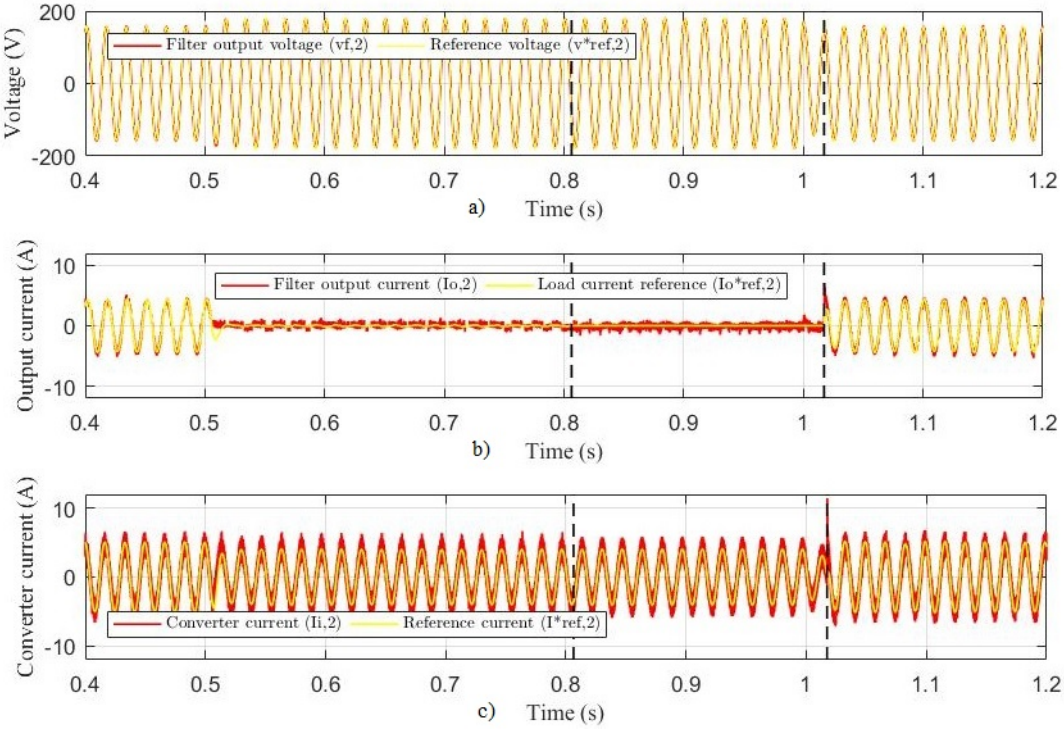

Source: From author (2021)

As the FCS-MPC control method is considered for the converter H-bridge primary controllers, it is therefore relevant to verify the control method capacity in tracking its given quality cost function references, as they are being dynamically adjusted in relation to the instantaneous active and reactive power demand according to the proposed adapted strategy droop curves. From observing Figures 4.21 and 4.22, it is possible to observe that even during the transitory event simulated with a operational control mode change of DG_2, the parallel converters implemented with FCS-MPC control method kept tracking its quality cost function references. In Figure 4.22 b) is possible to visualize the FCS-MPC tracking of a defined null filter output current reference, $i^*_{o,2} = 0$, while DG_2 operates in grid-feeding control mode.

4.5 Adapted economic power sharing strategy expandability verification

In order to verify the adapted power sharing strategy expandability capacity, a third cost-distinct distributed generation unity is considered to be connected in parallel to the evaluated low-voltage microgrid system as previously illustrated in Figure 3.12. With the exception of the included unit operational cost model, all other simulation parameters related to the converters and microgrid characteristics are considered to be similar as in the previously simulated two distributed generator system. The three converter microgrid simulation schematics is presented in Appendix A.

The hierarchical control structure is therefore modified for the considered situation. The proposed droop-based economic power dispatch strategy is adapted in order to include the new distributed generation unity cost parameters and, in sequence, implemented as the microgrid tertiary controller for the three converters operational limits and dispatch priority order definitions. The developed algorithm for the adapted droop-based economic power sharing strategy implementation as microgrid tertiary control level for the three distributed generators system can be visualized in Appendix B.

4.5.1 Tertiary control implementation - Three distributed generation units microgrid

The power sources operational cost function parameters and the considered island microgrid power quality reference ranges used as algorithm inputs are presented in Tables 3.3 and 3.4, respectively. The considered distributed generators 1, 2 and 3 normalized cost functions presented in Equations 3.42, 3.43 and 3.44 are illustrated in Figure 4.23.

Figure 4.23 – Normalized operational cost functions of distributed generators 1, 2 and 3.

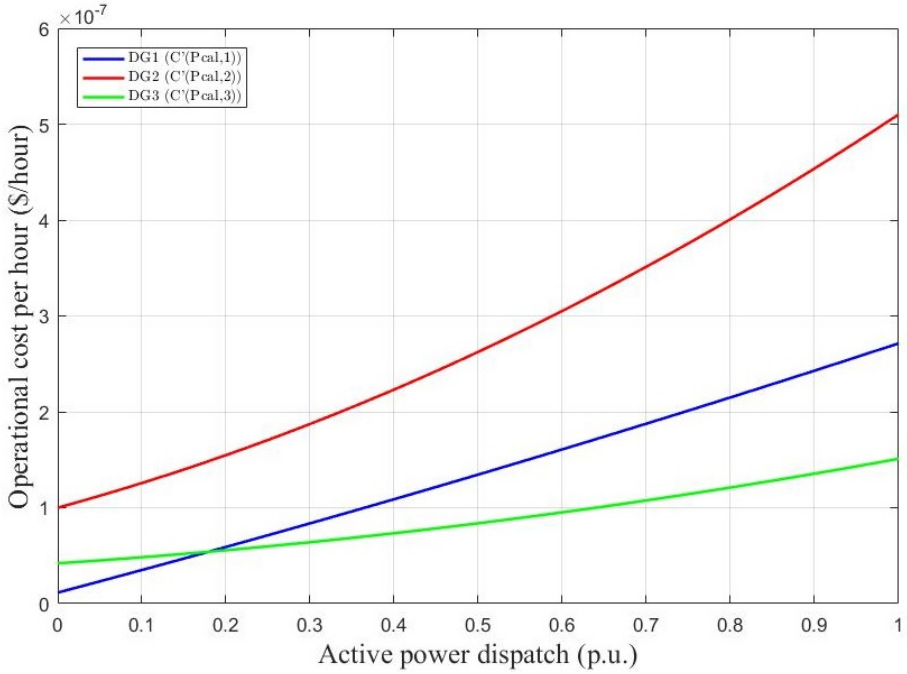

Source: From author (2021)

From the normalized cost curves, the average operational costs, $C'_{med,1}$, $C'_{med,2}$ and $C'_{med,3}$, could be obtained for DG_1, DG_2 and DG_3, respectively. In figure 4.23, it can be visualized the relative lower operational cost of DG_3 unit in relation to DG_1 and DG_2 for all its operational power dispatch range. As the new distributed generation unit is considered with the system lowest average operational cost ($C'_{med,3} < C'_{med,1} < C'_{med,2}$), the tertiary control rearrange the dispatch order within the island microgrid. According to the adapted economic strategy, DG_3 is given the microgrid highest dispatch priority, $N_3 = 1$, follow by units DG_1, $N_1 = 2$, and DG_2, $N_2 = 3$. The new dispatch priorities definition results are presented in Table 4.7.

Table 4.7 – Average operational costs and power dispatch priority for distributed generators 1, 2 and 3.

PARAMETERS	DG_1	DG_2	DG_3
Average normalized cost ($C'_{med,i}$)	19.76 $/hour	39.92 $/hour	12.70 $/hour
Power dispatch priority order (N_i)	2	3	1

Similarly as for the two distributed generator system simulations, the adapted strategy characteristic active power droop curves determined for three distributed generator also considers the island microgrid power quality parameters presented in Table 3.3. Same ΔV_{max}, ΔV_{min} and ΔP_{online} parameter values of 5V, 3V and 50% considered for the two distributed generator

microgrid simulations are adopted for the maximum and minimum voltage dispatch range and online power reserve, respectively.

Figures 4.24 and 4.25 presents the obtained adapted economic strategy *P-V* and *Q-f* droop-characteristic control curves for the considered three distributed generator microgrid.

Figure 4.24 – Adapted decentralized economic power sharing strategy P-V droop curves for distributed generator 1, 2 and 3.

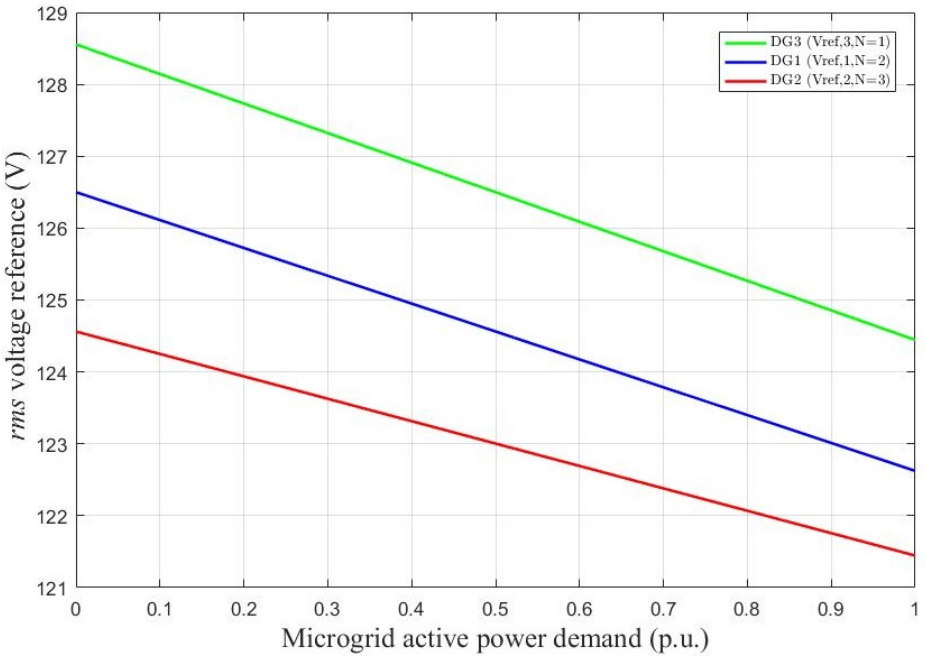

Source: From author (2021)

Table 4.8 summarizes the obtained maximum and minimum voltage and frequency operational references, and the droop curves inclination coefficients for the considered three distributed generator microgrid.

Table 4.8 – Adapted droop-based power sharing strategy tertiary control parameters definition for distributed generators 1, 2 and 3.

PARAMETERS	DG_1	DG_2	DG_3
Maximum operational *rms* voltage ($V_{max,i,N}$)	126.50 V	124.562 V	128.555 V
Minimum operational *rms* voltage ($V_{min,i,N}$)	122.624 V	121.445 V	124.445 V
Maximum operational frequency ($f_{max,MG}$)	60.5 Hz	60.5 Hz	60.5 Hz
Minimum operational frequency ($f_{min,MG}$)	59.5 Hz	59.5 Hz	59.5 Hz
Droop voltage curve coefficient ($k_{p,i,N}$)	3.876 V/$P_{1p.u.}$	3.117 V/$P_{2p.u.}$	4.110 V/$P_{3p.u.}$
Droop frequency curve coefficient ($k_{q,i,N}$)	1 V/$Q_{1p.u.}$	1 V/$Q_{2p.u.}$	1 V/$Q_{3p.u.}$

Figure 4.25 – Adapted decentralized economic power sharing strategy Q-f droop curves for distributed generator 1, 2 and 3.

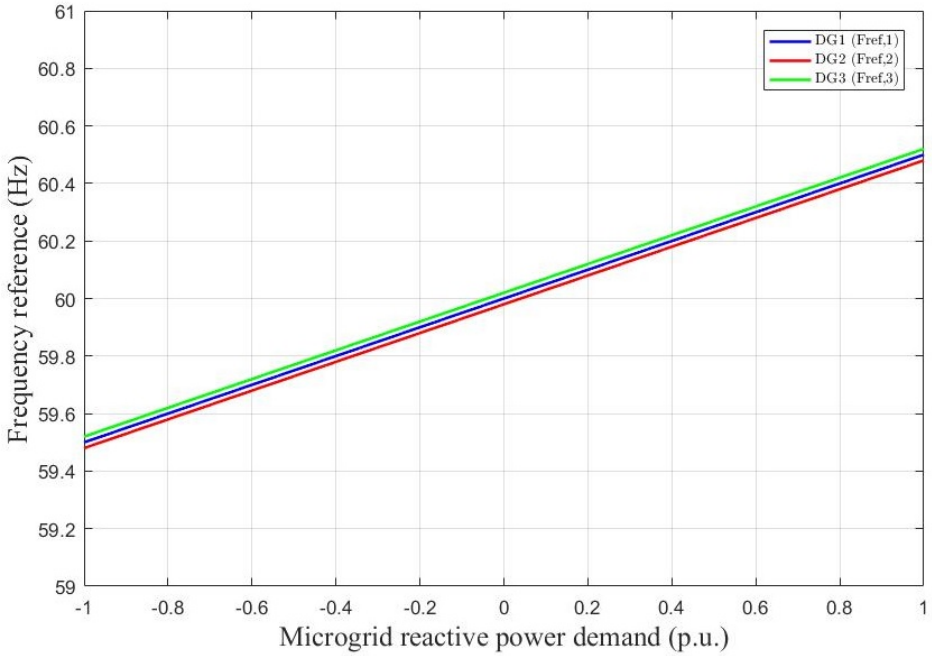

Source: From author (2021)

In accordance with the adapted economic strategy control logic, unit DG_3 is given the microgrid highest priority and hence, the voltage droop set references follows a relative higher curve in comparison to the other units.

From the tertiary control parameters definition presented in Table 4.8 integration on each respective converters primary controller, the power sharing simulations of the considered microgrid could then be performed.

4.5.2 Three DG units microgrid under active power demand - Case 1: R loads demand

To verify the adapted droop-based economic power sharing strategy response for a three distributed generator microgrid, initially a purely active power demand is considered. The load demand conditions are assumed the same as in for the two units simulations. Therefore, a three load steps of approximately 320VA under nominal voltage conditions were considered.

Figure 4.26 presents the active power sharing among the simulated three converter system with their respective internal droop-based voltage references under active load demand condition.

Figure 4.26 – Adapted economic strategy software simulation for three DG units microgrid - Case 1: R loads demand: a) Active power sharing; b) Microgrid *rms* voltages.

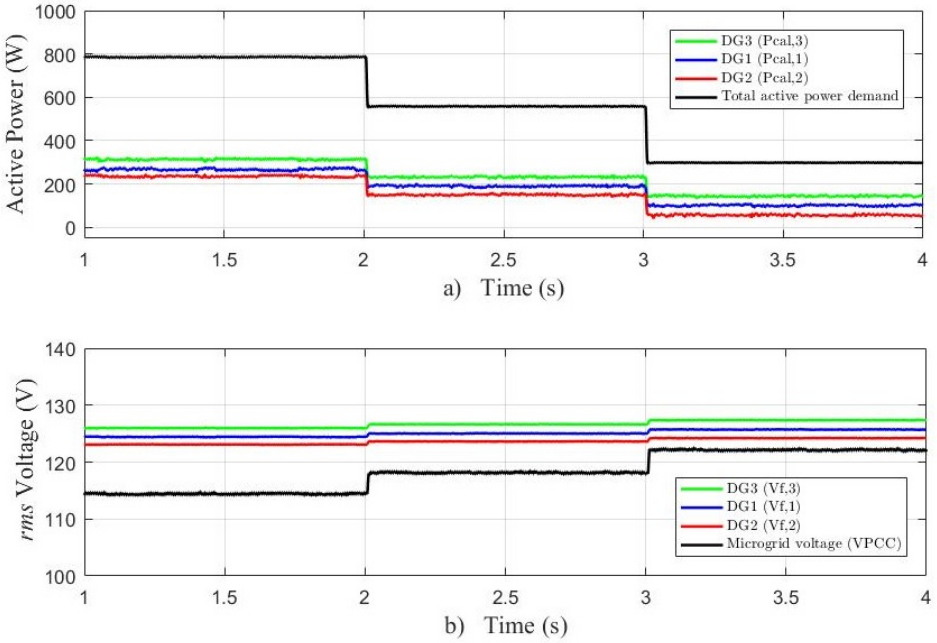

Source: From author (2021)

Figure 4.27 presents the reactive power sharing and converters internal droop-defined frequency references.

Figure 4.27 – Adapted economic strategy software simulation for three DG units microgrid - Case 1: R loads demand: a) Reactive power sharing; b) Microgrid frequencies.

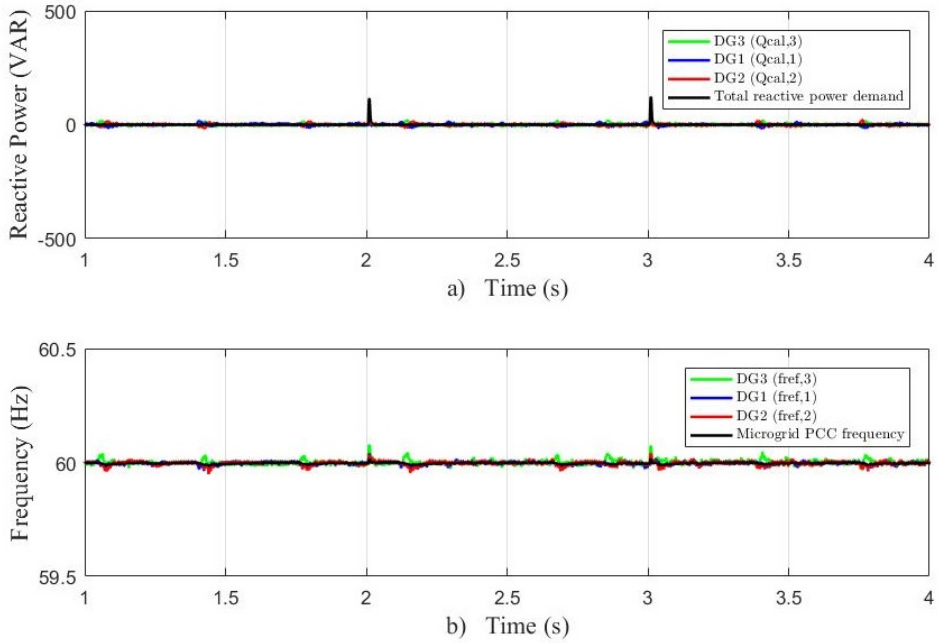

Source: From author (2021)

As can be seen, the active power sharing follows the predefined dispatch order set by the tertiary controller presented in Table 4.7. In comparison to the two converter simulation, as the same load demand level are being shared among three units instead, the microgrid PCC voltage amplitude level was raised, therefore improving power quality within the considered island system. The microgrid overall voltage amplitude serve as a control parameter to set the internal voltage amplitude reference of the local converters, therefore controlling the active power shared proportion.

As in the simulated two unit system, despite load transitory events, no reactive power was shared among the distributed generators as purely resistive loads were considered. Also no power coupling issue were verified as virtual resistance kept the system impedance behavior as being predominately resistive.

In Figure 4.28 it is possible to observe the three parallel FCS-MPC controlled converters capacity in maintaining sinusoidal voltages and currents, and also in performing a smooth transition under load variation. Converters output currents harmonic components are able to be identified circulating within the system.

Figure 4.28 – Adapted economic strategy software simulation for three DG units microgrid - Case 1: R loads demand: a) Voltage signals; b) Current signals.

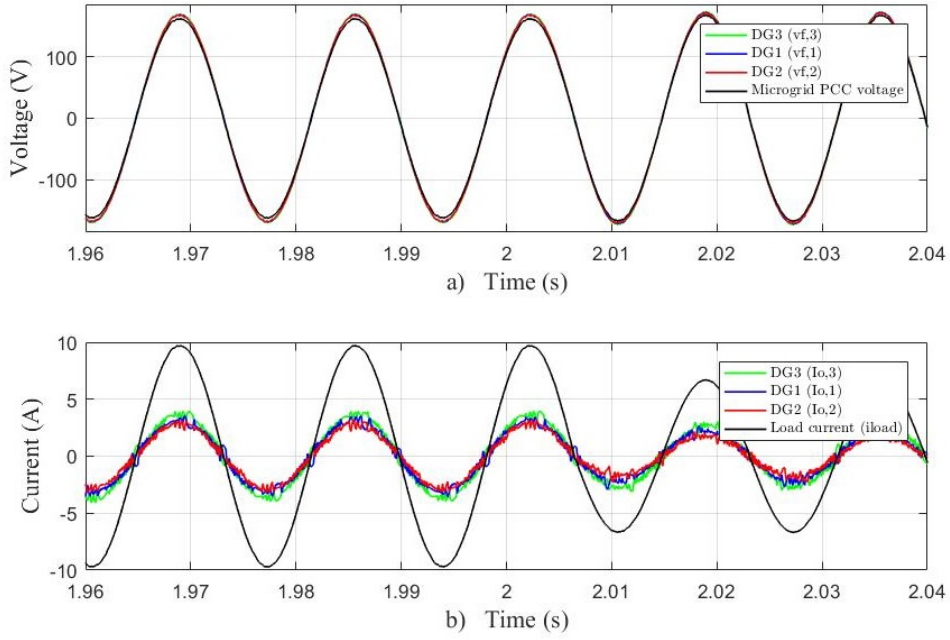

Source: From author (2021)

4.5.3 Three DG units microgrid under active and inductive-reactive power demand - Case 2: RL loads demand

For the active and reactive-inductive load demand simulation, similar RL load steps of approximately 320VA under nominal voltage conditions of 127V/60Hz were considered.

Figure 4.29 presents the active power sharing among the simulated three converter system with their respective internal droop-based voltage references considering an active and reactive-inductive load demand condition.

Figure 4.29 – Adapted economic strategy software simulation for three DG units microgrid - Case 2: RL loads demand: a) Active power sharing; b) Microgrid *rms* voltages.

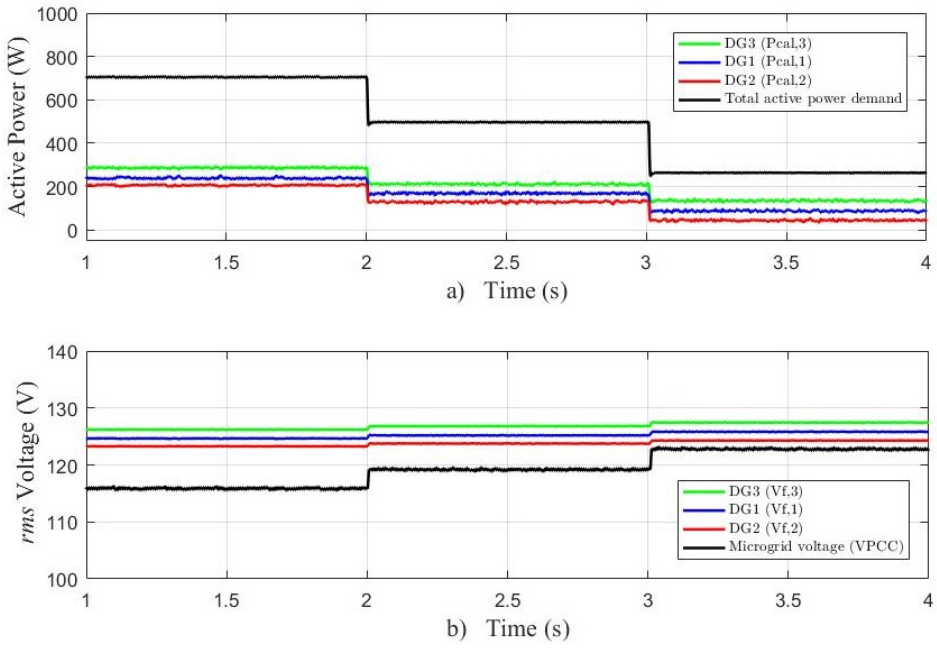

Source: From author (2021)

Also for the simulated RL load demand condition, proportional active power were shared among the distributed generators according to their respective dispatch priority order defined by the adapted economic strategy logic.

As demonstrated in Figure 4.30, the three converters shares equal amount of the total reactive power demand. Similarly as observed for the microgrid PCC voltage level raising effect with the addition of a new unit to the system, the microgrid frequency were approximated of standard nominal reference due to droop control characteristic curve, as smaller reactive power portions are being require from each converter.

Figure 4.30 – Adapted economic strategy software simulation for three DG units microgrid - Case 2: RL loads demand: a) Reactive power sharing; b) Microgrid frequencies.

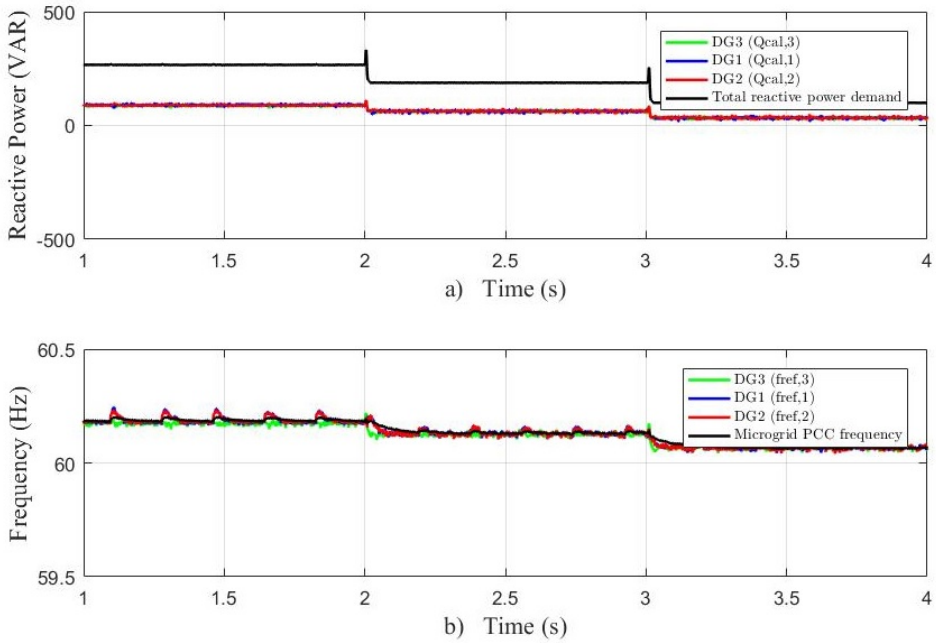

Source: From author (2021)

Also in the simulated RL demand condition, the parallel FCS-MPC control algorithms were able to keep sinusoidal voltage and current signal within the system while sharing reactive-inductive components as can be seen in Figure 4.31.

Figure 4.31 – Adapted economic strategy software simulation for three DG units microgrid - Case 2: RL loads demand: a) Voltage signals; b) Current signals.

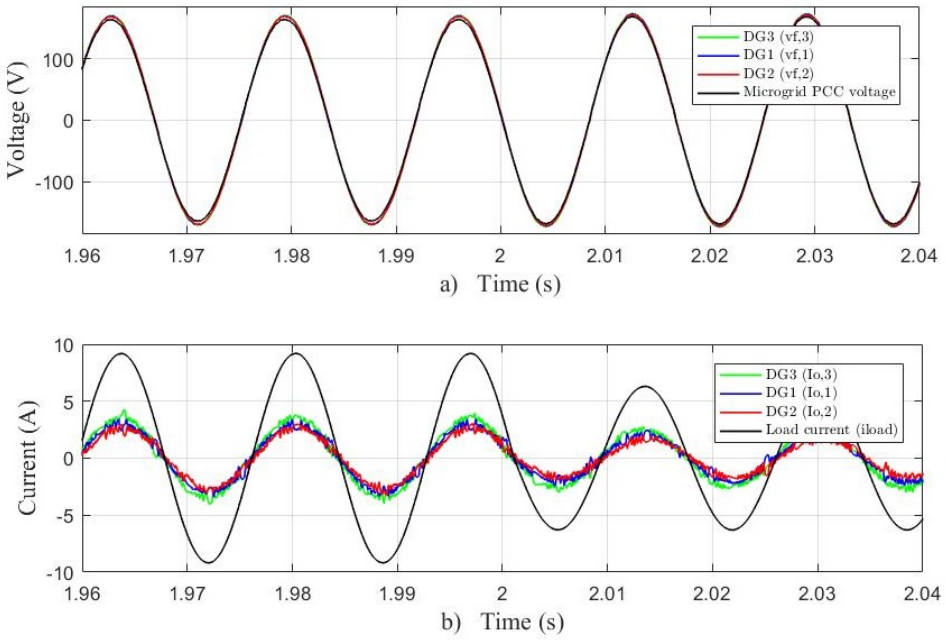

Source: From author (2021)

4.5.4 Three DG units microgrid under active and capacitive-reactive power demand - Case 3: RC loads demand

As in the RC simulation performed for two units microgrid, a set of RC loads with demand of approximately 300VA, 127V/60Hz, each was considered for the three converter system simulation. Similarly as observed in the previous R and RL simulations, the adapted strategy active power sharing proportion were also maintained for the RC load demand condition as can be verified in Figure 4.32.

Figure 4.32 – Adapted economic strategy software simulation for three DG units microgrid - Case 3: RC loads demand: a) Active power sharing; b) Microgrid *rms* voltages.

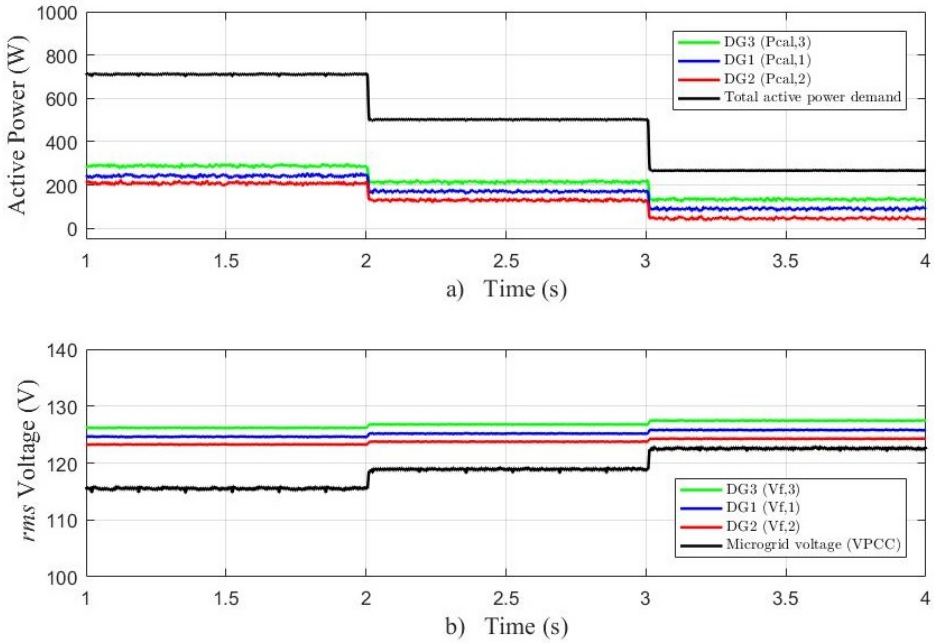

Source: From author (2021)

In Figure 4.33, the system frequency reduction effect due to reactive-capacitive load sharing can be verified. Also, the oscillatory effects in the ANF-FE reactive power measurement due to circulating harmonic current components were perceived.

Sinusoidal voltage and currents for the RC load condition can be verified in Figure 4.33 while sharing simultaneously active and reactive-capacitive powers. The presence of converters output harmonic currents can also be identified.

Figure 4.33 – Adapted economic strategy software simulation for three DG units microgrid - Case 3: RC loads demand: a) Reactive power sharing; b) Microgrid frequencies.

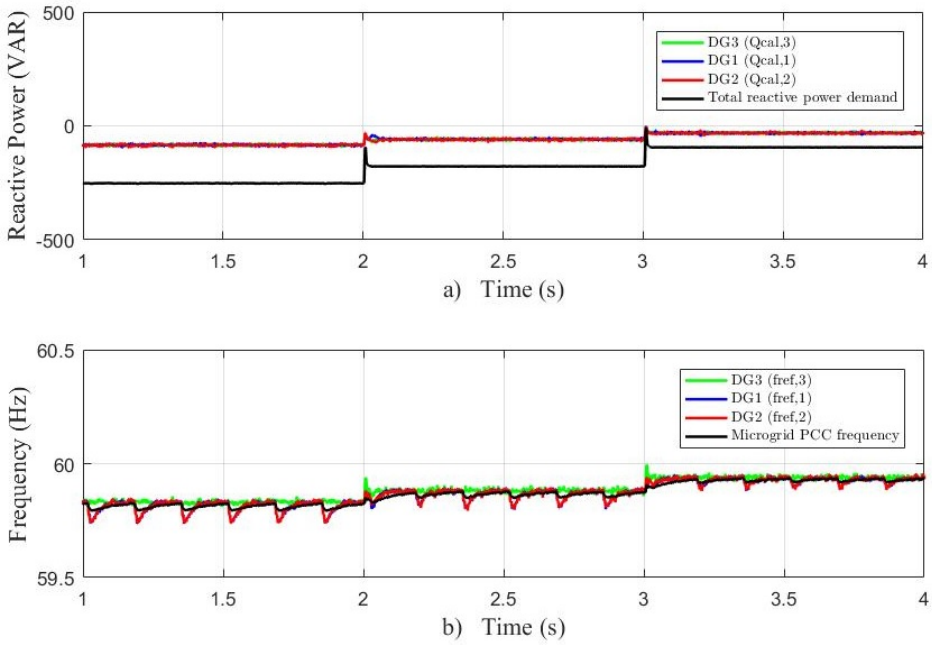

Source: From author (2021)

Figure 4.34 – Adapted economic strategy software simulation for three DG units microgrid - Case 3: RC loads demand: a) Voltage signals; b) Current signals.

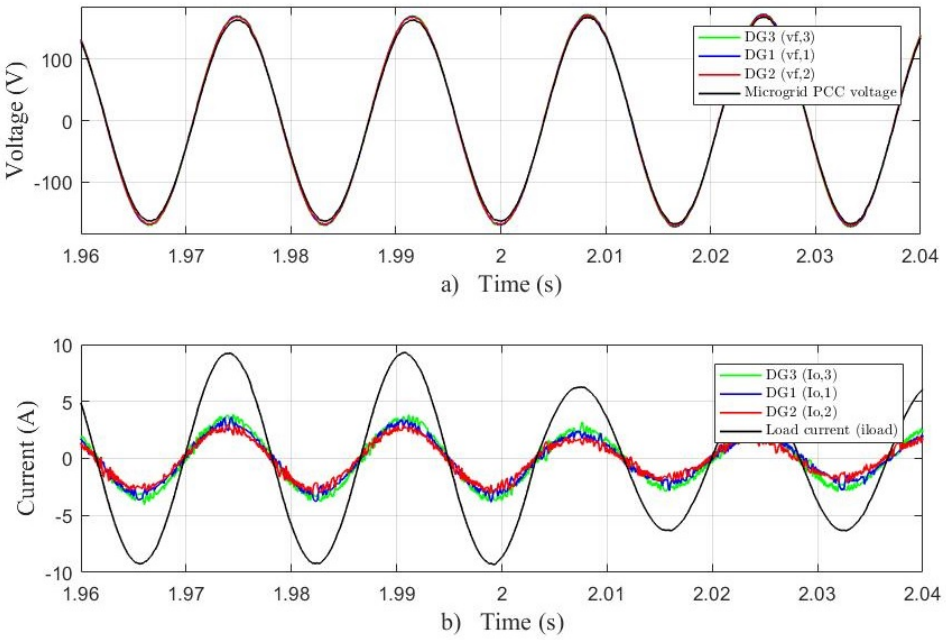

Source: From author (2021)

4.5.5 Three DG units microgrid under nonlinear loads power demand - Case 4: NL loads demand

A three set of single-phase rectifiers connected to RL loads with 50Ω resistance and 100mH inductance were considered to simulate the nonlinear loads demand in the three converter simulations. Each rectifier was considered with a power demand of approximately 280VA under nominal voltage of 127V/60Hz.

Figure 4.35 presents the active power sharing capacity of the primary controller in maintain the proportional dispatch priority reference as set by the adapted droop-based economic strategy, even while feeding nonlinear loads.

Figure 4.35 – Adapted economic strategy software simulation for three DG units microgrid - Case 4: NL loads demand: a) Active power sharing; b) Microgrid *rms* voltages.

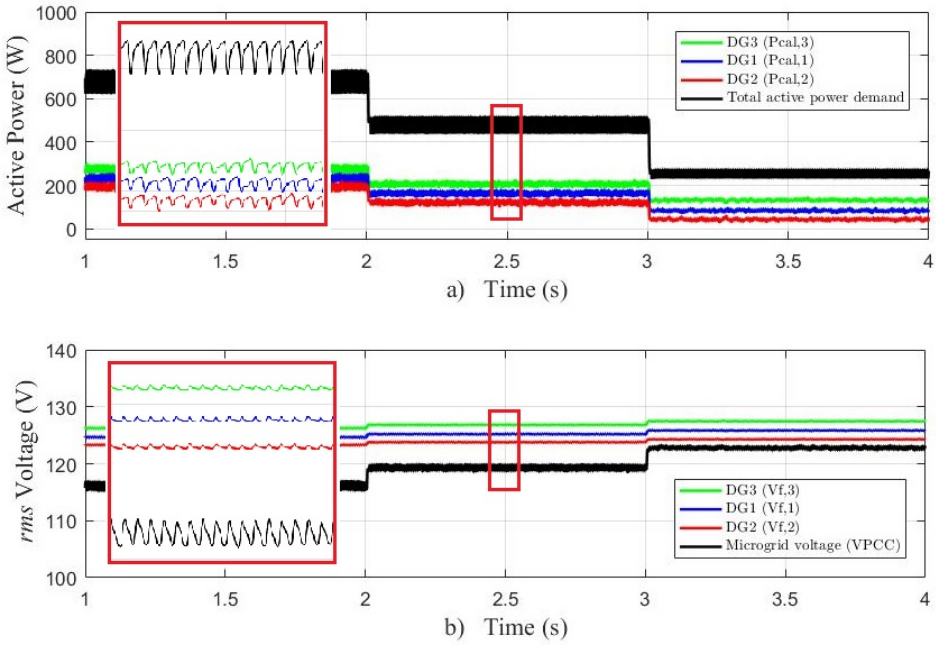

Source: From author (2021)

Figure 4.35 presents the reactive power sharing among the three converters with their respective frequency references. Oscillatory effects propagated over the control system power measurement and reference definitions due to the presence of harmonic currents can be observed in Figures 4.35 and 4.36. Nevertheless, the three converter control systems were able to keep following the droop-set references for proportional power dispatch.

Figure 4.36 – Adapted economic strategy software simulation for three DG units microgrid - Case 4: NL loads demand: a) Reactive power sharing; b) Microgrid frequencies.

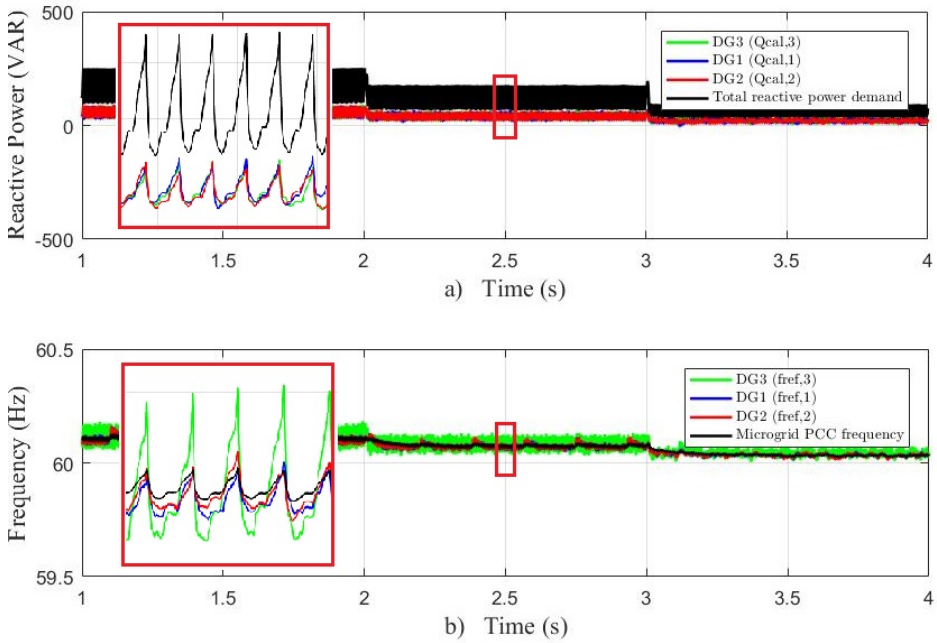

Source: From author (2021)

Figure 4.37 – Adapted economic strategy software simulation for three DG units microgrid - Case 4: NL loads demand: a) Voltage signals; b) Current signals.

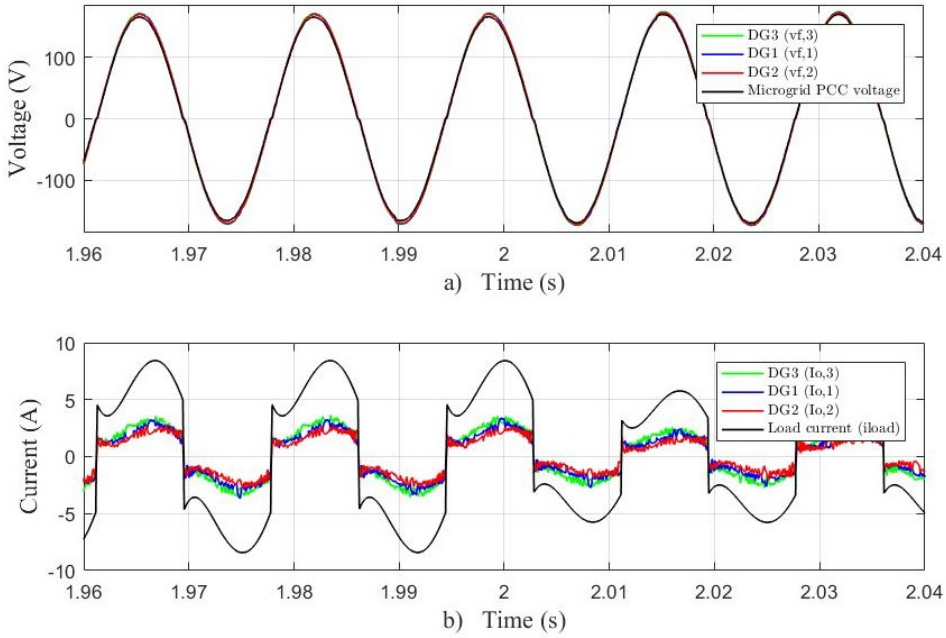

Source: From author (2021)

In Figure 4.37 it is possible to observe the FCS-MPC control capacity in maintaining a sinusoidal voltage under heavily distorted current signals considering the three parallel conver-

ters. Also, it is noticeable in this simulation the soft voltage and current signals transition due to load step variation.

4.5.6 Total harmonic distortion analysis - Three distributed generation units microgrid

Tables 4.9 and 4.10 presents the total harmonic distortion for voltage, THD_V, and current, THD_I, calculated for the considered R, RL, RC and nonlinear load demand conditions in the simulated three distributed generator microgrid.

Table 4.9 – Voltage signals THD analysis - Three distributed generator microgrid.

PARAMETERS	Total Harmonic Distortion - THD_V			
	Case 1: R	Case 2: RL	Case 3: RC	Case 4: NL
Filter output voltage ($v_{f,1}$)	0.58 %	4.41 %	3.7 %	2.3 %
Filter output voltage ($v_{f,2}$)	0.62 %	4.41 %	3.68 %	2.32 %
Filter output voltage ($v_{f,3}$)	0.62 %	4.4 %	3.71 %	2.29 %
Microgrid PCC voltage (v_{PCC})	0.46 %	4.4 %	3.67 %	2.9 %

Table 4.10 – Current signals THD analysis - Three distributed generator microgrid.

PARAMETERS	Total Harmonic Distortion - THD_I			
	Case 1: R	Case 2: RL	Case 3: RC	Case 4: NL
Filter output current ($i_{o,1}$)	8.87 %	10.32 %	9.77 %	28.48 %
Filter output current ($i_{o,2}$)	11.86 %	13.01 %	11.41 %	32.89 %
Filter output current ($i_{o,3}$)	9.35 %	9.87 %	11.72 %	38.55 %
Load current (i_{load})	0.46 %	4.06 %	3.97 %	31.26 %

An overall increase in THD_I for all simulated load conditions could be noticed when considering three parallel converters in relation to the two unit system as can be observed in Tables 4.5 and 4.10. Therefore, circulating harmonic currents increases among converters as the number of parallel FCS-MPC controlled systems in the simulated island microgrid increases.

The THD_I calculated in relation to the microgrid load current, i_{load}, is relative small in comparison to the THD_I values obtained for the converters output currents, $i_{o,i}$, for all simulated load demand conditions presented in Tables 4.5 and 4.10. Therefore, the presence of circulating harmonic components can be perceived among the parallel units for both the two and three converter system.

Comparing the simulated results of voltage total harmonic distortions presented in Tables 4.4 and 4.9, an overall downgrade in THD_V values could be perceived when the three converter system is concerned. For both two and three parallel distributed generator simulated

microgrid, the primary level FCS-MPC control demonstrated its harmonic rejection capacity while maintaining dynamically set sinusoidal output voltage signals in the diverse load demand conditions considered. Similar results were observed by Guimaraes (2019) for a single FCS-MPC controlled converter where, according to the author, one of the advantages in using the FCS-MPC in comparison to traditional PI controllers is its harmonic rejection capability without the necessity of additional control loops for individual harmonic frequencies.

Currently in Brazil there is no specific regulation for power quality considering microgrids or systems in island operation. However, for a conventional low-voltage distribution system, according to ANEEL/PRODIST (2018), the maximum voltage THD_V permitted is 10% for systems voltages under 1.000V. Considering the specified power quality values defined by PRODIST standard, the simulated island microgrid with parallel FCS-MPC controlled converters implementing the adapted droop-based economic power sharing strategy operates within acceptable harmonic distortion conditions.

4.5.7 Adapted droop-based economic power sharing strategy total generation costs comparative analysis - Three DG units microgrid

In order to validate de cost reduction efficiency of the adapted economic strategy for the simulated three distributed generation microgrid, a similar analysis as performed in results section 4.3 was conducted.

The microgrid total generation cost is calculated considering the active power shared based on the adapted economic strategy in every previously simulated load demand condition for the three distributed generators microgrid. Simulation were repeated considering the traditional droop method as the microgrid tertiary control for the considered three unit system feeding equal load demand condition for cost comparison purpose.

Total generation cost cumulative evolution over simulation time for both the adapted economic and the traditional droop strategies are illustrated in Figure 4.38.

Figure 4.38 – Microgrid total generation cost for the considered R, RL, RC and NL for the adapted economic and traditional droop strategies - Three distributed generation units microgrid.

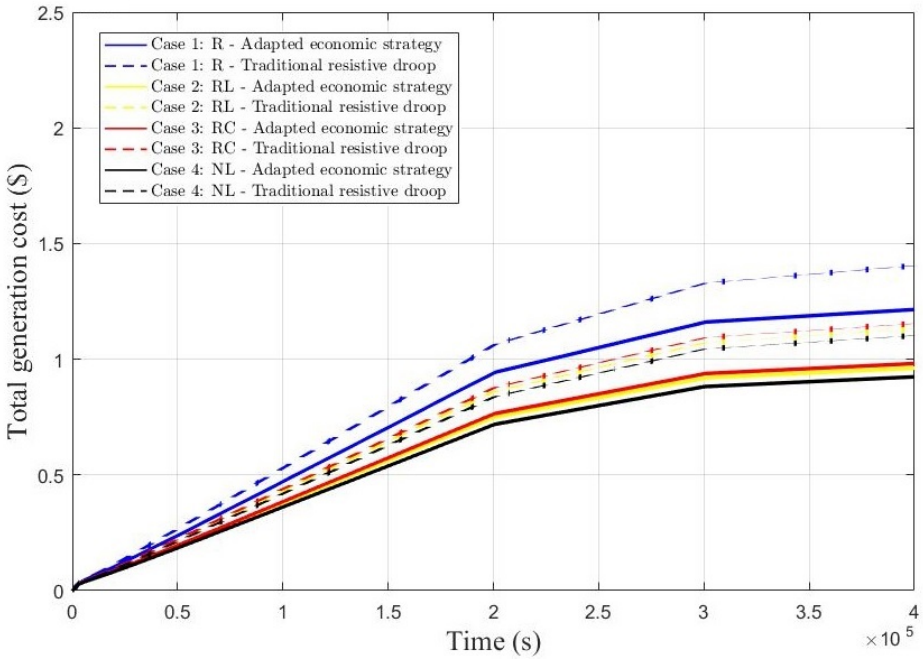

Source: From author (2021)

As can be seen in Figure 4.38, the microgrid TGC when implementing the adapted economic strategy presented relative lower values for all load demand simulations performed in comparison to the TGC calculated for the traditional droop scheme in the same circumstances. Table 4.11 presents the four load demand simulations TGC values for both tertiary control strategies implemented, as also the relative cost percentage reductions.

Table 4.11 – Total generation cost for a three distributed generator microgrid comparative analysis.

Power demand	Traditional droop strategy	Adapted economic strategy	TGC reduction
Case 1: R loads	1.40 $	1.21 $	13.5%
Case 2: RL loads	1.13 $	0.96 $	14.9%
Case 3: RC loads	1.15 $	0.98 $	15.0%
Case 4: NL loads	1.10 $	0.92 $	16.2%

As presented in Table 4.11, a total cost reduction of 13.5%, 14.9%, 15% and 16.2% were achieved for the R, RL, RC and nonlinear simulated load demand conditions when compared to the traditional droop control scheme. Nutkani et al. (2017) achieved cost reductions of 12.7%, 40.8% and 54.6% when comparing the original proposed economic dispatch strategy with the traditional droop method. However, these results were obtained for a predominately inductive microgrid, were resistive components in feeder lines could be neglected and no virtual

impedance adjustment were required. Nevertheless, the author states that better cost reduction results can be achieved by the adequate tuning of droop gradients and selecting a proper online power reserve.

As can be related from Tables 4.6 and 4.11, the inclusion of a less costly third unit reduced the overall microgrid cost in all simulated situation. The inclusion of a new unit enhances the cost reduction capability of the adapted economic strategy. Similar result was also observed by Nutkani et al. (2017) in the original scheme. However, as identified by the same author, there is trade-off between achieving better cost reduction performance by adding new DG units in the system with degrading power quality parameters within the island microgrid, as larger allowable operation voltage range is required to add more units in a proper droop-based scheme. Therefore, the adapted drop-based economic power sharing strategy for a low-voltage microgrid operational cost reduction performance was validated.

5 CONCLUSION

This work proposed an economic power management strategy for a low-voltage island microgrid based on droop concept. The proposed strategy avoided secondary communication system among distributed generators. Also, an operational control shift change was proposed to avoid a deactivation of a distributed generator during short-time load transients. All results observed were obtained through computer simulations of a hypothetical low-complexity single-phase microgrid.

Software simulations demonstrated the microgrid adapted economic power sharing strategy tertiary control implementation capability to define the distributed generators dispatch priority order based on each unit inherent average operational cost. In addition, the microgrid tertiary control demonstrated its capacity in setting each distributed generator maximum and minimum voltage amplitude and frequency references parameters to establish distinct cost-related droop curves for each converters primary control level. As stated by Han et al. (2017), when island microgrids are concerned, it is important to maintain system stability and achieve load power sharing among the multiple parallel-connected distributed generation units. Therefore, proper primary control structure for local distributed generators were also developed in order to perform software simulations of a considered low-voltage microgrid implementing the adapted power sharing strategy as tertiary control.

Considering the software sequential implementation of tertiary and primary control levels and later software simulation execution, it was possible to observe the proper functioning of the adapted economic strategy active and reactive power sharing management in a low-voltage island microgrid system with linear and nonlinear load demand conditions. Active and reactive power sharing together with voltage and frequency references tracking could be achieve among parallel connected grid-forming converter using FCS-MPC as control method. Also, as a secondary contribution of the present study, the proposed strategy presented adequate response in dealing with short-time power demand variations and operational cost reduction in relation to traditional droop scheme.

A drawback of the evaluated adapted economic power sharing strategy is the necessity of prior knowledge of the system feeders impedance in order to determine adequate virtual resistance values and to estimate the microgrid PCC voltage. Nevertheless, the use of virtual impedance method proved efficient while adjusting the system behavior from predominantly inductive to resistive and, therefore, ensuring the validity of *P-V/Q-f* droop relations for the

simulated low-voltage microgrid. Still, a trade-off between the system virtual resistive enhancement and the microgrid PCC voltage level could be identified.

While simulating linear loads power demand, the primary control integrated ANF-FE power measurement technique proved efficient in terms of accuracy and speed when calculation the active and reactive powers delivery by each converter in a system where the fundamental frequency varies continuously according to the instantaneous load demand. While dealing with non-linear loads, a reactive power demand could be identified as non-ideal diodes are being considered for the simulated rectifiers. The proposed strategy shared active and reactive powers among the local converters with an increase in oscillatory effects on control parameters when comparing with linear loads. Yet, the system were able to maintain the economic power sharing behavior as previously established by the tertiary control.

The evaluated microgrid control structure implemented in the present work consisted only of the primary and tertiary hierarchical control levels. Secondary control was not considered, which according to Guerrero et al. (2013) ensures that the frequency and voltage deviations are regulated toward zero after every change of load demand or generation inside the island microgrid. Also, harmonic compensation were not considered within the proposed scheme, which enhances the system power sharing capability when dealing with nonlinear loads and also avoid circulating harmonic currents among local converters.

Nevertheless, the adapted droop-based economic power sharing strategy cost reduction performance in comparison to the traditional droop control strategy was validated in software simulations, where microgrid total generation cost reduction could be observed for all considered power demand conditions.

The proposed adapted strategy also proved satisfactory response in power dispatch priority redistribution, active and reactive power sharing and cost reduction performance with the addition of a new cost-distinct power generation unity. A total harmonic distortion increase related to the current signal could be observed with the addition of a third grid-forming unit. Yet, the FCS-MPC control method implemented for the parallel converters demonstrated adequate behavior in following the dynamically droop-set sinusoidal voltage references, which were defined within a strict power quality parameters range. As prior demonstrated by Guimaraes (2019) for a single grid-forming FCS-MPC controlled converter, the simulated parallel connected grid-forming converters also kept the THD_V values within the ANEEL/PRODIST (2018) limit of 10 % for system under 1.000V.

The simulated converters control mode transition from grid-forming to grid-feeding control proved satisfactory during short-time low load variations. Similarly to the results obtained by Alhasheem et al. (2018) and Young e Bastias (2018) for parallel FCS-MPC grid-forming converters transient analysis, the observed transitory time between the control mode transition from grid-feeding to grid-forming unit and microgrid steady-state power sharing condition recovery were less than 0.2s. Also, the considered signal stabilization security factor proved effective in avoiding unnecessary control modes transitions.

The distributed generators operation as grid-feeding units during low load demand transitory events avoids units turning-off and re-synchronization procedures. Also, while on grid-feeding control mode, the distributed generators are still physically connected to the microgrid and keeps tracking the local voltage signal without power being delivered, permitting rapid transition to grid-forming control mode if system power demand suddenly increases. This improvement of the original Nutkani et al. (2017) economic strategy, together with the online power reserve method enhances system capacity in dealing with short-time load variations by improving power-sharing control redundancy and reliability for the island microgrid. As the online power reserve guarantees a gap in the next highest priority unit dispatch capacity to deal with a sudden increase in the microgrid load demand, the operational mode transition developed adds fast power-sharing recovery for converters during short-time load variations.

The adapted strategy presented, as in the original scheme proposed by Nutkani et al. (2017), allows the utilization of generic operational cost function models for the participating distributed generator units. This characteristic enhances the strategy versatility, permitting its further application for a vast quantity of low-voltage microgrid possibilities, where diverse power resources might be available. Additionally, as the proposed strategy is based on droop control method, it also incorporates the benefits of avoiding parallel communication systems for primary control coordination among the microgrid distributed generators, thus helping increase system reliability, modularity, and flexibility.

5.1 Further works

The following items can be further studied on in future works:

a) Implement a secondary control level at the microgrid hierarchical control structure in order to incorporate power quality management throughout the system, encompassing proper reactive power sharing and harmonic compensation mechanisms;

b) Implement an islanding detection algorithm with grid signal decoupling and resynchronization at tertiary control level in order to coordinate the microgrid connection and disconnection to the main power system;

c) Introduce a dynamic tuning for the virtual impedance at each converter primary control level, in order to ensure distinct feeder lines impedance adjustments while maintaining proper active and reactive power sharing in a low-voltage microgrid;

d) Verify the adapted economic strategy cost-saving performance in a long-term energy market parameters variation scenario, were a complex microgrid with several distinct distributed generators, feeders lines and loads could be considered;

e) Perform microgrid prototype simulations considering the adapted droop-based economic strategy for practical validation of the analyzed control scheme;

f) Compare the adapted economic dispatch strategy performance with other existing microgrid distributed and/or concentrated economic power management approaches.

5.2 Publications

During the course of this research, some publications were produced based on or somehow related to the content of this manuscript and those were listed below.

- PEDROSO, J. P. de C., FERREIRA, S. C. **"Análise das variações de potência ativa, reativa e distorções harmônicas en função da potência instalada de um gerador fotovoltaico operando como fonte de corrente,"** XXVII Congresso da Pós-Graduação da Universidade Federal de Lavras, 2018.

- PEDROSO, J. P. de C., FERREIRA, S. C., GUIMARÃES, R. A. **"Compartilhamento de potências ativa e reativa entre conversores formadores de rede em uma microrrede isolada empregando técnica droop,"** XXVIII Congresso da Pós-Graduação da Universidade Federal de Lavras, 2019.

- GUIMARÃES, R. A., FERREIRA, S. C., PACHECO, V. M., PEDROSO, J. P. de C., RIBEIRO, J. E., VIANA, O. S., LEITE, D. F. **"Controle preditivo baseado em modelo para conversores formadores de rede com operação ilhada,"** Simpósio Brasileiro de Automação Inteligente - SBAI 2019, 2019.

- PEDROSO, J. P. de C., FERREIRA, S. C., GUIMARÃES, R. A. **"Aplicação do FCS-MPC para despacho econômico em microrredes ilhadas,"** XXIII Congresso Brasileiro de Automática Lavras - CBA 2020, 2020.
- GUIMARÃES, R. A., FERREIRA, S. C., PEDROSO, J. P. de C., PACHECO, V. M., VIANA, O. S. **"Conversor formador de rede controlado por FCS-MPC com função custo multivariável,"** XXIII Congresso Brasileiro de Automática Lavras - CBA 2020, 2020.

APPENDIX A – Simulation Diagrams

The schematics used for the simulations are presented is presented in Figure 1

Figure 1 – Electrical diagram: Microgrid simulation for active and active-reactive demand.

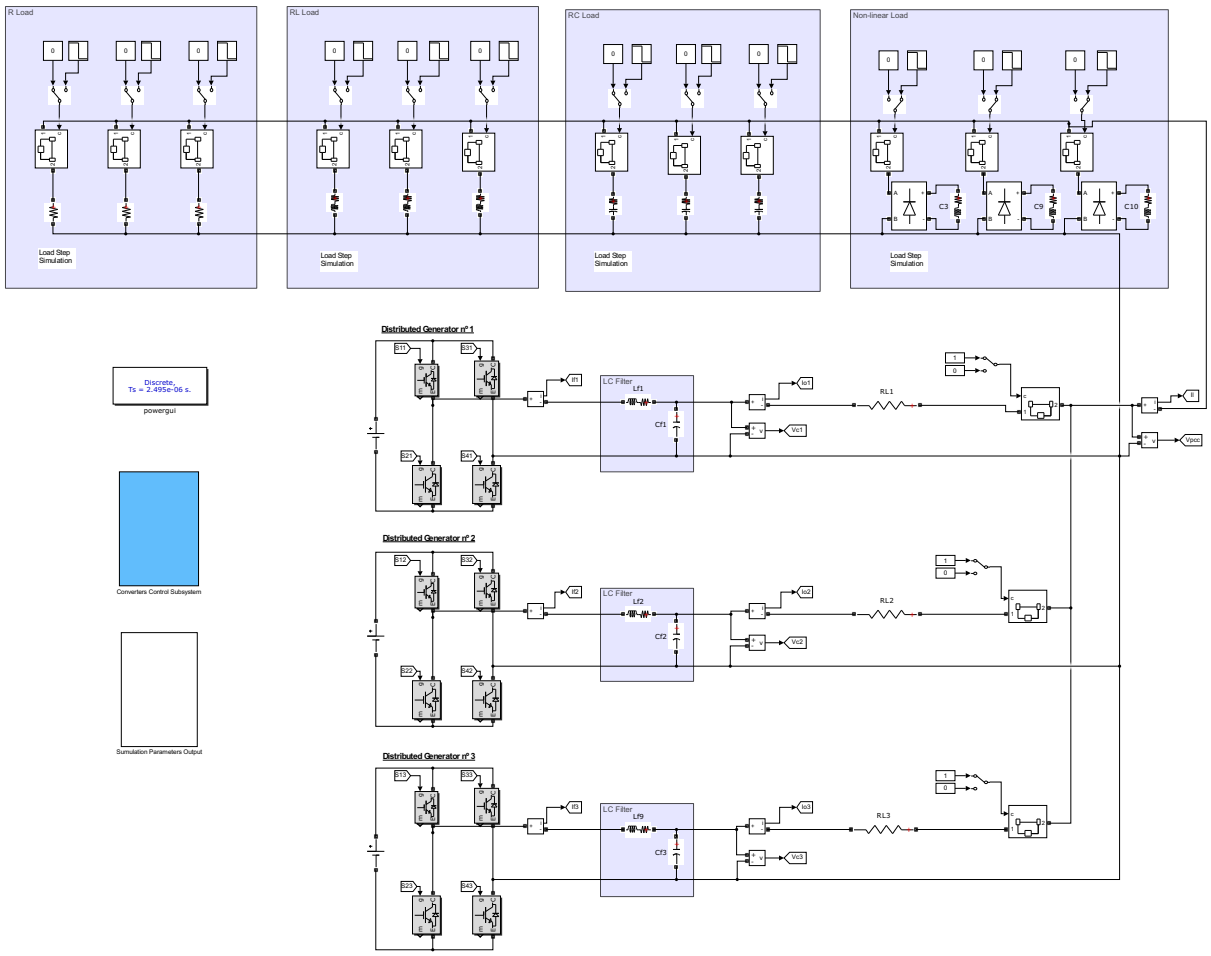

Source: From author (2021)

The control block used in this work can be seen in Figure 2

Figure 2 – Tertiary control for P-V/Q-f Droop scheme.

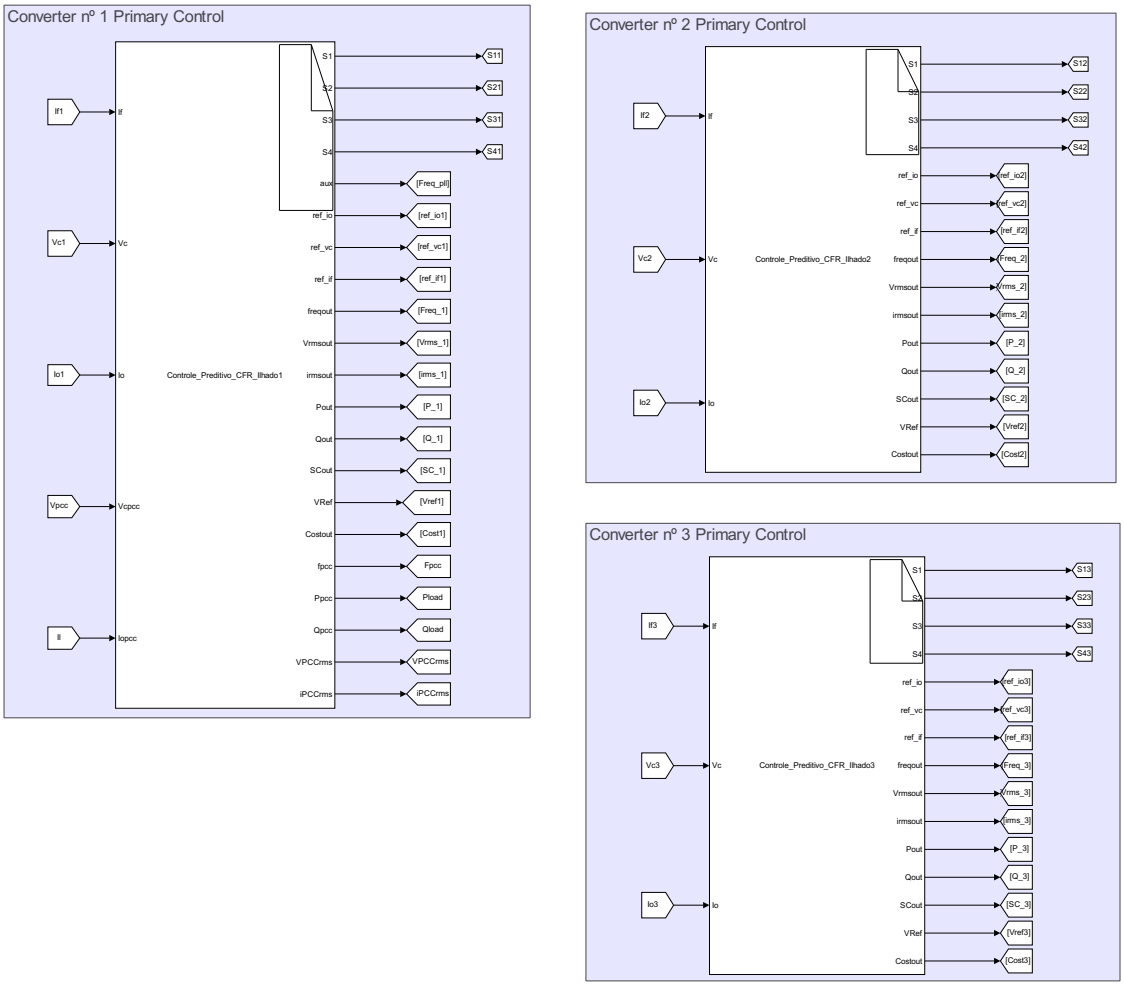

Source: From author (2021)

APPENDIX B – MATLAB/*Simulink* Control Algorithms

The following algorithms were developed in MATLAB .m and *Simulink* S-Function environments in order to implement both the conventional resistive droop control and the adapted economic dispatch strategy at tertiary and primary microgrid hierarchical control levels, respectively.

The primary control algorithm for both the conventional resistive droop method and the adapted economic dispatch strategy were implemented in *Simulink* S-Function control block using C programming language and is present presented first in Section .1.

The tertiary control algorithms for the traditional resistive droop control and for the adapted economic dispatch strategy are presented in Sections .2.1 and .2.2, respectively.

.1 Primary Control

Figure 3 – Primary control algorithm - Part I

```
//Primary Control Algorithm

//Microgrid control strategy selection
MCtrl = 1;//0 - Conventional droop or 1 - Adapted Dispatch Strategy
NGD = 3;//Number of microgrid distributed generators
N = 3;//Unit dispach priority - Tertiary control imput

//Droop control parameters initiation - Tertiary control imput
//Distributed generator rated parametes
Pmax = 500;//Active power maximum dispatch capacity [W]
Qmax = 500;//Reactive power maximum dispatch capacity [VAr]

RL = 0.5; //Feeder line resistence [Ohms]
Rv1 = 2.5;//Virtual resistence [Ohms]

//Voltage reference parameters definition
if (MCtrl == 0)
{
Vmax = 128.555;//Vmax,MG
Vmin = 121.445;//Vmin,MG
}

if (MCtrl == 0)
{
    if (NGD = 2)
    {
        if (N == 1)
        {
        Vmax = 128.555;//Vmax,1,1
        Vmin = 124.445;//Vmin,1,1
        }
        if (N == 2)
        {
        Vmax = 126.5;//Vmax,2,2
        Vmin = 121.445;//Vmin,2,2
        }
    }
    if (NGD = 3)
    {
        if (N == 1)
        {
        Vmax = 128.555;//Vmax,1,1
        Vmin = 124.445;//Vmin,1,1
        }
        if (N == 2)
        {
        Vmax = 126.5;//Vmax,2,2
        Vmin = 122.6235;//Vmin,2,2
        }
        if (N == 3)
        {
        Vmax = 124.5618;//Vmax,3,3
        Vmin = 121.445;//Vmin,3,3
        }
    }
}

//Frequency parameters definition
Fmax = 60.5;//Microgrid maximum frequency - FmaxMG
Fmin = 59.5;//Microgrid minimun frequency - FminMG
Fn = 60;    //Microgrid nominal frequency reference
```

Source: From author (2021)

Figure 4 – Primary control algorithm - Part II

```
//Global variables initiation
g_opt = 1e10;
i=0;
j=0;
raiz=0.707106781186547;

//Converter and LC filter parameters iniciation
C = 60e-6;   //Filter capacitance - Cf
L = 2.0e-3;  //Filter inductance - Lf
R = 0.1;     //Filter inner resistence - Rf
Vdc=310;     //DC link volatage

//FCS-MPC imput parameters - Converter local sensors
vck = Vc[0]; //Filter output coltage
ifk = If[0]; //Converter output current
iok = Io[0]; //Filter output current

//Voltage vector initiation
v[0]  = 0;
v[1]  = Vdc;
v[2]  = -Vdc;
v[3]  = 0;

//Swiching states setting
S1[0] = states[x_opt][0];
S2[0] = states[x_opt][1];
S3[0] = states[x_opt][2];
S4[0] = states[x_opt][3];

//FCS-MPC fisrt prediction step - k+1
ifk1 = (1-(R*Ts/L))*ifk - (Ts/L)*vck + (Ts/L)*v[x_old];
vck1 = vck + (Ts/C)*ifk1 - (Ts/C)*iok;

//Adaptatice filter for converter output current
u=0.01;
io1 = w3*X_sen + w4*X_cos;
w3 = w3 + u*erro_io*X_sen;
w4 = w4 + u*erro_io*X_cos;
erro_io = iok - io1;

//Adaptative filter for PCC voltage
u=0.25;
vs1 = w5*X_sen + w6*X_cos;
w5 = w5 + u*erro_vs*X_sen;
w6 = w6 + u*erro_vs*X_cos;
erro_vs = vsk - vs1;

//Adaptive notch filter for LC filter output voltage - Vf
gamav = 0.09;
w1_pllv= w1_pllv - Ts*gamav*x1v*w1_pllv*e1v;
xd1v = xd1v + Ts*(2*0.707*w1_pllv*e1v-(w1_pllv*w1_pllv*x1v));
x1v  = x1v + Ts*xd1v;
xd5v = xd5v + Ts*(2*0.3*w1_pllv*e1v-(25*w1_pllv*w1_pllv*x5v));
x5v  = x5v + Ts*xd5v;
e1v= vck - (xd1v+xd5v);

//Adaptive notch filter for LC filter output current - Io
xd1i = xd1i + Ts*(2*0.707*w1_pllv*e1i-(w1_pllv*w1_pllv*x1i));
x1i  = x1i + Ts*xd1i;
xd5i = xd5i + Ts*(2*0.3*w1_pllv*e1i-(25*w1_pllv*w1_pllv*x5i));
x5i  = x5i + Ts*xd5i;
```

Source: From author (2021)

Figure 5 – Primary control algorithm - Part III

```
e1i = iok - (xd1i+xd5i);

//Outuput vaoltage and current RMS determination
Vrms=raiz*sqrt((xd1v*xd1v)+(w1_pllv*x1v)*(w1_pllv*x1v));
irms=raiz*sqrt((xd1i*xd1i)+(w1_pllv*x1i)*(w1_pllv*x1i));

//Active and Reactive power calculation
P = ((w1_pllv*w1_pllv*x1v*x1i + xd1i*xd1v)*0.5);
Q = (-w1_pllv*(xd1v*x1i - x1v*xd1i)*0.5);

//PCC volatege estimation
vsk = vck-x1i*(RL + Rv1);

//Droop control reference determination
kp = (Vmax-Vmin)/(-Pmax);
kq = (Fmax-Fmin)/(-Qmax);
Vref = Vmax+kp*P;
Fref = Fn-kq*Q;

//Converter operational control mode definition
if (N == 1)//Highest priority operate as grid-forming converter
{
ctrl = 1;
}
if (N =! 1)//Other priority units control mode selection
{
if ((Vrms>=(Vmax - 0.1)))
{
    cont_sup = cont_sup + 1;
    cont_inf = 0;
}
if (Vrms<(Vmax - 0.1))
{
    cont_inf = cont_inf + 1;
    cont_sup = 0;
}
if ((cont_sup>668) || (flag_sup == 1))
{
    ctrl = 0;
    flag_sup = 1;
    flag_inf = 0;
}
else
{
    ctrl=1;
}
if ((cont_inf>668) || flag_inf == 1)
{
    ctrl = 1;
    flag_sup = 0;
    flag_inf = 1;
}
}

// Reference signals detemination
if (ctrl == 0)//Grid-feeding signal reference
{
    X_sen = X_sen_pll;
    X_cos = X_cos_pll;
    wt_pll_ref = wt_pll;
    wt_ref = wt_pll_ref;
```

Source: From author (2021)

Figure 6 – Primary control algorithm - Part IV

```
}

if (ctrl ==1)//Grid-forming signal reference
{
    f_ref = Fref;
    w_ref = 2*pi*f_ref;
    if ((i2>6680) && (vc_ref>=0) && (Vsk_1<0) && (Rsoma<0))
    {
    wt_ref = 0;
    i2 = 0;
    }
    i2=i2 + 1;
    wt_ref = wt_ref + Ts*w_ref;
    Rsoma = Vsk_2 + Vsk_3 + Vsk_4 + Vsk_5;
    Vsk_5 = Vsk_4;
    Vsk_4 = Vsk_3;
    Vsk_3 = Vsk_2;
    Vsk_2 = Vsk_1;
    Vsk_1 = vc_ref;
    X_sen = sin(wt_ref);
    X_cos = cos(wt_ref);
}

//FCS-MPC internal reference signals determination
if (ctrl == 0)
{
    Io_refd = 0; //Null current reference
    Io_refq = 0; //Null current reference
    Vc_refd = w5;
    Vc_refq = w6;
    If_refd = Io_refd - (w1_pll*C)*Vc_refq;
    If_refq = Io_refq + (w1_pll*C)*Vc_refd;
}

if (ctrl == 1)
{
    Io_refd = w3;
    Io_refq = w4;
    Vc_refd = Vref*sqrt(2);
    Vc_refq = 0;
    If_refd = Io_refd - (2*pi*f_ref*C)*Vc_refq;
    If_refq = Io_refq + (2*pi*f_ref*C)*Vc_refd;
}

//Converter inner reference determination - Io, Vf, If
io_ref = Io_refd*X_sen + Io_refq*X_cos;
vc_ref = Vc_refd*X_sen + Vc_refq*X_cos - Rv1*io1;
if_ref = If_refd*X_sen + If_refq*X_cos;

//FCS-MPC execution
while (i<=2)
{
    //FCS-MPC second prediction step - k+2
    ifk2 = (1 - (R*Ts/L))*ifk1 - (Ts/L)*vck + (Ts/L)*v[i];
    vck2 = vck1 + (Ts/C)*ifk2 - (Ts/C)*iok;

    //Switching state selection regulator
    if ((cont==50) && (i==x_old))
    {
        ke=10e10;
    }
```

Source: From author (2021)

Figure 7 – Primary control algorithm - Part V

```
    else
    {
        ke=0;
    }

    //Quality const function
    g_i = (if_ref - ifk2)*(if_ref - ifk2);//Current quality cost
function
    g_v = (vc_ref - vck2)*(vc_ref - vck2);//voltage quality cost
function

    if (ctrl == 0)   g = 100*g_i + g_v + ke;//Grid-feeding quality
cost function
    if (ctrl == 1)   g = g_i + g_v +ke;//Grid-forming quality cost
function

    //Optimal values selection
    if (g<g_opt)
    {
        g_opt = g;
        x_opt = i;
    }
     i=i+1;
}

//Switching states limiter
if (x_opt == x_old)
    cont = cont + 1;
else
    cont = 0;

x_old = x_opt;

//ANF-FE based PLL for microgrid PCC
gama = 20000;
w1_pll= w1_pll - Ts*gama*x1*w1_pll*e1;
xd1 = xd1 + Ts*(2*0.707*w1_pll*e1-(w1_pll*w1_pll*x1));
x1  = x1 + Ts*xd1;
xd5 = xd5 + Ts*(2*0.707*w1_pll*e1-(25*w1_pll*w1_pll*x5));
x5  = x5 + Ts*xd5;
e1= vsk/180 - (xd1+xd5);
a = sqrt((xd1*xd1) + (w1_pll*w1_pll*x1*x1));
X_sen_pll = xd1/a;
X_cos_pll = -w1_pll*x1/a;
wt_pll = atan2(X_sen_pll,X_cos_pll);
if(wt_pll<0) wt_pll = wt_pll + 2*pi;
VPCCrmsFAS=raiz*sqrt((xd1*xd1)+(w1_pll*x1)*(w1_pll*x1));
FreqPCCFAS=w1_pll/(2*pi);

//Instantaneous operational cost calculation
if (N == 1)
{
cF=0.01;//Fuel cost conversion factor [$/kW]
cM=0.02;//Maintenance cost conversion factor [$/kW]
ce=0.001;//Emission cost conversion factor [$/kW]
Cost = (cM*P+(cF*(2+1*P+2*P*P))+(ce*(1-
1*P+5.5*(P*P)+0.0002*pow(3*sqrt(P*P),2.71828))))/(Pmax*3600*1000000/
1000);//Operational cost function - DG1
}
if (N == 2)
{
```

Source: From author (2021)

Figure 8 – Primary control algorithm - Part VI

```
cF=0.1;//Fuel cost conversion factor [$/kW]
cM=0.01;//Maintenance cost conversion factor [$/kW]
ce=0.005;//Emission cost conversion factor [$/kW]
Cost =
((cF+cM+ce)*(P+0.05+0.01*P+0.12*P*P))/(Pmax*3600*1000000/1000);
//Operational cost function - DG2

}
if (N == 3)
{
cF=0.01;//Fuel cost conversion factor [$/kW]
cM=0.02;//Maintenance cost conversion factor [$/kW]
ce=0.01;//Emission cost conversion factor [$/kW]
Cost = (cM*P+(cF*(4+12*P+2*P*P))+(ce*(1-
2*P+6.5*(P*P)+0.0002*pow(3*sqrt(P*P),2.71828))))/(Pmax*3600*1000000/
1000); //Operational cost function - DG3
}

//Output variables exibition
ref_io[0] = io_ref;
ref_vc[0] = vc_ref;
ref_if[0] = if_ref;
Vrmsout[0] = Vrms;
irmsout[0] = irms;
freqout[0] = w1_pll/(2*pi);
Pout[0] = P;
Qout[0] = Q;
SCout[0] = ctrl;
VRef[0] = Vref;
Costout[0] = Cost;
```

Source: From author (2021)

.2 Tertiary Control

.2.1 Microgrid traditional resistive droop control tertiary control algorithm

Figure 9 – Tertiary control algorithm for traditional resistive droop control strategy - Part I

```
%Tertiary Control Algorithm - Conventional Droop Control
clc;
clear all;

%Number of DG units to participate in economic dispach scheme
N == 3;

%Power quality parameters difinition
Vref = 127;%Voltage reference [V]
VmaxSTANDARD = 133;%Brasilian standart maximum voltage for low
voltage distribution systems - ANEEL/PRODIST [V]
VminSTANDARD = 117;%Brasilian standart minimum voltage for low
voltage distribution systems - ANEEL/PRODIST [V]
FmaxSTANDARD = 60.5;%Microgrid defined maximum frequency for low
voltage distribution systems [Hz]
FminSTANDARD = 59.5;%Microgrid defined minimum frequency for low
voltage distribution systems [Hz]

%Converters power ratings definition
Pmax=1;%Maximum dispatchable power for each generator [p.u.]
Pmin=0;%Minimum dispatchable power for each generator [p.u.]
Qmax=1;%Maximum reactive dispatchable power for each generator
[p.u.]
Qmin=-1;%Minimum reactive dispatchable power for each generator
[p.u.]

%Resistive droop P-V/Q-f general parameters limits
deltaVmax = 5;%Maximum voltage range [V]
deltaVmin = 3;%Minimun voltage range [V]
var = 3.5;%Maximum tolerated voltage amplitude deviation [%]
Vmax = VmaxSTANDARD-(var/100)*Vref;%Microgrid defined maximun
voltage amplitude [V]
Vmin = VminSTANDARD+(var/100)*Vref;%Microgrid defined minimum
frequency [V]
Fmax = FmaxSTANDARD;%Maximum allowed frequency [Hz]
Fmin = FminSTANDARD;%Minimum allowed frequency [Hz]

n=0.000001;
P=Pmin:n:Pmax;
Q=Qmin:n:Qmax;

if N == 2
{
%Active Power Droop Curves - Proportional P-V droop curves
VGDP1=Vmax-P*(Vmax-Vmin)/(Pmax-Pmin);
VGDP2=Vmax-P*(Vmax-Vmin)/(Pmax-Pmin);

%Reactive Power Droop Curves - Proportional Q-f droop curves
FGDP1=Fmin-Q*((Fmax-Fmin)/(Qmin-Qmax))+2;
FGDP2=Fmin-Q*((Fmax-Fmin)/(Qmin-Qmax))+2;

%Print Graphs
figure(1)
plot(P,VGDP1,'b',P,VGDP2,'r','Linewidth',1.5)
ylim([120 130])
xlabel('Active power demand P_{i} - p.u.','FontSize',15)
ylabel('{\it rms} Voltage reference V_{i} - V','FontSize',15)
grid on

figure(2)
plot(Q,FGDP1,'b',Q,FGDP2,'r','Linewidth',1.5)
```

Source: From author (2021)

Figure 10 – Tertiary control algorithm for traditional resistive droop control strategy - Part II

```
ylim([59 61])
xlabel('Reactive power demand Q_{i} - p.u.','FontSize',15)
ylabel('Frequency reference f_{i} - Hz','FontSize',15)
grid on
}

if N == 3
{
%Active Power Droop Curves - Proportional P-V droop curves
VGDP1=Vmax-P*(Vmax-Vmin)/(Pmax-Pmin);
VGDP2=Vmax-P*(Vmax-Vmin)/(Pmax-Pmin);
VGDP3=Vmax-P*(Vmax-Vmin)/(Pmax-Pmin);

%Reactive Power Droop Curves - Proportional Q-f droop curves
FGDP1=Fmin-Q*((Fmax-Fmin)/(Qmin-Qmax))+0.5;
FGDP2=Fmin-Q*((Fmax-Fmin)/(Qmin-Qmax))+0.5;
FGDP3=Fmin-Q*((Fmax-Fmin)/(Qmin-Qmax))+0.5;

%Print Graphs
figure(1)
plot(P,VGDP1,'b',P,VGDP2,'r',P,VGDP3,'g','Linewidth',1.5)
ylim([120 130])
xlabel('Active power demand P_{i} - p.u.','FontSize',15)
ylabel('{\it rms} Voltage reference V_{i} - V','FontSize',15)
grid on

figure(2)
plot(Q,FGDP1,'b',Q,FGDP2,'r',Q,FGDP3,'g','Linewidth',1.5)
ylim([59 61])
xlabel('Reactive power demand Q_{i} - p.u.','FontSize',15)
ylabel('Frequency reference f_{i} - Hz','FontSize',15)
grid on
}

%Print Results
for i=1:N
fprintf('DG unit n°: %6.0f \n',i)
fprintf('Maximum dispatch voltage = %6.3f [V]\n', Vmax)
fprintf('Minimum dispatch voltage = %6.3f [V]\n', Vmin)
fprintf('Maximum dispatch frequency = %6.3f [Hz]\n', Fmax)
fprintf('Minimum dispatch frequency = %6.3f [Hz]\n', Fmin)
fprintf('\n')
end
```

Source: From author (2021)

.2.2 Microgrid adapted economic dispatch strategy tertiary control algorithm

Figure 11 – Tertiary control algorithm for adapted economic dispatch strategy - Part I

```
%Tertiary Control Algorithm - Adapted Droop-based Economic Power
Sharing Strategy for Low-voltage Microgrids
clc;
clear all;

%Number of DG units to participate in economic dispach scheme
N == 3;

%Power quality parameters difinition
Vref = 127;%Voltage reference [V]
VmaxSTANDARD = 133;%Brasilian standart maximum voltage for low
voltage distribution systems - ANEEL/PRODIST [V]
VminSTANDARD = 117;%Brasilian standart minimum voltage for low
voltage distribution systems - ANEEL/PRODIST [V]
FmaxSTANDARD = 60.5;%Microgrid defined maximum frequency for low
voltage distribution systems [Hz]
FminSTANDARD = 59.5;%Microgrid defined minimum frequency for low
voltage distribution systems [Hz]

%Converters power ratings definition
Pmax=1;%Maximum dispatchable power for each DG [p.u.]
Pmin=0;%Minimum dispatchable power for each DG [p.u.]
Qmax=1;%Maximum reactive dispatchable power for each DG [p.u.]
Qmin=-1;%Minimum reactive dispatchable power for each DG [p.u.]

%Online power reserve definition
deltapstep = 0.5;% [p.u.]

%Resistive droop P-V/Q-f general parameters limits
var = 3.5;%Maximum tolerated voltage amplitude deviation [%]
Vmax = VmaxSTANDARD-(var/100)*Vref;%Microgrid defined maximun
voltage amplitude [V]
Vmin = VminSTANDARD+(var/100)*Vref;%Microgrid defined minimum
voltage amplitude [V]
Fmax = FmaxSTANDARD;%Maximum allowed frequency [Hz]
Fmin = FminSTANDARD;%Minimum allowed frequency [Hz]

n = 0.000001;
P = Pmin:n:Pmax;
Q = Qmin:n:Qmax;
LIM = [Pmin Pmax];

%DG n°1 Parameters
GD1 = 1;%Unit designation number
F1 = 0.1;%Fuel cost conversion factor [$/kW]
M1 = 0.01;%Maintenance cost conversion factor [$/kW]
e1 = 0.005;%Emission cost conversion factor [$/kW]
Pmax1 = 500;%Maximum active DG rated power [W]
Qmax1 = 500;%Maximum reactive DG rated power [VAR]

%Operational cost function of DG n° 1
C1 = @(P)((F1+M1+e1)*(P+0.05+0.01*P+0.12*P.^2))/(Pmax1*6.93*10^-7);
C11 = ((F1+M1+e1)*(P+0.05+0.01*P+0.12*P.^2))/(Pmax1*6.93*10^-7);

%Normalized total generation cost for DG n°1
Cmed1 = (integral(C1,0,Pmax)/(Pmax-Pmin));
Cmax1 = C1(Pmax);
Cmin1 = C1(Pmin);


%Normalized total generation cost without no-load cost for DG n°1
```

Source: From author (2021)

Figure 12 – Tertiary control algorithm for adapted economic dispatch strategy - Part II

```
C12 = C11-Cmin1;
Cmed12 = Cmed1-Cmin1;
Cmin12 = C1(Pmin)-Cmin1;
Cmax12 = C1(Pmax)-Cmin1;

%DG n°2 Parameters
GD2 = 2;%Unit designation number
F2 = 0.01;%Fuel cost conversion factor [$/kW]
M2 = 0.02;%Maintenance cost conversion factor [$/kW]
e2 = 0.01;%Emission cost conversion factor [$/kW]
Pmax2 = 500;%Maximum active DG rated power [W]
Qmax2 = 500;%Maximum reactive DG rated power [VAR]

%Operational cost function of DG n° 2
C2 = @(P)((M2*P+(F2*(4+12*P+2*P.^2))+(e2*(1-
2*P+6.5*(P.^2)+0.0002*exp(3*sqrt(P.^2) ))))/(Pmax2*6.93*10^-7);
C21 = ((M2*P+(F2*(4+12*P+2*P.^2))+(e2*(1-
2*P+6.5*(P.^2)+0.0002*exp(3*sqrt(P.^2) ))))/(Pmax2*6.93*10^-7);

%Normalized total generation cost for DG n°2
Cmed2 = (integral(C2,0,Pmax)/(Pmax-Pmin));
Cmax2 = C2(Pmax);
Cmin2 = C2(Pmin);

%Normalized total generation cost without no-load cost for DG n°2
C22 = C21-Cmin2;
Cmed22 = Cmed2-Cmin2;
Cmin22 = C2(Pmin)-Cmin2;
Cmax22 = C2(Pmax)-Cmin2;

%DG n°3 Parameters
GD3 = 3;%Unit designation number
F3 = 0.01;%Fuel cost conversion factor [$/kW]
M3 = 0.02;%Maintenance cost conversion factor [$/kW]
e3 = 0.001;%Emission cost conversion factor [$/kW]
Pmax3 = 500;%Maximum active DG rated power [W]
Qmax3 = 500;%Maximum reactive DG rated power [VAR]

%Operational cost function of DG n° 3
C3 = @(P)((M3*P+(F3*(2+1*P+2*P.^2))+(e3*(1-
1*P+5.5*(P.^2)+0.0002*exp(3*sqrt(P.^2) ))))/(Pmax3*6.93*10^-7);
C31 = ((M3*P+(F3*(2+1*P+2*P.^2))+(e3*(1-
1*P+5.5*(P.^2)+0.0002*exp(3*sqrt(P.^2) ))))/(Pmax3*6.93*10^-7);

%Normalized total generation cost for DG n°3
Cmed3 = (integral(C3,0,Pmax)/(Pmax-Pmin));
Cmax3 = C3(Pmax);
Cmin3 = C3(Pmin);

%Normalized total generation cost without no-load cost for DG n°3
C32 = C31-Cmin3;
Cmed32 = Cmed3-Cmin3;
Cmin32 = C3(Pmin)-Cmin3;
Cmax32 = C3(Pmax)-Cmin3;

if N == 2
{
%Maximum dispatchable active and reactive power for each DG unit
Pactive=[Pmax1 Pmax2];
Qreactive=[sqrt((Qmax1^2)-(Pmax1^2)) sqrt((Qmax2^2)-(Pmax2^2))];
```

Source: From author (2021)

Figure 13 – Tertiary control algorithm for adapted economic dispatch strategy - Part III

```
%Dispatch priority order assingnement
M1=[GD1, Cmed1];
M2=[GD2, Cmed2];
O=[1:N];

%Unity dispatch priority definition
if Cmed1>Cmed2
    M=[M2;M1];
elseif Cmed2>Cmed1
    M=[M1;M2];
else
    M=[M1;M2];
end
M=[M,O'];
l=size(M);

%Highest dispatch priority DG reference voltage limits
VmaxGDP1=Vmax;
VminGDP1=Vmin+deltaVmin;

%Intermediary dispatch priority DG reference voltage limits
lamb1=(VmaxGDP1-VminGDP1)/Pmax;
Vmax1=Vmax-deltaVmax*((M(2,3)-1)/(N-1));
Vmax2=VminGDP1+lamb1*deltapstep;
if Vmax1>=Vmax2
    VmaxGDP2=Vmax1;
else
    VmaxGDP2=Vmax2;
end
VminGDP2=Vmin;
Vmaxmin=[VmaxGDP1 VminGDP1;VmaxGDP2 VminGDP2];
M=[M Vmaxmin];

%Dispatch curves inner parameters calculation
func=[];
for i=1:N
b=M(i,4);
a=(M(i,5)-b)/Pmax;
func(i,1)=a;
func(i,2)=b;
end
M=[M func];

%Active Power Economic Droop Curves - Drive voltage apltitude
determination of subsequent generation units due to power reserve
VGDP1=P*M(1,6)+M(1,7);
VGDP2=P*M(2,6)+M(2,7);
Vmed1=deltapstep*M(1,6)+M(1,7);
Vmed2=deltapstep*M(2,6)+M(2,7);
Vmed=[Vmed1;Vmed2];
M=[M Vmed];

%Reactive Power Droop Curves
FGDP1=Fmin-Q*((Fmax-Fmin)/(Qmin-Qmax))+0.5;
FGDP2=Fmin-Q*((Fmax-Fmin)/(Qmin-Qmax))+0.5;

%Print Results
fprintf('ECONOMIC DISPACH AND MICROGRID GENERAL PARAMETERS\n\n')
fprintf('A)Microgrid general parameters\n')
fprintf('Microgrid maximun voltage amplitude = %6.2f [V]\n', Vmax)
fprintf('Microgrid minimum voltage amplitude = %6.2f [V]\n', Vmin)
```

Source: From author (2021)

Figure 14 – Tertiary control algorithm for adapted economic dispatch strategy - Part IV

```
fprintf('Maximum voltage amplitude range = %6.2f [V]\n', deltaVmax)
fprintf('Minimum voltage amplitude range = %6.2f [V]\n', deltaVmin)
fprintf('Online power reserve = %6.2f [p.u.]\n', deltapstep)
fprintf('\n')
fprintf('B) DG Cost Functions:\n')
fprintf('Number of generation units participating on the economic
dispatch scheme : n°: %6.0f \n\n',N)
fprintf('DG unit n°: %6.0f \n',GD1)
fprintf('Normalized minimum cost = %6.4f [C´min]\n', Cmin1)
fprintf('Normalized average cost = %6.4f [C´med]\n', Cmed1)
fprintf('Normalized maximum cost = %6.4f [C´max]\n', Cmax1)
fprintf('Normalized minimum cost without no-load operation cost =
%6.4f [C"min]\n', Cmin12)
fprintf('Normalized average cost without no-load operation cost =
%6.4f [C"med]\n', Cmed12)
fprintf('Normalized maximum cost without no-load operation cost =
%6.4f [C"max]\n', Cmax12)
fprintf('\n')
fprintf('DG unit n°: %6.0f \n',GD2)
fprintf('Normalized minimum cost = %6.4f [C´min]\n', Cmin2)
fprintf('Normalized average cost = %6.4f [C´med]\n', Cmed2)
fprintf('Normalized maximum cost = %6.4f [C´max]\n', Cmax2)
fprintf('Normalized minimum cost without no-load operation cost =
%6.4f [C"min]\n', Cmin22)
fprintf('Normalized average cost without no-load operation cost =
%6.4f [C"med]\n', Cmed22)
fprintf('Normalized maximum cost without no-load operation cost =
%6.4f [C"max]\n', Cmax22)
fprintf('\n')
fprintf('C) Dispatch Priority Definition\n\n')
for i=1:N
fprintf('Dispatch Priority = %6.0f\n', M(i,3))
fprintf('DG unit n°: %6.0f \n',M(i,1))
fprintf('Cost curve moving average = %6.4f [C´med]\n', M(i,2))
fprintf('Maximum voltage amplitude = %6.3f [V]\n', M(i,4))
fprintf('Minimum voltage amplitude = %6.3f [V]\n', M(i,5))
fprintf('DG maximum dispatchable active power = %6.0f [kW]\n',
Pactive(1,i))
fprintf('DG maximum dispatchable reactive power = %6.0f [kVar]\n',
Qreactive(1,i))
fprintf('\n')
end
fprintf('\n')
fprintf('Matrix - DG unit n°|Average cost|Dispatch
priority|Vmax[V]|Vmin[V]|Coef. a|Coef. b|Voltage Drive Online
Reserve')
M
C3=0;
C32=0;
VGDP3=0;
FGDP3=0;
}

if N == 3
{

CNormNL=[Cmed12 Cmed22 Cmed32];

%Maximum dispatchable active and reactive power for each DG unit
Pactive=[Pmax1 Pmax2];
Qreactive=[sqrt((Qmax1^2)-(Pmax1^2)) sqrt((Qmax2^2)-(Pmax2^2))];
```

Source: From author (2021)

Figure 15 – Tertiary control algorithm for adapted economic dispatch strategy - Part V

```
%Dispatch priority order assingnement
M1=[GD1, Cmed1*(10^9), Cmed12];
M2=[GD2, Cmed2*(10^9), Cmed22];
M3=[GD3, Cmed3*(10^9), Cmed32];
O=[1:N];

%Unit dispatch priority definition
if Cmed1>Cmed2 && Cmed3>Cmed2
    if Cmed1>Cmed3
        M=[M2;M3;M1];
    elseif Cmed3>Cmed1
        M=[M2;M1;M3];
    else
        M=[M2;M1;M3];
    end
 end
 if Cmed2>Cmed1 && Cmed3>Cmed1
    if Cmed2>Cmed3
        M=[M1;M3;M2];
    elseif Cmed3>Cmed2
        M=[M1;M2;M3];
    else
        M=[M1;M2;M3];
    end
 end
 if Cmed1>Cmed3 && Cmed2>Cmed3
    if Cmed2>Cmed1
        M=[M3;M1;M2];
    elseif Cmed1>Cmed2
        M=[M3;M2;M1];
    else
        M=[M3;M2;M1];
    end
 end
if Cmed1==Cmed2 && Cmed2==Cmed3
    M=[M1;M2;M3];
end
M=[M,O'];
l=size(M);

%Highest dispatch priority DG reference voltage limits
VmaxGDP1=Vmax;
VminGDP1=Vmin+deltaVmin;

%Intermediary dispatch priority DG reference voltage limits
lamb1=(VmaxGDP1-VminGDP1)/Pmax;
Vmax11=Vmax-deltaVmax*((M(2,4)-1)/(N-1));
Vmax21=VminGDP1+lamb1*deltapstep;
if Vmax11>=Vmax21
    VmaxGDP2=Vmax11;
else
    VmaxGDP2=Vmax21;
end
VminGDP2=Vmin+deltaVmin*((max(CNormNL)-M(2,3))/(max(CNormNL)-
min(CNormNL)));

%Lowest dispatch priority DG reference voltage limits
lamb2=(VmaxGDP2-VminGDP2)/Pmax;
Vmax12=Vmax-deltaVmax*((M(3,4)-1)/(N-1));
Vmax22=VminGDP2+lamb2*deltapstep;
```

Source: From author (2021)

Figure 16 – Tertiary control algorithm for adapted economic dispatch strategy - Part VI

```
if Vmax12>=Vmax22
    VmaxGDP3=Vmax12;
else
    VmaxGDP3=Vmax22;
end
VminGDP3=Vmin;
Vmaxmin=[VmaxGDP1 VminGDP1; VmaxGDP2 VminGDP2; VmaxGDP3 VminGDP3];
M=[M Vmaxmin];

%Dispatch curves inner parameters calculation
for i=1:N
b=M(i,5);
a=(M(i,6)-b)/Pmax;
func(i,1)=a;
func(i,2)=b;
end
M=[M func];

%Active Power Economic Droop Curves - Drive voltage apltitude
determination of subsequent generation units due to power reserve
VGDP1=P*M(1,7)+M(1,8);
VGDP2=P*M(2,7)+M(2,8);
VGDP3=P*M(3,7)+M(3,8);
Vmed1=deltapstep*M(1,7)+M(1,8);
Vmed2=deltapstep*M(2,7)+M(2,8);
Vmed3=deltapstep*M(3,7)+M(3,8);
Vmed=[Vmed1;Vmed2;Vmed3];
M=[M Vmed];

%Reactive Power Droop Curves
FGDP1=Fmin-Q*((Fmax-Fmin)/(Qmin-Qmax))+0.5;
FGDP2=Fmin-Q*((Fmax-Fmin)/(Qmin-Qmax))+0.5;
FGDP3=Fmin-Q*((Fmax-Fmin)/(Qmin-Qmax))+0.5;

%Print Results
fprintf('ECONOMIC DISPACH AND MICROGRID GENERAL PARAMETERS\n\n')
fprintf('A)Microgrid general parameters\n')
fprintf('Microgrid maximun voltage amplitude = %6.2f [V]\n', Vmax)
fprintf('Microgrid minimum voltage amplitude = %6.2f [V]\n', Vmin)
fprintf('Maximum voltage amplitude range = %6.2f [V]\n', deltaVmax)
fprintf('Minimum voltage amplitude range = %6.2f [V]\n', deltaVmin)
fprintf('Online power reserve = %6.2f [p.u.]\n', deltapstep)
fprintf('\n')
fprintf('B) DG Cost Functions:\n')
fprintf('Number of generation units participating on the economic
dispatch scheme : n°: %6.0f \n\n',N)
fprintf('DG unit n°: %6.0f \n',GD1)
fprintf('Normalized minimum cost = %6.4f [C´min]\n', Cmin1)
fprintf('Normalized average cost = %6.4f [C´med]\n', Cmed1)
fprintf('Normalized maximum cost = %6.4f [C´max]\n', Cmax1)
fprintf('Normalized minimum cost without no-load operation cost =
%6.4f [C"min]\n', Cmin12)
fprintf('Normalized average cost without no-load operation cost =
%6.4f [C"med]\n', Cmed12)
fprintf('Normalized maximum cost without no-load operation cost =
%6.4f [C"max]\n', Cmax12)
fprintf('\n')
fprintf('DG unit n°: %6.0f \n',GD2)
fprintf('Normalized minimum cost = %6.4f [C´min]\n', Cmin2)
fprintf('Normalized average cost = %6.4f [C´med]\n', Cmed2)
fprintf('Normalized maximum cost = %6.4f [C´max]\n', Cmax2)
```

Source: From author (2021)

Figure 17 – Tertiary control algorithm for adapted economic dispatch strategy - Part VII

```
fprintf('Normalized minimum cost without no-load operation cost =
%6.4f [C"min]\n', Cmin22)
fprintf('Normalized average cost without no-load operation cost =
%6.4f [C"med]\n', Cmed22)
fprintf('Normalized maximum cost without no-load operation cost =
%6.4f [C"max]\n', Cmax22)
fprintf('\n')
fprintf('DG unit n°: %6.0f \n',GD3)
fprintf('Normalized minimum cost = %6.4f [C´min]\n', Cmin3)
fprintf('Normalized average cost = %6.4f [C´med]\n', Cmed3)
fprintf('Normalized maximum cost = %6.4f [C´max]\n', Cmax3)
fprintf('Normalized minimum cost without no-load operation cost =
%6.4f [C"min]\n', Cmin32)
fprintf('Normalized average cost without no-load operation cost =
%6.4f [C"med]\n', Cmed32)
fprintf('Normalized maximum cost without no-load operation cost =
%6.4f [C"max]\n', Cmax32)
fprintf('\n')
fprintf('C) Dispatch Priority Definition\n\n')
for i=1:N
fprintf('Dispatch Priority = %6.0f\n', M(i,4))
fprintf('DG unit n°: %6.0f \n',M(i,1))
fprintf('Cost curve moving average = %6.4f [C´med]\n', M(i,2))
fprintf('Maximum voltage amplitude = %6.3f [V]\n', M(i,5))
fprintf('Minimum voltage amplitude = %6.3f [V]\n', M(i,6))
fprintf('\n')
end
fprintf('\n')
fprintf('Matrix - DG unit n°|Average cost x10^-9|Averga no-load
cost|Dispatch priority|Vmax[V]|Vmin[V]|Coef. a|Coef. b|Voltage Drive
Online Reserve')
M
}

figure(1)
plot(P,C11,'b',P,C21,'r',P,C31,'g','Linewidth',1.5)
xlabel('Active power demand P_{i} - p.u.','FontSize',15)
ylabel('Operational cost per hour C´_{i}(P_{i}) -
$/hour','FontSize',15)
grid on
figure(2)
plot(P,C12,'b',P,C22,'r',P,C32,'g','Linewidth',1.5)
xlabel('Active power demand P_{i} - p.u.','FontSize',15)
ylabel('No-load operational cost per hour C"_{i}(P_{i}) -
$/hour','FontSize',15)
grid on
figure(3)
plot(P,VGDP1,'g',P,VGDP2,'b',P,VGDP3,'r','Linewidth',1.5)
xlabel('Active power demand P_{i} - p.u.','FontSize',15)
ylabel('{\it rms} Voltage reference V_{i} - V','FontSize',15)
grid on
figure(4)
plot(Q,FGDP1,'b',Q,FGDP2,'r',Q,FGDP3,'g','Linewidth',1.5)
ylim([59 61])
xlabel('Reactive power demand Q_{i} - p.u.','FontSize',15)
ylabel('Frequency reference f_{i} - Hz','FontSize',15)
grid on
```

Source: From author (2021)

APPENDIX C – MATLAB/*Simulink* virtual resistance analysis algotithm

The following algorithm was developed in MATLAB .m software environment to analyze the virtual resistance parameter variation effect over the considered microgrid resistive behavior.

Figure 18 – Virtual resistance analysis algorithm

```
%Virtual Resistance Verifivation - System equivalent impedance
elctrical model
clear all;
clc;

%Microgrid and converters LC impedance parameters
RL=0.5;%Feeder line ressitence [Ohms]
f=60;%Microgrid nominal frequency reference [Hz]
Cf=60e-6;%Filter capacitance [µC]
Lf=2e-3;%Filter inductance [mH]
Rf=0.1;%Filter inner resistance [Ohms]
Pnom=500;%Converter rated active power [W]
VminMG=121.445;%Microgrid minimum voltage [V]

%Virtual resistance evaluation range definition
RVmax=6;%Maximum RV value [Ohms]
n=0.1;
RV=0:n:RVmax;

i=length(RV);
Imax=Pnom/VminMG;

%System electrical model - Thevenin equivalent circuit
k=(sqrt((Rf^2)+(2*pi*f*Lf)^2))/(2*pi*f*Cf*(sqrt((Rf^2)+(2*pi*f*Lf-
1/(2*pi*f*Cf))^2)));
alpha=atan((2*pi*f*Lf/Rf))+atan(-pi/2)-atan((2*pi*f*Lf)-
(1/(2*pi*f*Cf)));

%Real and imaginary system impedance parts
Req=RV+RL+k*cos(alpha);
Xeq=k*sin(alpha);

%Percentual voltage drop estimation
Vlosspercent=((RV+RL)*Imax*100/VminMG)';

%System impedance ratio
Ratio=(Req/Xeq)';

M=[RV' Req' Vlosspercent Ratio]

%Print Graph
plot(Ratio, Vlosspercent,'k')
xlim([0.2681 8])
ylim([0 20])
xlabel('Thevenin equivalent circuit R_{eq}/X_{eq}
ratio'),ylabel('Estimated microgrid PCC percentual voltage drop
(%)')
grid on
```

Source: From author (2021)

REFERENCES

ABDELAZIZ, M. M. A. et al. A multistage centralized control scheme for islanded microgrids with pevs. **IEEE Transactions on Sustainable Energy**, v. 5, n. 3, p. 927–937, July 2014.

ALHASHEEM, M. et al. Parallel operation of dual vscs regulated by fcs-mpc using droop control approach. **2018 20th European Conference on Power Electronics and Applications (EPE'18 ECCE Europe)**, v. 20, n. 1, p. 1–10, 2018.

ALVAREZ, E. et al. On-line minimization of running costs, greenhouse gas emissions and the impact of distributed generation using microgrids on the electrical system. **2009 IEEE PES/IAS Conference on Sustainable Alternative Energy (SAE)**, p. 1–10, Sep. 2009.

ANEEL/PRODIST. **Procedimentos de Distribuição de Energia Elétrica no Sistema Elétrico Nacional – PRODIST - Módulo 8 – Qualidade da Energia Elétrica.** 2018. Disponível em: <http://www.aneel.gov.br/modulo-8>.

ARAUJO, L. S. de. **Controle de Conversores em Microrredes Autônomas com Sistemas de Armazenamento Distribuídos**. Dissertação (Mestrado) — UNIVERSIDADE ESTADUAL DE CAMPINAS, 2017.

AUGUSTINE, N. et al. Economic dispatch for a microgrid considering renewable energy cost functions. **2012 IEEE PES Innovative Smart Grid Technologies (ISGT)**, p. 1–7, Jan. 2012.

BARKLUND, E. et al. Energy management system with stability constraints for stand-alone autonomous microgrid. **2007 IEEE International Conference on System of Systems Engineering**, p. 1–6, Apr. 2007.

BIALASIEWICZ, J. T. Renewable energy systems with photovoltaic power generators: Operation and modeling. **IEEE Transactions on Industrial Electronics**, v. 55, n. 7, p. 2752–2758, July 2008.

BLAABJERG, F.; CHEN, Z.; KJAER, S. B. Power electronics as efficient interface in dispersed power generation systems. **IEEE Transactions on Power Electronics**, v. 19, n. 5, p. 1184–1194, Sep. 2004. ISSN 0885-8993.

BLAABJERG, F. et al. Overview of control and grid synchronization for distributed power generation systems. **IEEE Transactions on Industrial Electronics**, v. 53, n. 5, p. 1398–1409, Oct 2006. ISSN 0278-0046.

BODSON, M.; DOUGLAS, S. Adaptive algorithms for rejection of sinusoidal disturbances with unknown frequencies. **Proc. 13th IFAC World Conference**, p. 1–5, jul 1996. San Francisco.

BRABANDERE, K. D. et al. A voltage and frequency droop control method for parallel inverters. **IEEE Transactions on Power Electronics**, v. 22, n. 4, p. 1107–1115, July 2007.

CALDOGNETTO, T.; TENTI, P. Microgrids operation based on master–slave cooperative control. **IEEE Journal of Emerging and Selected Topics in Power Electronics**, v. 2, n. 4, p. 1081–1088, Dec 2014.

CHANDORKAR, M. C.; DIVAN, D. M.; ADAPA, R. Control of parallel connected inverters in standalone ac supply systems. **IEEE Transactions on Industry Applications**, v. 29, n. 1, p. 136–143, Jan 1993. ISSN 0093-9994.

CHEN, J.-F.; CHU, C.-L. Combination voltage-controlled and current-controlled pwm inverters for ups parallel operation. **IEEE Transactions on Power Electronics**, v. 10, n. 5, p. 547–558, Sep. 1995.

CLARKE, E. Steady-state stability in transmission systems calculation by means of equivalent circuits or circle diagrams. **Transactions of the American Institute of Electrical Engineers**, XLV, p. 22–41, Jan 1926. ISSN 0096-3860.

CORTES, P. et al. Predictive control in power electronics and drives. **IEEE Transactions on Industrial Electronics**, v. 55, n. 12, p. 4312–4324, Dec 2008. ISSN 0278-0046.

DRAGIčEVIć, T. Model predictive control of power converters for robust and fast operation of ac microgrids. **IEEE Transactions on Power Electronics**, v. 33, n. 7, p. 6304–6317, July 2018.

DRIESSE, A.; JAIN, P.; HARRISON, S. Beyond the curves: Modeling the electrical efficiency of photovoltaic inverters. **2008 33rd IEEE Photovoltaic Specialists Conference**, p. 1–6, May 2008. ISSN 0160-8371.

EL-SHARKH, M. Y. et al. Cost related sensitivity analysis for optimal operation of a grid-parallel pem fuel cell power plant. **J. Power Sources**, v. 161, n. 2, p. 1198–1207, jul 2006.

FARHANG-BOROUJENY. **Adaptive Filters: Theory and Applications**. second. [S.l.]: John wiley and sons, 1998. 800 p.

FERREIRA, S. C. **Aplicação de Filtros Adaptativos em Compensadores Híbridos de Reativo**. Dissertação (Mestrado) — Universide Federal de Itajubá, Itajubá, MG, 2012.

GONZATTI, R. B. et al. Using smart impedance to transform high impedance microgrid in a quasi-infinite busbar. **IEEE Transactions on Smart Grid**, v. 8, n. 1, p. 428–436, Jan 2017. ISSN 1949-3053.

GREEN, T. C.; PRODANOVIC, M. Control of inverter-based micro-grids. **Electr. Power Syst. Res. Distrib. Generation**, v. 77, n. 9, p. 1204–1213, July 2007. ISSN 1551-3203.

GUERRERO, J. M. et al. Advanced control architectures for intelligent microgrids—part i: Decentralized and hierarchical control. **IEEE Transactions on Industrial Electronics**, v. 60, n. 4, p. 1254–1262, April 2013. ISSN 0278-0046.

GUERRERO, J. M. et al. Output impedance design of parallel-connected ups inverters with wireless load-sharing control. **IEEE Transactions on Industrial Electronics**, v. 52, n. 4, p. 1126–1135, Aug 2005. ISSN 1557-9948.

GUIMARAES, R. A. **Controle Preditivo Baseado em Modelo para Conversres Formadores de Rede com Operação Ilhada**. Dissertação (Mestrado) — Programa de Pós-graduação em Engenharia de Ssitemas e Automação da Universidade Federal de Lavras, september 2019.

HAN, H. et al. Review of power sharing control strategies for islanding operation of ac microgrids. **IEEE Transactions on Smart Grid**, v. 7, n. 1, p. 200–215, Jan 2016. ISSN 1949-3053.

HAN, Y. et al. Review of active and reactive power sharing strategies in hierarchical controlled microgrids. **IEEE Transactions on Power Electronics**, v. 32, n. 3, p. 2427–2451, March 2017. ISSN 0885-8993.

HAO, M.; ZHEN, X. A control strategy for voltage source inverter adapted to multi — mode operation in microgrid. **2017 36th Chinese Control Conference (CCC)**, p. 9163–9168, July 2017. ISSN 1934-1768.

HE, J.; LI, Y. W. An enhanced microgrid load demand sharing strategy. **IEEE Transactions on Power Electronics**, v. 27, n. 9, p. 3984–3995, Sep. 2012. ISSN 1941-0107.

HETZER, J.; YU, D. C.; BHATTARAI, K. An economic dispatch model incorporating wind power. **IEEE Transactions on Energy Conversion**, v. 23, n. 2, p. 603–611, June 2008. ISSN 1558-0059.

HSU, L.; ORTEGA, R.; DAMM, G. A globally convergent frequency estimator. **IEEE Transactions on Automatic Control**, v. 44, n. 4, p. 698–713, April 1999. ISSN 2334-3303.

HUANG, R. et al. Optimal design of hybrid energy system with pv/wind turbine/storage: A case study. **2011 IEEE International Conference on Smart Grid Communications (SmartGridComm)**, p. 511–516, Oct. 2011.

IEEE. Ieee application guide for ieee std 1547(tm), ieee standard for interconnecting distributed resources with electric power systems. **IEEE Std 1547.2-2008**, p. 1–217, 2009.

IEEE. Ieee guide for conducting distribution impact studies for distributed resource interconnection. **IEEE Std 1547.7-2013**, p. 1–137, Feb 2013.

IEEE. Ieee standard for interconnecting distributed resources with electric power systems - amendment 1. **IEEE Std 1547a-2014 (Amendment to IEEE Std 1547-2003)**, p. 1–16, 2014.

KARIMI, H.; NIKKHAJOEI, H.; IRAVANI, R. Control of an electronically-coupled distributed resource unit subsequent to an islanding event. **2008 IEEE Power and Energy Society General Meeting - Conversion and Delivery of Electrical Energy in the 21st Century**, p. 1–1, July 2008. ISSN 1932-5517.

KATIRAEI, F.; IRAVANI, M. R.; LEHN, P. Microgrid autonomous operation during and subsequent to islanding process. **IEEE Power Engineering Society General Meeting, 2004.**, p. 2175 Vol.2–, June 2004.

LAAKSONEN, H.; SAARI, P.; KOMULAINEN, R. Voltage and frequency control of inverter based weak lv network microgrid. **IEEE Transactions on Power Electronics**, v. 22, n. 4, p. 6 pp.–6, Nov 2005.

LASSETER, B. Microgrids [distributed power generation. **Conference Proceedings**, v. 1, p. 146–149 vol.1, Jan 2001.

LASSETER, B. Microgrids. **Conference Proceedings**, v. 1, p. 305–308 vol.1, Jan 2002.

LI, Y. W.; KAO, C. An accurate power control strategy for power-electronics-interfaced distributed generation units operating in a low-voltage multibus microgrid. **IEEE Transactions on Power Electronics**, v. 24, n. 12, p. 2977–2988, Dec 2009. ISSN 1941-0107.

LIN, P. et al. A distributed control architecture for global system economic operation in autonomous hybrid ac/dc microgrids. **IEEE Transactions on Smart Grid**, v. 10, n. 3, p. 2603–2617, May 2019. ISSN 1949-3061.

MINXIAO, H. et al. Transient analysis and control for microgrid stability controller. **2013 IEEE Grenoble Conference**, p. 1–6, June 2013.

MIRANDA, U. A.; ROLIM, L. G. B.; AREDES, M. A dq synchronous reference frame current control for single-phase converters. **2005 IEEE 36th Power Electronics Specialists Conference**, p. 1377–1381, June 2005. ISSN 0275-9306.

MUMTAZ, F. et al. A novel approach to solve power flow for islanded microgrids using modified newton raphson with droop control of dg. **IEEE Transactions on Sustainable Energy**, v. 7, n. 2, p. 493–503, April 2016. ISSN 1949-3037.

NUTKANI, I. U.; LOH, P. C.; BLAABJERG, F. Autonomous droop scheme with reduced generation cost. **2013 15th European Conference on Power Electronics and Applications (EPE)**, p. 1–7, Sep. 2013. ISSN 0275-9306.

NUTKANI, I. U.; LOH, P. C.; BLAABJERG, F. Droop scheme with consideration of operating costs. **IEEE Transactions on Power Electronics**, v. 29, n. 3, p. 1047–1052, 2014.

NUTKANI, I. U. et al. Cost-prioritized droop schemes for autonomous ac microgrids. **IEEE Transactions on Power Electronics**, v. 30, n. 2, p. 1109–1119, Feb 2015. ISSN 1941-0107.

NUTKANI, I. U. et al. Decentralized economic dispatch scheme with online power reserve for microgrids. **IEEE Transactions on Smart Grid**, v. 8, n. 1, p. 139–148, Jan 2017. ISSN 1949-3053.

OLIVARES, D. E. et al. Trends in microgrid control. **IEEE Transactions on Smart Grid**, v. 5, n. 4, p. 1905–1919, July 2014. ISSN 1949-3053.

PANTEN, N.; HOFFMANN, N.; FUCHS, F. W. Finite control set model predictive current control for grid-connected voltage-source converters with lcl filters: A study based on different state feedbacks. **IEEE Transactions on Power Electronics**, v. 31, n. 7, p. 5189–5200, 2016.

PEI, Y. et al. Auto-master-slave control technique of parallel inverters in distributed ac power systems and ups. **2004 IEEE 35th Annual Power Electronics Specialists Conference**, p. 2050–2053 Vol.3, June 2004.

PENG, F. Z.; LI, Y. W.; TOLBERT, L. M. Control and protection of power electronics interfaced distributed generation systems in a customer-driven microgrid. **2009 IEEE Power Energy Society General Meeting**, p. 1–8, July 2009.

PETRUZZIELLO, F.; ZIOGAS, P. D.; JOOS, G. A novel approach to paralleling of power converter units with true redundancy. **21st Annual IEEE Conference on Power Electronics Specialists**, p. 808–813, July 1990.

QUEIROZ, A. d. P. D. et al. Single-phase ac-dc-ac multilevel converter based on h-bridges and three-leg converters connected in series. **017 IEEE Energy Conversion Congress and Exposition (ECCE)**, p. 2129–2136, Oct 2017.

ROCABERT, J. et al. Control of power converters in ac microgrids. **IEEE Transactions on Power Electronics**, v. 27, n. 11, p. 4734–4749, Nov 2012. ISSN 0885-8993.

RODRIGUEZ, J. et al. State of the art of finite control set model predictive control in power electronics. **IEEE Transactions on Industrial Informatics**, v. 9, n. 2, p. 1003–1016, May 2013. ISSN 1551-3203.

SHANXU, D. et al. Parallel operation control technique of voltage source inverters in ups. **Proceedings of the IEEE 1999 International Conference on Power Electronics and Drive Systems. PEDS'99**, p. 883–887 vol.2, July 1999.

SILVA, M. J. **Avaliação de desempenho de algoritmos de sincronismo com a rede elétrica**. Dissertação (Mestrado) — Programa de Pós-graduação em Engenharia de Sistemas e Automação da Universidade Federal de Lavras, april 2019.

SIRI, K.; LEE, C. Q. Current distribution control of converters connected in parallel. **Conference Record of the 1990 IEEE Industry Applications Society Annual Meeting**, p. 1274–1280 vol.2, Oct 1990.

TULADHAR, A. et al. Parallel operation of single phase inverter modules with no control interconnections. **Proceedings of APEC 97 - Applied Power Electronics Conference**, p. 94–100 vol.1, Feb 1997.

TULADHAR, A. et al. Control of parallel inverters in distributed ac power systems with consideration of line impedance effect. **IEEE Transactions on Industry Applications**, v. 36, n. 1, p. 131–138, Jan 2000. ISSN 1939-9367.

VANDOORN, J. D. M. D. K. T. L.; MEERSMAN, B. Review of primary control strategies for islanded microgrids with power-electronic interfaces. **Renew. Sustain. Energy Rev.**, v. 19, p. 613–628, March 2013. ISSN 1364-0321.

VAZQUEZ, S. et al. Model predictive control: A review of its applications in power electronics. **IEEE Industrial Electronics Magazine**, v. 8, n. 1, p. 16–31, March 2014. ISSN 1932-4529.

VERGARA, P. P. et al. Economic impact of the active power droop gain in droop-based islanded microgrids. **2019 IEEE Milan PowerTech**, p. 1–6, June 2019.

VERGARA, P. P. et al. Distributed strategy for optimal dispatch of unbalanced three-phase islanded microgrids. **IEEE Transactions on Smart Grid**, v. 10, n. 3, p. 3210–3225, May 2019. ISSN 1949-3061.

YAZDANI, D.; BAKHSHAI, A.; JAIN, P. K. A three-phase adaptive notch filter-based approach to harmonic/reactive current extraction and harmonic decomposition. **IEEE Transactions on Power Electronics**, v. 25, n. 4, p. 914–923, April 2010. ISSN 1941-0107.

YAZDANI, D. et al. A real-time extraction of harmonic and reactive current in a nonlinear load for grid-connected converters. **IEEE Transactions on Industrial Electronics**, v. 56, n. 6, p. 2185–2189, 2009.

YOUNG, C. H.; BASTIAS, A. Finite-control-set predictive voltage control of paralleled inverters in an islanded microgrid. **2018 IEEE 27th International Symposium on Industrial Electronics (ISIE)**, p. 395–400, June 2018. ISSN 2163-5145.